ABSTRACT.

The acoustic emission of automobile finishes on a steel substrate has been investigated. An automobile finish consists of several coatings, namely a phosphate coat, an electrocoat, a surfacer coat and a topcoat. (The phosphate coat is a type of conversion coating and the others are types of paint coats.) Several types of phosphates and electrocoats have been studied, both as part of the complete finish and as several subsystems of the finish.

When only a phosphate coat is present on the steel it has been found that the majority of the acoustic emission occurs at low strains and can be attributed to cracking and adhesion loss of the phosphate needles. When a paint coating is present this inhibits the needles cracking, but adhesion loss continues to occur within the phosphate layer. The acoustic emission from paint coats, whether as part of the complete finish or as a subsystem, occurs in two regions of high activity. The acoustic emission at lower strains has been correlated with microcracking and minor adhesion loss. It has also been established that the acoustic emission at the higher strain is related to gross damage, visible on the surface of the specimen. This high strain damage is in the form of localised peeling in diamond shaped areas which crack, followed by gross peeling.

The amplitude distributions were found to consist of a series of peaks. Using the above observations it is possible to attribute each of these peaks to a single failure process.

The Acoustic Emission and Failure Mechanisms of Automotive Finishes.

Thesis submitted for the degree of Doctor of Philosophy by

Josephine Anne Rooum.

The deed is done. Didst thou not hear a noise?

Scene 2.

Act 2.

Macbeth.

INDEX.

Chapter 1. Introduction.

A newly developed paint is subjected to a wide variety of tests before it is put on the market. Amongst the most important are tests of the paint's adhesion to its substrate and the deformation characteristics of the full paint system. These tests can be broadly categorised into two groups. Firstly there are those which can be easily performed, such as scratching with a coin, and secondly those which imitate in-service conditions, such as the "gravellometer" which simulates stone chipping. The results are assessed either by an experienced eye, or by comparative photographs, and suffer from being subjective, non-quantitative and requiring a high level of staff training. They also take no account of sub-surface damage which may occur.

Paints generally fail through some form of cracking, either within the paint or along the interface with its substrate. Such processes are liable to generate stress waves which travel through the material and can be detected at the surface. This type of phenomenon is exploited in several areas of materials testing and is known as acoustic emission.

This project investigates the acoustic emission of a particular paint system, that of an automobile finish, during tensile testing. The acoustic emission data is correlated with failure mechanisms, to assess the feasibility of this technique in the field of paint testing.

Chapter 2. Paint.

2.1 General.

A paint consists of three main components, a binder, a pigment and a solvent. In a liquid paint the solvent is the carrier for the binder and the pigment. As the paint dries the solvent evaporates and the binder usually undergoes a cross-linking process. The dry paint is a thin polymer film (of the order of 20μm thick) consisting of the binder with a dispersion of fine, coloured pigment particles. The drying time and weather resistance of the paint are determined by the binder. Some binders give unsuitably hard and brittle films, in which case a plasticiser can be added. This behaves like a non-volatile solvent, reducing the bonding between the polymer chains in the binder to give a more supple film.

The mechanism of the adhesion of the paint film to the substrate surface depends on the forces operating at the interface. The forces that operate are van der Waals attractions, hydrogen bonding and chemisorption (ionic and covalent bonds) between the paint and the substrate, but the exact nature of these effects and their relative importance have not yet been established (Myers and Long, 1969). It is known, however that it is important that the substrate surface is thoroughly cleaned before painting as this removes any impurities from the active centres for adhesion. On metal substrates any loose oxide film

should also be removed as this would interfere with adhesion between the paint and the metal. An uneven substrate surface has a beneficial effect on adhesion, providing a greater surface area than a smooth surface and hence more active sites.

The mechanical properties of a paint film fall between those of an elastic solid and those of a viscous fluid, hence it is known as "viscoelastic". In common with other viscoelastic materials paints exhibit glass transition temperatures. Below this temperature the paint is in a "glassy" state and is hard and brittle since there is no large scale molecular motion, atoms and groups of atoms moving only about their equilibrium positons. The glass transition corresponds to the onset of motion of much longer segments of molecules, characteristic of the rubbery state. The glass transition temperature is usually determined by volume coefficient measurements. In the rubbery region the motion requires a much larger free volume so at the glass transition temperature there is a change in slope of the temperature v. volume coefficient curve. Figure 2.1A shows this effect for polystyrene. For paints this type of measurement is impractical and instead the brittleness of the film is measured as a function of temperature by impact testing (see experimental section). Again the curve will show a change of slope at the glass transition temperature.

Similarly the mechanical properties will depend on the time of the application of the force. In a short time the molecules cannot distort substantially so the material appears hard and brittle. At longer times the chain segments reorientate to relieve local stresses and the material appears more flexible.

Hence the glass transition temperature will depend on the technique by which it is measured. An impact test for instance, which takes place suddenly will give a higher Tg than a more gradual test.

The main reason for painting steel car bodies is to protect them from corrosion. Potential differences arise on a bare steel surface by, for example, local variations in the composition of the steel so that if oxygen and water are both present then a corrosion current is set up, the reactions being

1 $4Fe \rightarrow 4Fe^{2+}+8e^{-}$

2 $8e^{-}+4H_2O+2O_2 \rightarrow 8OH^{-}$

see figure 2.1B. The reaction products diffuse from the surface and react with hydrated oxygen to form rust

3 $4Fe^{2+}+8OH^{-} \rightarrow 4Fe(OH)_2+O_2 \rightarrow 2Fe_2O_3\ H_2O+2H_2O.$

The rust is precipitated at a region intermediate between the anode and the cathode, so it does not act to inhibit the corrosion reaction. Corrosion can be prevented by stopping the flow of the corrosion currents in the cell which can be done by suppressing either the anodic or cathodic reactions, or by putting a high resistance in the path of the current. In some cases zinc oxide pigments are introduced in the paint film in order to suppress the anodic reaction. For some time it was thought that paint acted by suppressing the cathodic reaction, preventing the access of water and oxygen to the steel surface. Work by Mayne (1957) however, demonstrated that the permeabilities of paint films to water and oxygen are usually so great that access of water and oxygen is virtually unhindered. It

follows that in most cases the paint protects against corrosion by impeding the movement of ions between the anodic and cathodic sites. Bacon et al (1948) measured the resistance of various paint films and found these corresponded to the protection afforded by the paints.

2.2 The automobile finish.

Car bodies are usually formed from mild steel, with a paint finish consisting of several coats, as shown in figure 2.2A. A typical finishing process is shown in figure 2.2B. As stated in section 2.1, the substrate must be clean to allow adhesion of the paint to the surface. Wojtkowiak and Bender (1978) have shown that differences in corrosion about a line scribed through paint and phosphate on a steel substrate can be attributed to oil and grease present on the substrate surface before coating.

The phosphating and electrocoating processes will be described more fully in the following sections. These processes rarely level out any imperfections in the smoothness of the substrate and a surfacer coat is applied in order that the topcoat is applied onto a smooth surface. The binder of the surfacer coat is either an epoxy ester or an oil-free alkyd resin and its filling properties are derived from a variety of additions, mainly baryates. There are two types of topcoat in common use, employing either thermoplastic or thermosetting resins with conventional pigments.

The topcoat is the main contributor to the appearance of the finish, giving the colour and the gloss, but the behaviour and

protective properties of the finish depend on all the coats and on their compatibility.

2.2.1 The phosphate layer.

The phosphate layer contains the substrate surface as an integral part of the coating and is therefore a type of conversion coating. The phosphating is achieved by spraying or dipping the substrate in a bath which consists of phosphoric acid, a metal phosphate (usually zinc) and an accelerator (usually sodium chlorate). The following reactions take place:

1 $Fe - xe^- \rightarrow Fe^{x+}$

2 $xH_3O^+ + xe^- \rightarrow x/2H_2\uparrow + xH_2O$

3 $2H_2PO_4^- + 3Zn^{2+} \rightarrow Zn_3(PO_4)_2 + 4H^+$

4 $ClO_3^- + 6H^+ + 6e^- \rightarrow Cl^- + 3H_2O$

As the acid attacks the metal (equations 1 and 2) the evolution of hydrogen gas reduces the acid concentration at the interface, displacing the equilibrium of equation 3 to the right. The action of the accelerator is to further reduce the acid concentration (equation 4). The phosphate is nucleated at microanodic sites on the steel substrate, precipitating as mixed iron and zinc phosphates of undefined formulae, known as phosphophyllite. As the anodes become covered with crystallites the attack becomes more uniform and the growth of zinc phosphate predominates. This is the orthorhombic $Zn_3(PO_4)_2 4H_2O$ and is called hopeite.

The paint adheres more strongly to the phosphate surface than it would to the substrate alone and, if the paint film is damaged, the phosphate inhibits the spread of underfilm

corrosion.

The phosphate coat is water rinsed before painting in order to remove any residual acid or chloride ions from the bath, which would otherwise cause corrosion. There is some evidence that rinsing further improves the adhesion of the substrate to the paint (Cooke, 1979).

2.2.2 Electrocoat or electrodeposited primer.

Electrocoating is basically a dipping process, where charged paint particles (binder and pigments) are attracted to the car body. The car forms one electrode and the sides of the dipping tank the other. The car is usually the anode, although cathodic depositon is sometimes used. The main reactions that take place at the substrate are, for anodic deposition:

1 $4H_2O \rightarrow 4H^+ + O_2 + 4e^-$

2 $Fe \rightarrow Fe^{x+} + xe^-$

3 $RCOO^- + H^+ \rightarrow RCOOH$

4 $RCOO^- + Fe^{x+} \rightarrow (RCOO)_x\text{-}Fe$ and for cathodic deposition (Anderson et al, 1978):

5 $2H_2O + 4e^- \rightarrow 4OH^- + 2H_2$

6 $Fe + 4OH^- \rightarrow (FeO_2)^{x-} + 2H_2O + (4-x)e^-$

7 $R_3NH^+ + OH^- \rightarrow R_3N + H_2O$

8 $xR_3NH^+ + (FeO_2)^{x-} \rightarrow (R_3NH)_x\text{-}(FeO_2)$

It can be seen that the metal ions from the substrate play an important role in the coating process. These diffuse through the paint layer to the surface after the initial deposition.

The process is self regulating and gives a coat of uniform

thickness. The outer surfaces of the car are quickly coated but as the paint layer builds up its resistance increases and eventually the current it allows to pass is insufficient for further coating in these regions. Deposition in the box section interiors will then occur, at the bare surface just beyond the coating edge. This continues until the entire car body is coated.

As the car is removed from the tank it collects a layer of paint of high water content which is rinsed off before the electrocoat is stoved.

2.3 Paint testing.

In the paint industry little attempt is made to predict a paint's performance from its constituents. Instead, newly developed paints are extensively tested in order to predict their behaviour during service. The two reasons for painting are to protect and decorate the substrate, and the colour, gloss and corrosion resistance are important among the many properties tested. For the paint to continue to provide resistance to corrosion under service conditions it must remain a continuous film and adhered to the substrate. Thus it must be able to conform to any movement or deformation the substrate is likely to encounter. A measure of this ability is given by its flexibility.

2.3.1 Flexibility testing.

In a flexibility test the whole paint system, including the substrate is tested. This has the advantage that the paint

film(s) are subjected to similar strains and will behave in the same way as would occur under actual service conditions.

The test is commonly performed by bending painted panels over a series of mandrels of increasing radius, usually by hand. The strain to which the paint is subjected is known from the radius of the mandrel and the thickness of the painted panel, the flexibility being given by the highest strain the paint can undergo before it ruptures. The test can also be performed by direct extension of the paint system, in a tensile testing machine. In this case the strains can be more easily controlled and measured. Schuh and Theuerer (1937) compared results between bending and direct extension tests of the flexibility for a number of paint films. They found that, in some cases, the values given by the bend tests were considerably below those for the direct extension tests. They were able to attribute this to differences in the strain rates at which these tests were performed.

As a paint film gets older it becomes more brittle and will, eventually, crack on the substrate. This is discussed further in section 2.4.1. The time at which this failure occurs depends on the paint and is usually greater than six years. Jacobsen (1938) found that the rate and the character of this film failure are closely related to the paint's ability to retain its flexibility with age.

The flexibility that is exhibited by a paint system depends, not only on the stress-strain properties of the paint, but also on the adhesion between the paint and its substrate. In a system consisting of several layers it will also depend on the intercoat

adhesion. Both the adhesion and the properties of the paint itself can be tested seperately.

2.3.2 Adhesion tests.

There are a great many procedures used for testing adhesion, the most frequently used being subjective tests, such as scratching with a coin or a fingernail. The various testing procedures are described in detail by Schurr (1972). Two commonly used tests that give comparative data for the tested paint films are the crosscut test and the tensile test. For the crosscut test a fine grid of scratches is cut through the paint, sellotape is attached then pulled away and the number of squares remaining adhered to the substrate give an estimate of the adhesion. In the tensile test the load is applied normally to the substrate surface, by glueing a paint panel to tensile testing machine grips and then recording the stress at which the paint losses adhesion. One problem with this test is that the glue may affect the properties of the paint film.

2.3.3 Properties of detached paint films.

It is possible to detach paint films from their substrates by inserting a knife along the interface, or by painting onto tin plate and "floating off" the paint with mercury. The films can be strained in tensile testing machines and their tensile strength and elongation to failure are useful in evaluating the effect of additional plasticisers and pigments on paint films.

Jacobsen (1938) studied the tensile properties of detached

paint films in various two-coat paint systems. He found the results consistent with those from flexibility tests on the whole system.

2.4 Environmental effects.

As discussed in section 2.1, the behaviour of a paint film will depend on the temperature and on the strain rate at which it is tested. At higher temperatures and lower strain rates the film will appear more flexible. This effect has been shown experimentally for strain rate (Schuh and Theuerer,1937) and for temperature (Elm,1953). The behaviour will also depend on the humidity, and in general tests are designed to take place at 25∓5°C and 50∓1% relative humidity. This control is not always possible, in which case the temperature and the humidity are recorded with the test data. The conditions in which the coatings have been stored are also important in determining their behaviour.

2.4.1 Ageing and weathering of paint coats.

Once formed, a paint coat will begin to age, becoming more brittle with time (Schurr,1972). The two main factors that cause a film to break down are ultraviolet light and water. Extremes of temperature also have some effect (Nylen and Sunderland,1968). In order to determine the useful lifetime of a paint, samples are weathered and inspected during ageing for defects such as flaking, cracking, colour change and mould growth. The weathering

can be either naturally or under accelerated conditions. Various machines exist for accelerated weathering tests, all expose the paint to a very severe environment, with greater exposure to water and ultraviolet light than will be encountered in practice, typically for three months. If the paint performs adequately further samples are exposed to natural weathering, where the panels are left outside for several years.

2.4.2 The effect of water.

Water acts as a plasticiser, so in conditions of higher humidity, when more water is absorbed, the flexibility of the paint will increase. Hence the need to specify the humidity when testing.

Paints are often exposed, not only to variations in humidity, but also to the direct action of water (as rain, for instance). To test that a paint's performance is still adequate the paint panels are often totally immersed in water (S.M.M.T.,1956), for several days. After soaking, paints are generally found to adhere less well to their substrates (Walker,1965). As the water evaporates out the paint usually regains its original properties within a few hours.

An estimate of the quantity of water contained in a paint film can be obtained by measuring its dielectric constant. The metal substrate forms one plate of a capacitor and a layer of mercury placed on the paint surface forms the other, as shown in figure 2.4A. The capacitance is measured and the percentage of water contained in the paint film is given by

$$V = \frac{100 \times \log(C_1/C_2)}{\log 80}$$

where C_1 is the measured capacitance and C2 is the capacitance of the dry paint film (Gentles,1963).

2.5 Microscopy of paint films.

Light microscopy is widely used in the study of paint films. It is particuarly useful for the examination of weathering effects such as cracking, chalking and mildew. Many pigment particles are large enough to be identified and their dispersion studied under the light microscope, but smaller ones are examined in the form of thin films in the transmission electron microscope.

The thickness of a paint coat is often determined by a microscopical examination of a cross section of the paint, still attached to its substrate. Examination in cross section is also used to investigate the penetration of the paint into wood and, using specimens set in resin and then polished, it is also possible to study adhesion failure between paints and metal substrates (Myers and Long,1969).

Surfaces of paints were studied in the electron microscope as early as 1944 (Bell,1960) this was done using replica techniques but, with the arrival of the scanning electron microscope replica work became virtually obsolete. The study of coatings using the scanning electron microscope is mainly used as an extension to light microscopy, allowing higher magnifications and a greater depth of field.

FIGURE 2.1A

A temperature vs. volume coefficient curve for polystyrene, taken from Treloar L. Introduction to polymer science, pub. Wykeham Science Series, 1970.

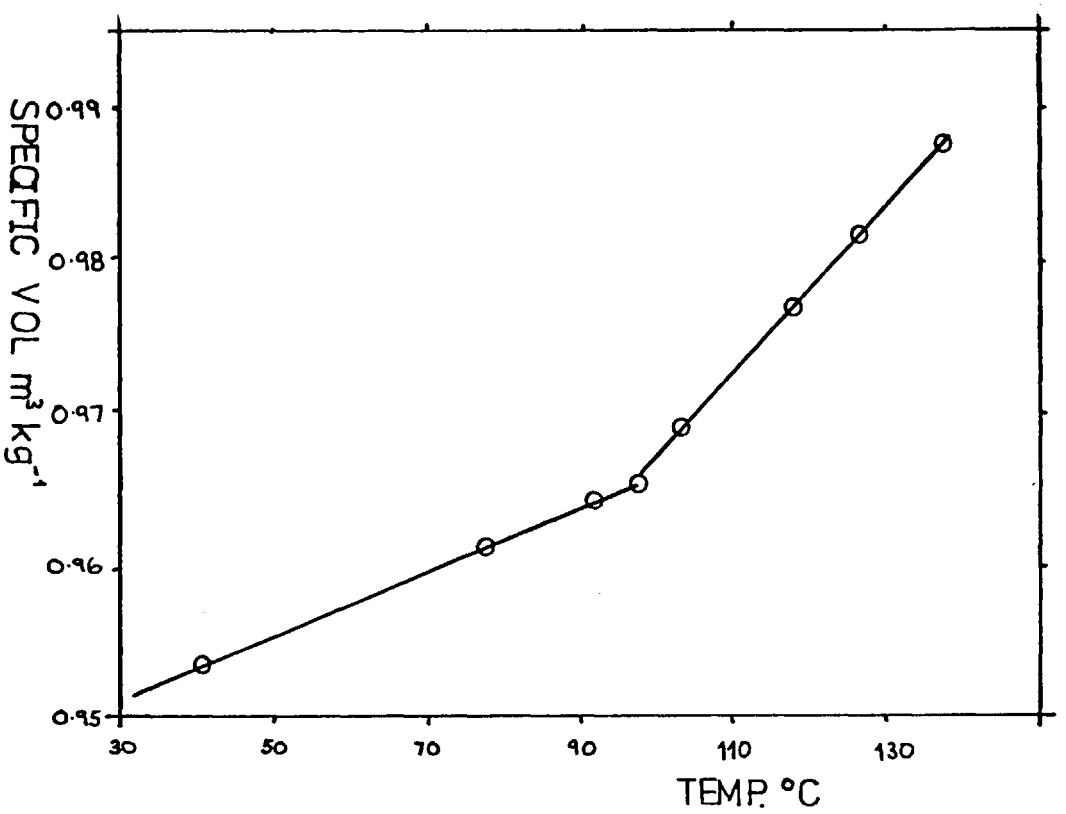
SPECIFIC VOL m³ kg⁻¹
0·99
0·98
0·97
0·96
0·95
30
50
70
90
110
130
TEMP. °C

FIGURE 2·1B

Corrosion reactions on iron.

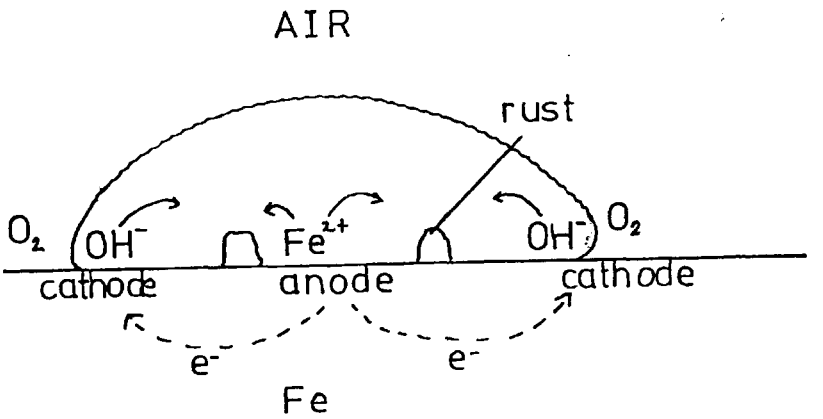

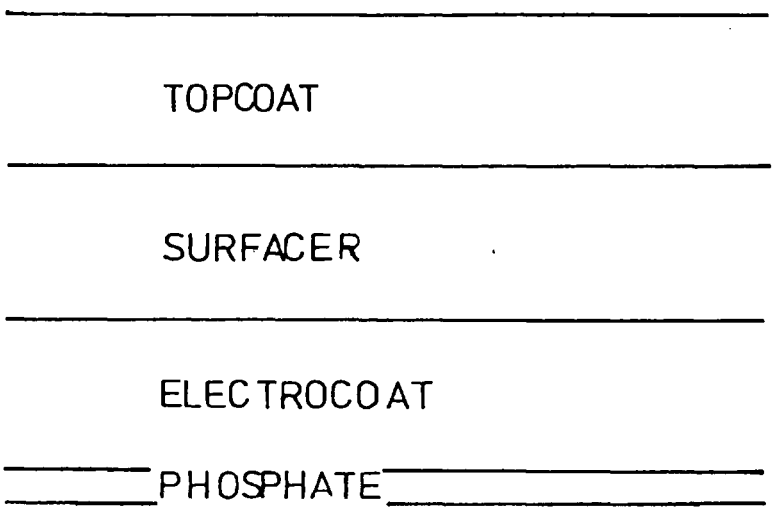

FIGURE 2-2 A
Typical automobile finish.

FIGURE 2.2B

TYPICAL AUTOMOBILE FINISHING PROCESS.

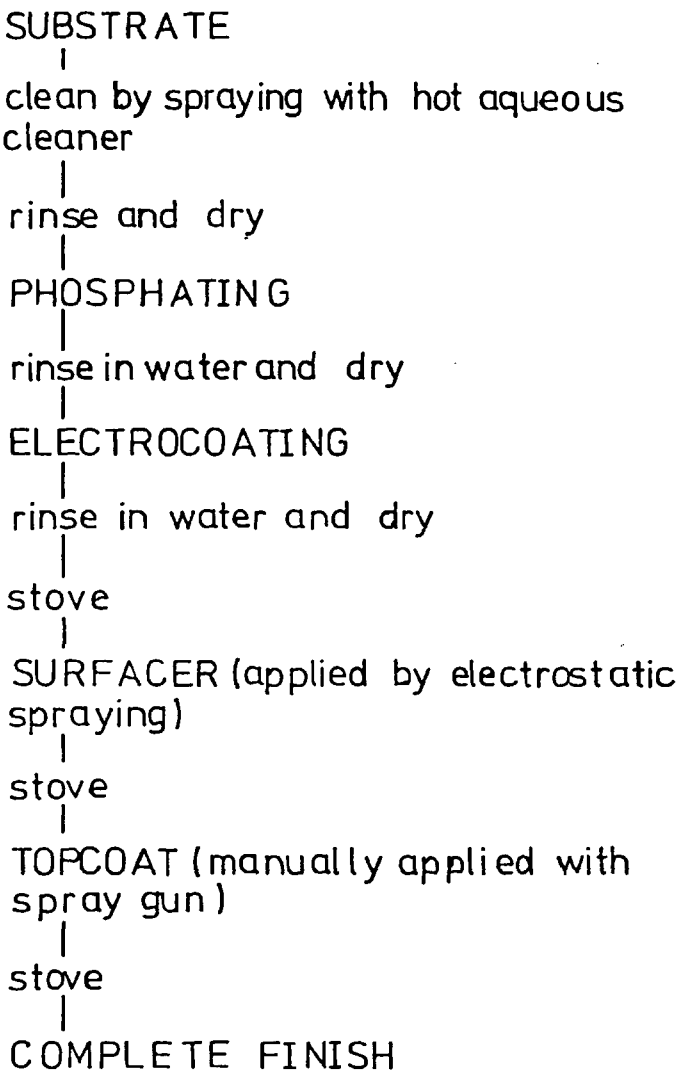

FIGURE 24 A

Schematic diagram of apparatus to measure water content of paint films.

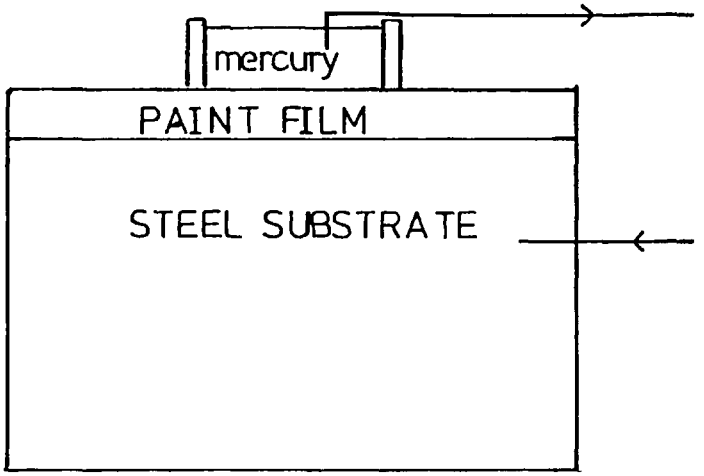

Chapter 3. Acoustic Emission.

Acoustic emission is the term used to describe the generation of stress waves as a material is deformed. The waves are generated at areas of abrupt local deformation, such as a crack tip, and propagate through the material, to be detected as small displacements on the specimen's surface.

Early studies using acoustic emission were performed on geological materials (Hardy,1972) during research into mine design and rock burst prevention. Early work in materials science includes that by Mason (1948) who investigated twinning in tin and Kaiser (1950) who studied wood and a large number of metals. Kaiser noticed that if a specimen had been previously loaded there was no emission on subsequent loading until the previous maximum stress was reached. This is known as the Kaiser effect. Acoustic emission has also been used in the study of composites (Guild et al,1975) and ceramics (Swindlehurst and Wilshaw,1976).

The propagation, detection and processing techniques of acoustic emission will now be discussed in more detail.

3.1 Propagation.

An abrupt redistibution of the internal stresses in a structure, for instance a crack propagating or dislocations moving, causes a stress wave to be generated in the material. Pollock (1973) uses the analogy of a mass held in tension between

two springs to describe the system. If one of the springs is instantaneously weakened the mass will begin oscillating about a new equilibrium position with damping forces eventually bringing it to rest. The waves thus produced are longitudinal, with oscillations occuring in the direction of the propagation of the wave (figure 3.1A).

From a single source within a specimen stress waves will radiate in all directions, at the velocity of sound ($\sim 2000 ms^{-1}$, for metals). The initial waves produced by a source are longitudinal. However when a wave reaches a boundary, such as an interface boundary or the specimen surface, transverse waves may also be produced. The situation is shown in figure 3.1B., and is known as mode conversion. If a longitudinal wave hits a boundary at other than normal incidence then both longitudinal and transverse waves are transmitted and reflected, similarly for a transverse wave. This is often observed experimentally and can be predicted from a consideration of the boundary conditions (Pollard,1977). For a transverse wave the oscillations are normal to the direction of propagation (figure 3.1C), they propagate only in solids and at lower velocities than longitudinal waves. (If the boundary is the specimen surface then surface waves will be produced (figure 3.1D). These extend only a small distance into the material, typically of the order of one wavelength, and propagate only along the surface.) The amount of reflection and transmission at a boundary can be determined by considering the acoustic impedances of the two materials. The acoustic impedance is given by

material density x velocity of sound in the material

The more similar the acoustic impedances of the two materials the greater the fraction of the wave that is transmitted. This effect is of particular importance if the signal is to be detected. The acoustic impedance of the detecting transducer must be similar to that of the material under study. Air has an extremely small acoustic impedance, thus it is essential that there should be no air gap between the material and the transducer. This is achieved by using a couplant of suitable impedance, which thoroughly wets both surfaces, araldite and silicon grease are commonly used. It is important that the couplant layer is not too thick, as this would set up reflections within the couplant (Redwood, 1964).

Along with reflections and mode conversion, further complications to the signal arise through attenuation, the loss of energy into the material as the wave travels through it. For longitudinal waves heat exchange between the contracted and expanded sections of the material can occur (Mason, 1958) causing attenuation proportional to the square of the frequency. In a metal energy will also be lost by the unpinning of dislocations and Swindlehurst (1973) has shown that transverse waves suffer greater attenuation than longitudinal waves.

Displacements on the surface will arise from the interference of a large number of waves of different frequencies, amplitudes and directions. The reflections within a specimen depend on the size and the geometry of the specimen. This gives rise to a complicated situation which can sometimes cause confusion. A particularly good example of this is the inflection noticed in the ΔK vs. count rate curves obtained in fatigue

experiments on standard C.T.S. specimens, interpreted as a change in fracture mode (Harris et al,1974). This is shown in figure 3.1E. Hamel et al (1979) have shown that this can be accounted for entirely by geometrical effects. It is possible, in some instances, to predict the wave patterns by calculating the reflections and interferences that occur. Fitch (1969) was able to do this for a single source in a thin plate, and found the calculations correlated well with experiment.

3.2 Detection.

The displacements on a specimen, caused as stress waves reach the surface, are of the order of $10^{-13}\mu m$. Such displacements are readily detected by piezoelectric crystals. The piezoelectric effect occurs in some ionic crystals. When ionic crystals are subjected to a pressure the positive ions will move with respect to the negative ones. If the crystal has a centre of symmetry the ions will distort about the centre and electrical neutrallity will be maintained. If, however, the crystal has no centre of symmetry the distortion will cause an electrical potential between the faces of the crystal, proportional to the change in the crystal thickness,

$$V=h\Delta t$$

where V=voltage, Δt=change in thickness and h=piezoelectric deformation constant(volts/m). The deformation constant varies with the crystal material. Several materials exhibit the piezoelectric effect, quartz being one of the most common. For the purpose of acoustic emission lead zirconium titanate (P.Z.T.)

is widely used, as its high dielectric constant (1,200 compared with 4.5 for quartz) means that capacitive effects in the coaxial cable will produce less distortion in the signal.

A piezoelectric transducer is produced by depositing thin layers of conducting material onto the crystal faces which allow the potential across the crystal to be measured. A diagram of a transducer is shown in figure 3.2A.

The stress waves have a wide range of frequencies. Often transducers are used that have a flat frequency response to only a narrow band centred on their resonant frequency. These are known as narrow band transducers. There are also a variety of wide band transducers with a flat frequency response to a larger range of frequencies (typically 0 to 500kHz). These include, along with piezoelectric types, the capacitive transducer (Scruby and Wadley,1978), which measures the capacitance between a plate and the specimen, from which the width of the air gap and hence the displacements on the surface can be calculated. Although the wide band transducers are less sensitive they allow a range of frequencies to be scanned. Ono and Usick (1976), working on aluminium alloys, found that results of frequency analysis were due largely to resonances in the specimen and transducer, and concluded that the frequency spectrum was otherwise flat. This suggests that little information is lost when a narrow band transducer is employed.

It is possible to choose the frequency about which a narrow band transducer will operate, as the crystal resonances depend on its thickness. Early workers used frequencies of less than 60kHz, which caused many experimental problems. A significant advance in

acoustic emission was the raising of the frequencies monitored to above the level of the majority of the background noise (Dunegan et al, 1964). Higher frequency signals are attenuated more, however and this sets an upper limit to the frequencies that can be used.

A typical narrow band transducer operates at about 150kHz. The transducer responds to a single pressure change by a sharp voltage peak followed by a gradual decay with the voltage oscillating about zero. This effect is known as ringing down and is shown diagrammatically in figure 3.2B. The frequency of the ringing is a characteristic of the transducer. The signal is typically of the order of 0.5millivolts and lasts for approximately 100microseconds. The signal is filtered and amplified before processing. To reduce the distortion introduced by the cables the signal is preamplified near the transducer and then further amplified. Typically the total amplification is between 40 and 100dB, depending on the analysing techniques used. A dB or decibel is a measure of amplifier gain and is given by

$$dB = 20\log(V_{in}/V_{out})$$

3.3 Signal processing techniques.

In order to compare results from various tests the transducer signal has to be converted into some manageable form. Often data is stored on tape for later processing, but usually the signal is analysed directly. A typical voltage output is shown in figure 3.3A. The background noise appears as a continuous, low level signal and the stress waves as bursts in

the voltage. The background noise is eliminated by setting a threshold, below which the signal is not monitored. Sometimes the acoustic emission is made up of low amplitude, unresolvable bursts, which may appear to be a change in the background noise level. This is termed "continuous emission" and is commonly associated with dislocation movement (Webborn, 1979).

The methods of signal analysis in general use include r.m.s. monitoring, ringdown and event counting and amplitude and frequency analysis, as summarised in figure 3.3B. Frequency analysis was described in section 3.2, the other techniques will be described in the following sections.

3.3.1 R.M.S. monitoring.

This technique monitors the square root of the mean transducer voltage, through the test, using a conventional r.m.s. voltmeter. The backgound noise is monitored as a continuous signal with the acoustic emission superimposed. As no threshold level need be set this method is particularly suitable for characterising continuous-type emission. With other processing techniques it is difficult to set the threshold to eliminate all the background noise while preserving all the acoustic emission. R.M.S. monitoring is also found to be less sensitive to small changes in gain (which can occur by the amplifier drifting) than the other techniques (Hamstad and Mukherjee, 1974).

For the more usual burst-type emission the rather slow response times of most meters(~2μsecs) make it impossible to distinguish a series of small, quick bursts from one large one.

In this case counting methods are generally more useful.

3.3.2 Event counting.

The transducer output as shown in figure 3.2B can be attributed to one event occurring in the specimen (an increment of crack growth for instance). This technique counts each such sinusoidal decay of the transducer as one event. This is achieved by the introduction of dead times, during which the counter does not operate. As a signal crosses the threshold a count is registered and a preset dead time (usually of the order of milliseconds) begins. Ideally the dead time ends immediately after the burst has occurred, ready for the process to be repeated as the signal next crosses the threshold. A signal as shown in figure 3.3A would register 5 events.

3.3.3 Ringdown counting.

This technique records the number of times the transducer output crosses the threshold. The signal of figure 3.2B would register 3 ringdown counts. Ringdown counting requires simpler electronics than event counting, and will weight some types of noise less heavily. For instance electrical noise often occurs in the form of a spike which would be counted as one event and one ringdown count. Typically over an entire test the ringdown counts will number ten or a hundred times more than the event counts. An

electrical spike will, then, form a much smaller fraction of the total ringdown counts than of the total events. Ringdown counting gives more weight to higher energy signals, as these take longer to ringdown. The number of ringdown counts, N_r, can be related to the peak voltage, V_p, of a burst by

$$N_r = ft \ln(V_p/V_t)$$

where f is the resonant frequency of the transducer, t is the time the burst lasts and V_t is the threshold voltage.

3.3.4 Amplitude analysis.

The peak voltage monitored during an event is known as its amplitude (see figure 3.2A). The amplitude is related to the energy of the event. Classical wave theory predicts that

$$E \propto (V_p)^2$$

where E is the energy. This is a rather simplified equation, as it will also depend on the time duration of the pulse (Holt,1972). Amplitudes are usually presented in the form of amplitude distributions which are histograms, giving the number of the events in each of several ranges of amplitude, with data collected from a whole test. The amplitude is usually given in decibels,

$$dB = 20\log(V_p/V_o)$$

where V_o is a reference voltage. The amplitude distribution is usually recorded by feeding the signal into a multilevel sorter which records each time any of a series of threshold levels is crossed (Pollock,1973). A simple amplitude sorter registers the number of events above each level and the events in each range is found by subtraction.

The amplitude distribution is not significantly altered by reflections in the sample or by transducer effects. This was demonstrated by Holt (1976) who compared the amplitude distributions from an electrical signal fed directly into a multilevel sorter with that obtained if the signal was used to excite a transducer attached to a specimen, the pulses being

detected by acoustic emission equipment. The two distributions were very similar and he concluded that an amplitude distribution accurately reflects the amplitudes of the stress waves in the specimen.

Amplitude distributions are commonly characterised by their "b-value". The distribution is approximated to a power law of the form

$$n(V) = (V/V_t)^{-b}$$

where n(V) is the fraction of the population with amplitude exceeding V, V_t is the lowest detectable voltage and b is constant. The b-value is thus the slope of the straight line given when log n(V) is plotted against log V. A similar power law distribution is also used in geological applications (Schlotz,1968). If the curve is better approximated by two or more straight lines these are often attributed to two or more deformation mechanisms in the specimen. Becht et al (1976) use different b-values to distinguish between fibre failure and interfibre failure in glass reinforced plastic tubes and similarly Williams and Lee (1979) distinguished between flawed and unflawed laminated graphite/epoxy composites.

It is enlightening to work back from an idealised log-log plot setting b=1 (a typical value for b (Pollock,1973)). This is shown in figure 3.3C. It can be seen that the amplitude distribution is physically unacceptable at low amplitudes, and the peak shape is unlike that found experimentally. Holt (1976) suggests that the distribution is better approximated by a log-normal curve (figure 3.3D). He shows that this approximates to a power law distribution at amplitudes much greater than V_m

the modal value of the amplitude. This type of description seems more realistic. Nevertheless the power law description is of some value. If a process proceeds by a large number of small steps then it will have a high b-value and if it proceeds by a small number of large steps it will have a low b-value. Furthermore a clearly defined bi-modal b-value corresponds to two peaks in the amplitude distribution curve.

3.4 The acoustic emission of coatings.

Acoustic emission has been used to monitor several types of coatings and in various deformation modes. Fisher and Lally (1977) tensile tested iron and copper in both electropolished and oxidised states. They found the responses very similar, indicating that the oxide layer had little effect. Palmer (1973) however, took a cracked steel specimen and oxidised it at 650°C for one hour. On tensile testing at room temperature this gave a large amount of emission at low strains some of high amplitudes, unlike a similar, but not oxidised specimen. Palmer attributed the acoustic emission to the oxide layer cracking on the faces of the crack. Brindley and Harrison (1972) also found that oxide layer cracking on steel gave rise to acoustic emission at low strains. In both this and Palmer's work the acoustic emission was exhausted at low loads, however at elevated temperatures the oxide layer is continually reforming and cracking (Williams,1973). In an attempt to eliminate this oxide spalling in his post weld relief cracking studies Clark (1978) coated steel specimens with various organic films. On heating he found

that most of the films did not emit and he was able to recommend two coatings that were quiet and also prevented oxide formation.

Cracking of electroplate coatings has also been investigated. In three point bending tests Filatov et al (1973) found that a nickel coating on steel that deforms plastically gives fewer counts than a chromium coat that cracks. Indeed it has recently been suggested that acoustic emission can be used to monitor cracking during the electrocoating process (Peters and Larson,1976). The effect of various thicknesses of zinc coats on steel during tensile testing has also been examined (Mosle,1978). Differences in the acoustic emission monitored were attributed to differences in the failure mechanisms.

Mosle (1979) has also monitored the acoustic emission from several paint systems during tensile testing, and quotes his results as the rate of ringdown counting. His work on phosphated steel indicated that a thicker phosphate coat gave an earlier onset of more acoustic emission than a thin one. He attributes this to the fracture of more and coarser crystals. He also examined the effect of coating the phosphate with an acrylic paint coat. The coat was found to emit less if baked at a temperature higher than recommended by the manufacturer. A painted sheet with no phosphate generally gave less emission, and emitted more if baked at a high temperature.

Mosle also studied a four coat paint system consisting of a phosphate coat, two undercoats and a topcoat. If the second of the undercoats showed poor adhesion the acoustic emission began at earlier strains and gave increased ringdown counts. He also did some soaking tests on a one coat epoxy based paint and found

that the acoustic emission began at earlier strains with increasing immersion times. This he attributes (1979a) to the condensation of water along the steel/paint interface, which he verified by the existance of pores, visible on the back of the paint coat in the scanning electron microscope.

He has also examined the effect of the thickness of a one coat acrylic paint, and suggests that the coating thickness has no significant effect. This seems unlikely as conventional tests (Schuhetal, 1937) indicate that the coating thickness dramatically affects the flexibility of a paint. Indeed on closer examination of the results presented by Mosle (figure 3.4A) the 80μm coat appears to give more emissions than the 20μm one. Measurements from these graphs indicate that the difference is 25 to 30%, which may be significant .

FIGURES 3.1A,C and D

Showing the movement of the material as the longitudinal, transverse and surface waves respectively pass through it. Diagrams are taken from Krautkramer J. Ultrasonic testing of materials, pub. 1965.

FIGURE 3.1B

The mode conversion experienced by a longitudinal wave when it impinges on a boundary between two solids.

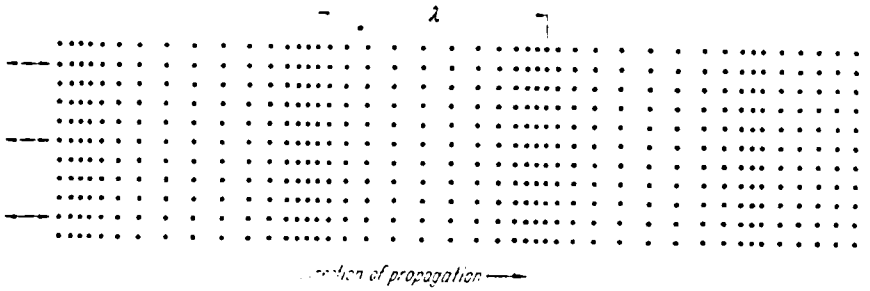

FIGURE 3.1A Longitudinal waves.

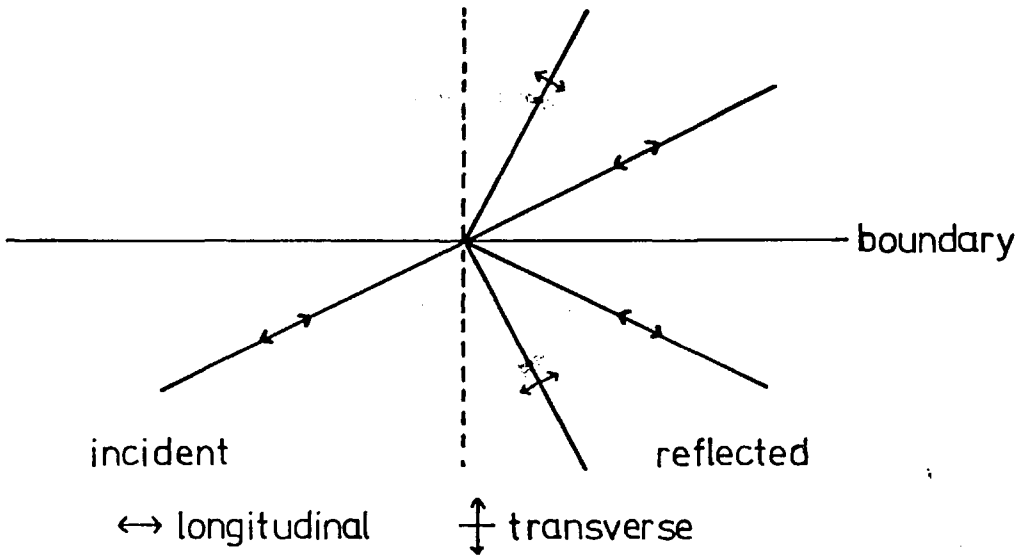

FIGURE 3·1B
Mode conversion.

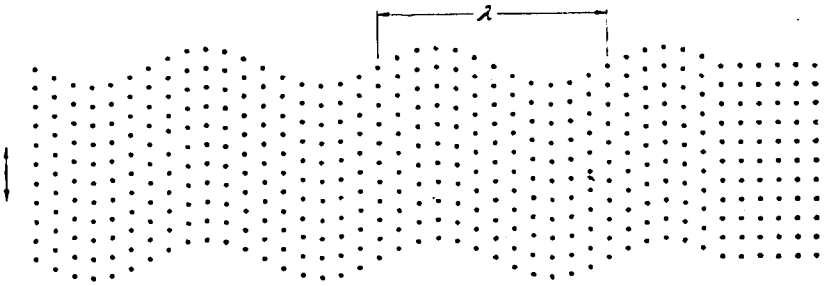

FIGURE 3·1C Transverse waves.

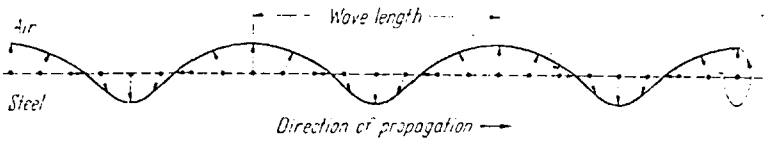

FIGURE 3.1D Surface waves.

FIGURE 3·1E

Inflection in the ΔK vs count rate curve that can be accounted for by geometrical effects.

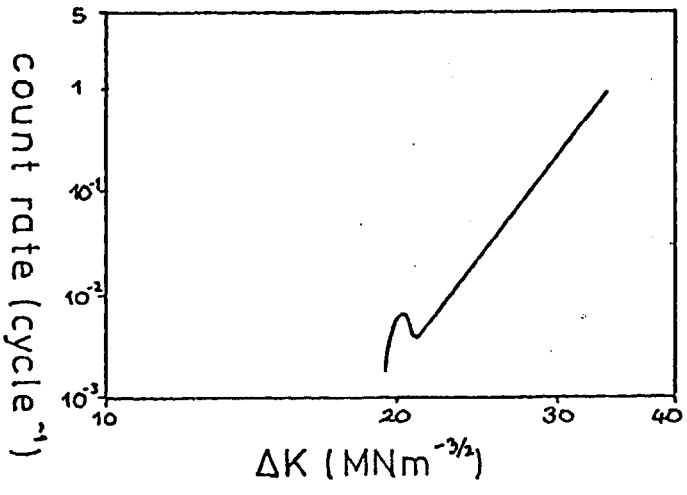

FIGURE 3.2A

Schematic representation of a piezoelectric transducer.

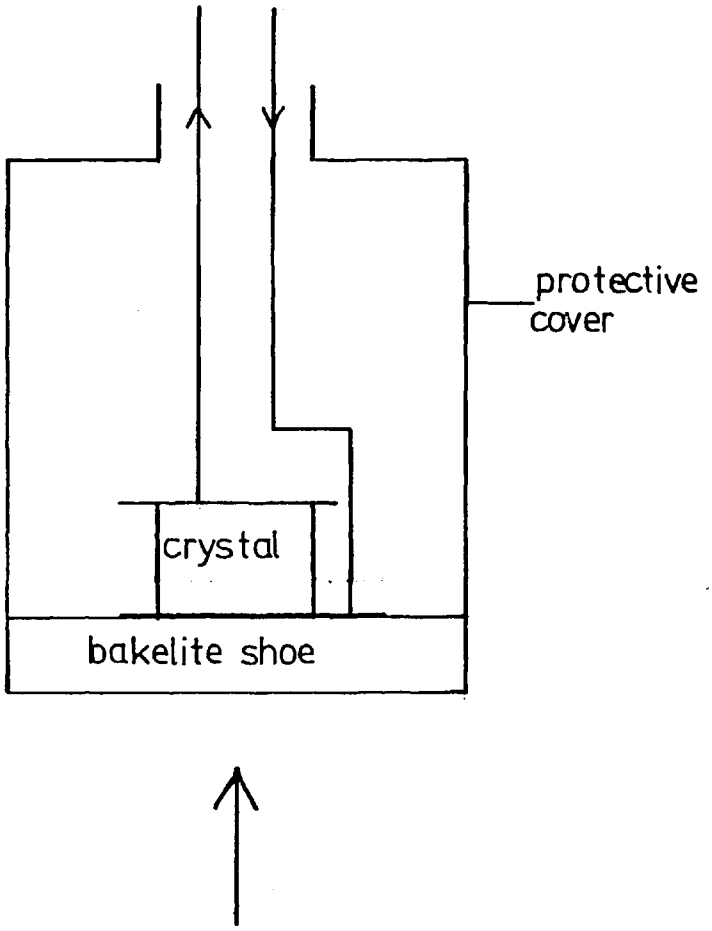

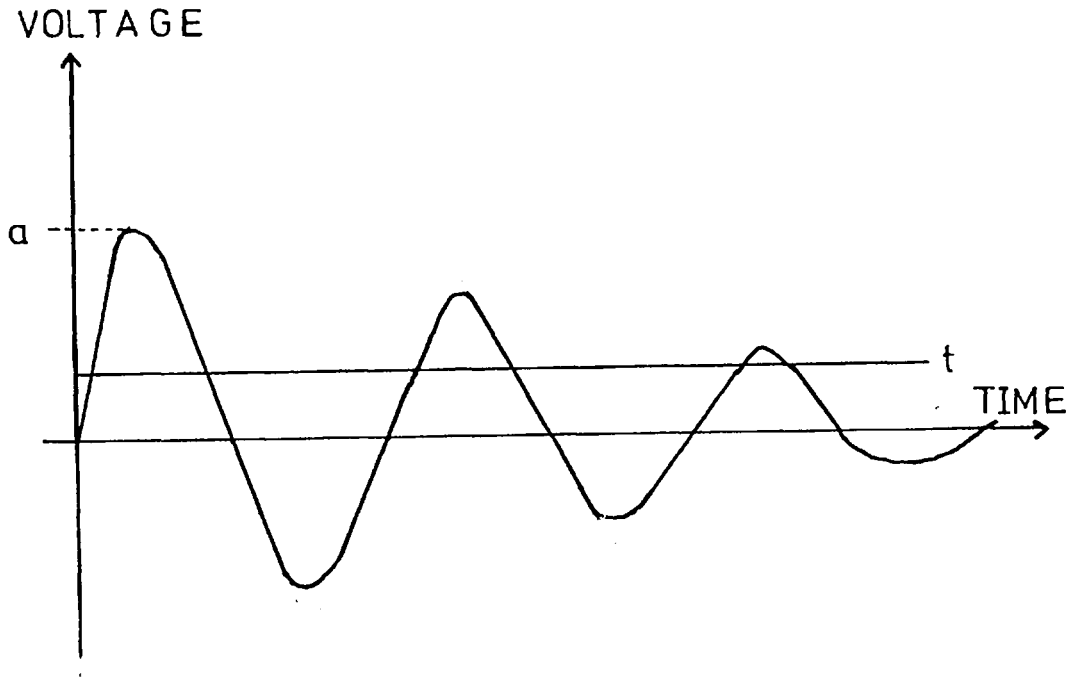

t - threshold
a - amplitude

FIGURE 3·2B

The ringing down of the transducer.

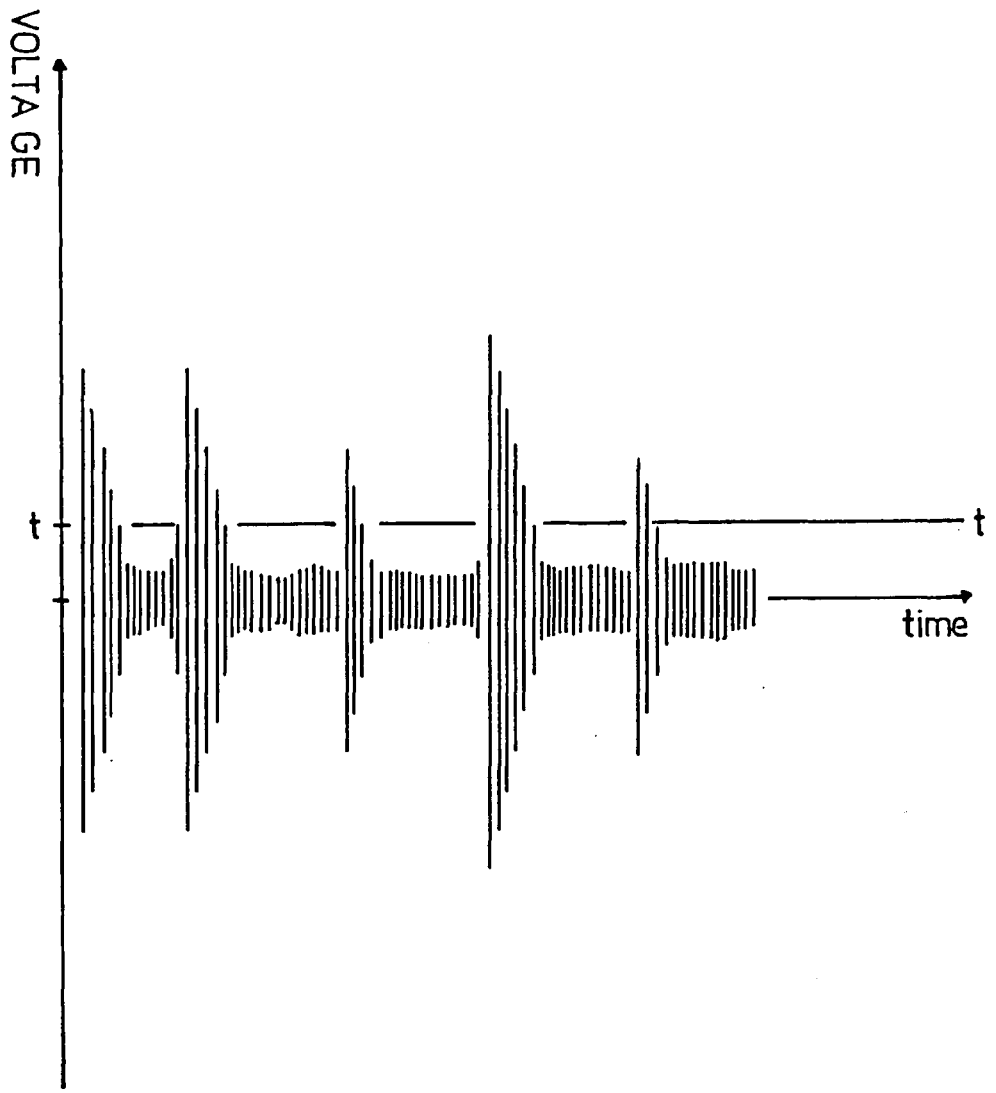

FIGURE 3.3A
Typical voltage output.

FIGURE 3.3B

Single processing techniques.

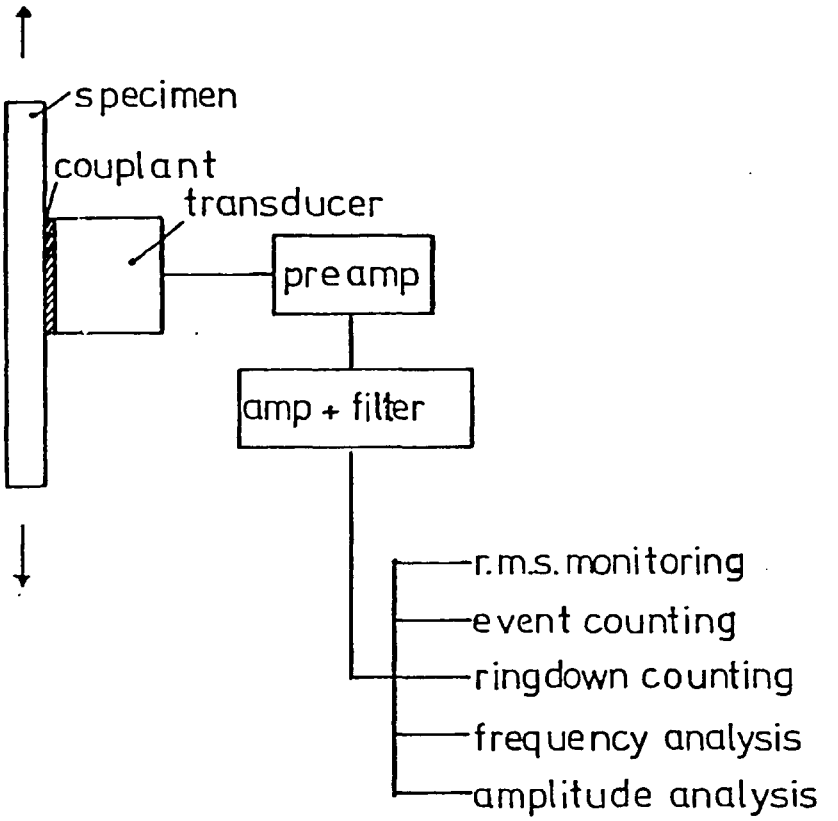

FIGURE 3·3C Working back from an idealised cumulative-log plot.

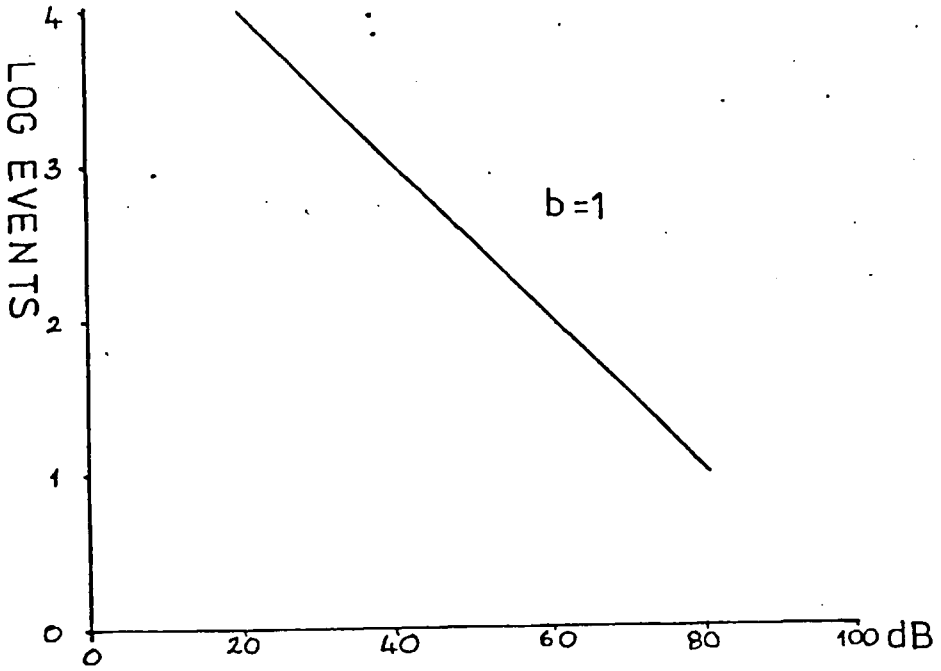

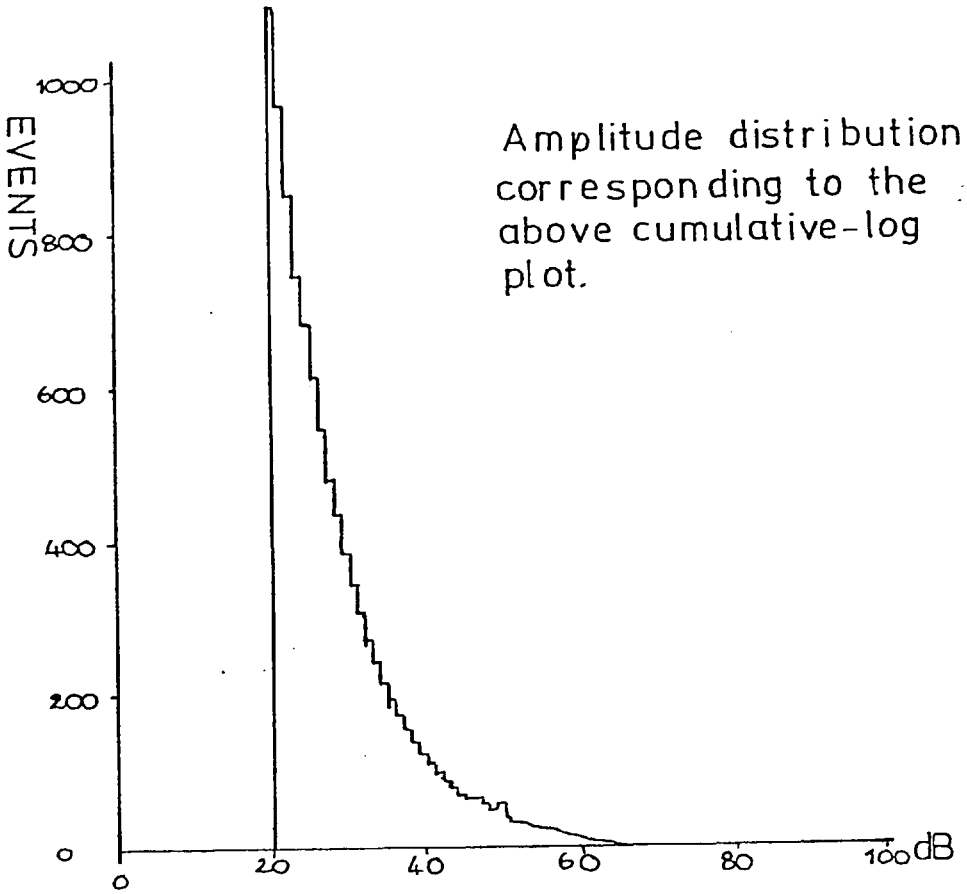

Amplitude distribution corresponding to the above cumulative-log plot.

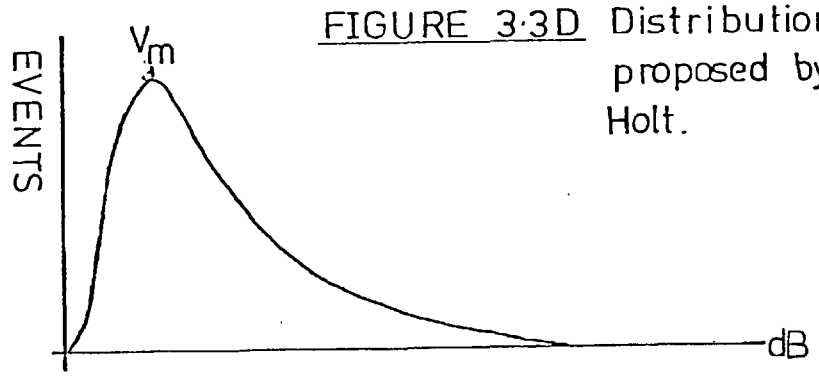

FIGURE 3·3D Distribution proposed by Holt.

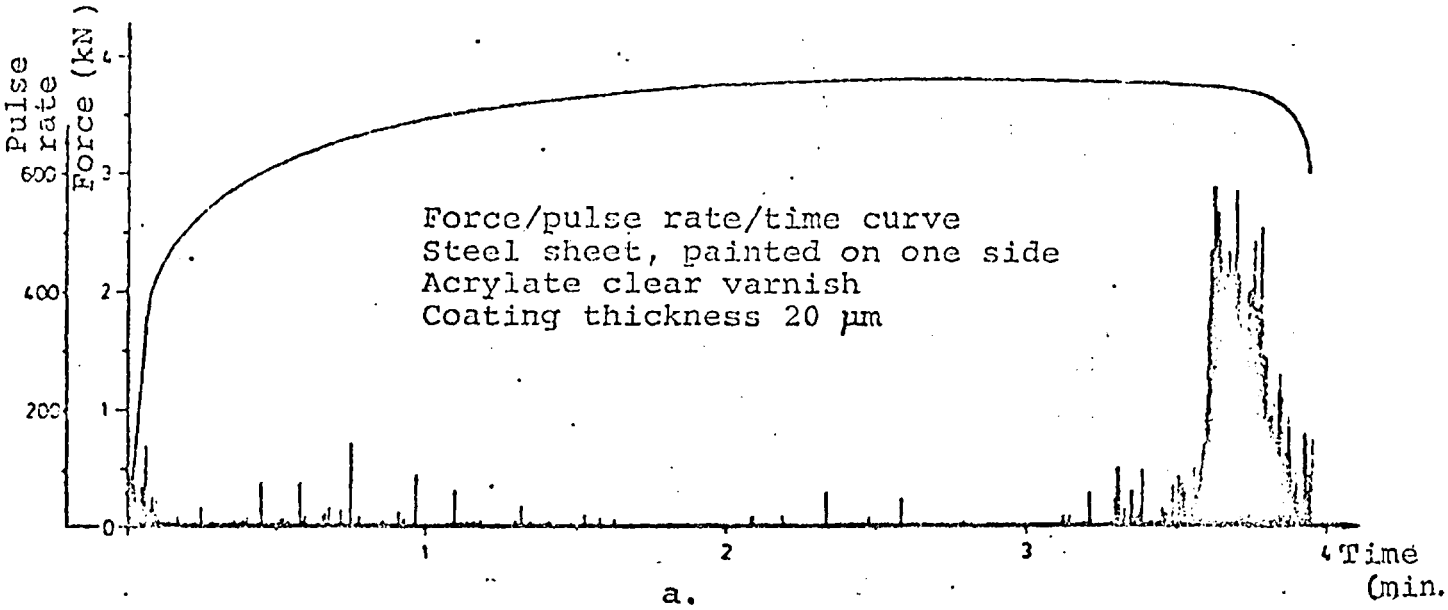

a.

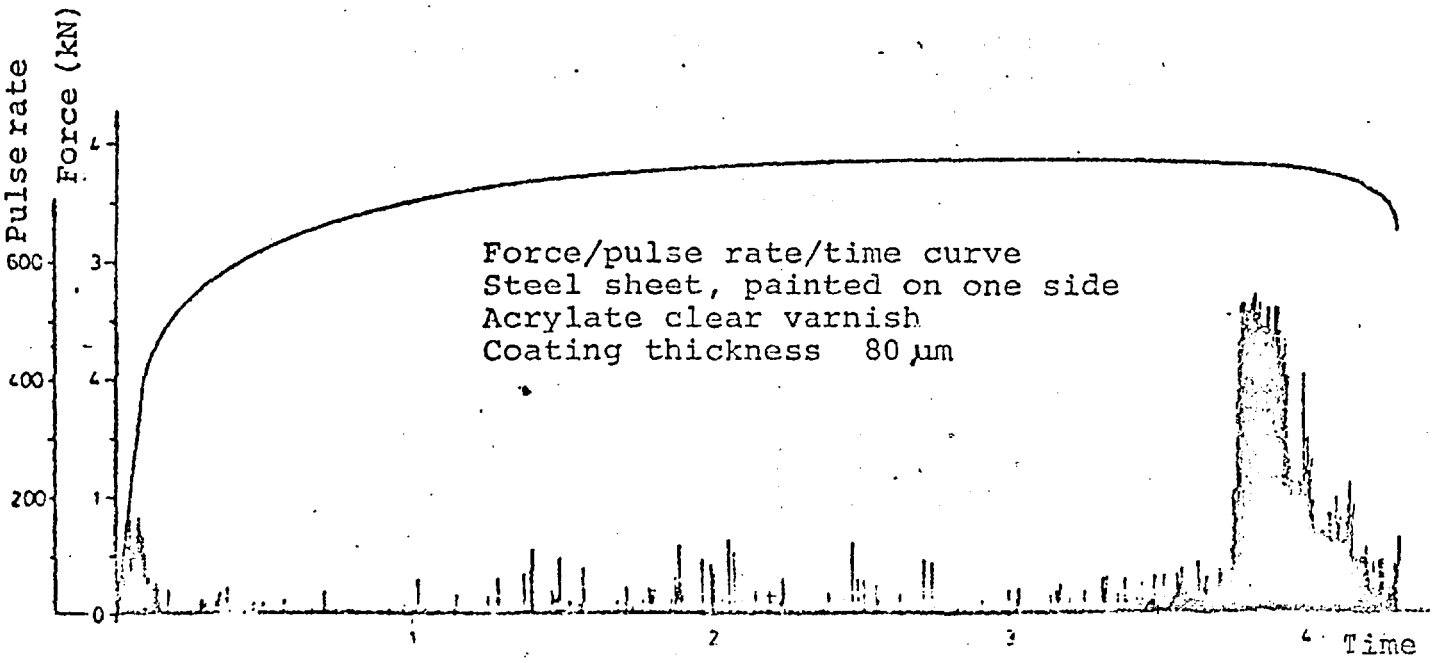

b.

AEA on painted standard steel rods with different paint thickness. Force/pulse rate/time curve.

a) 20 ± 2 µm paint thickness.

b) 80 ± 2 µm paint thickness.

FIGURE 3·4A

Curves obtained by Mosle to determine the effect of coating thickness.

Chapter 4. Materials and experimental.

4.1 Materials.

Mild steel panels measuring 101.6mm by 152.4mm by 0.7mm were treated as shown in figure 4.1A. The steel was ~ 0.2% C and ~ 0.08% Mn by weight and was phosphated by the Ford Motor Company, using the Granodine 16S system, then rinsed in Deoxylyte 76. The electrocoat primers were applied at the Imperial Chemical Industries Paints Division Laboratory, an anodic electrocoat to a thickness of 30μm and a cathodic electrocoat (designated cathodic 1) to a thickness of 20μm. The panels were phosphated and electrocoated on both sides, but further coats (an oil free alkyd resin surfacer coat, and a melamine formaldehyde thermosetting resin topcoat) were applied on one side only. To ease the comparison between specimens, the appropriate side of the specimen was ground down to the steel (using water lubricated silicon grinding papers) for a number of tests. These tests shall be descibed as coated on one side only.

At each stage in the preparation process several panels were put aside for testing and, for brevity, these will be designated by letters, as shown in table 4.1A, a fold out copy of which is attached to the final page of this work. Some panels were phosphated and given an alternative cathodic electrocoat, designated cathodic 2, to a thickness of 16μm, but no further coats. Several panels were not phosphated but an anodic or

TABLE 4.1A.

SYMBOL	SPECIMEN
S	Steel
S/P(R)	Steel with a phosphate coat (rinsed)
S/P	Steel with a phosphate coat (unrinsed)
S/P(R)/A	Steel with a rinsed phosphate & anodic electrocoat
S/P/A	Steel with an unrinsed phosphate & anodic electrocoat
S/P(R)/C1	Steel with a rinsed phosphate & cathodic 1 "
S/P/C1	Steel with an unrinsed phosphate & cathodic 1 "
S/P(R)/C2	Steel with a rinsed phosphate & cathodic 2 "
S/P/C2	Steel with an unrinsed phosphate & cathodic 2 "
S/A	Steel with anodic electrocoat applied directly
S/C2	Steel with cathodic 2 electrocoat applied directly
F/S A(R)	Steel with a rinsed phosphate & anodic electrocoat, with surfacer and topcoat on one side
F/S A	Steel with an unrinsed phosphate & anodic electrocoat with surfacer and topcoat on one side
F/S C1(R)	Steel with a rinsed phosphate & cathodic 1 coat with surfacer and topcoat on one side
F/S C1	Steel with an unrinsed phosphate & cathodic 1 coat with surfacer and topcoat on one side
Systems with the coating only on one side.	
S/P(R)/A(1)	Steel with a rinsed phosphate & anodic electrocoat
S/P/A(1)	Steel with an unrinsed phosphate & anodic electrocoat
S/P(R)/C1(1)	Steel with a rinsed phosphate & cathodic 1 "
S/P/C1(1)	Steel with an unrinsed phosphate & cathodic 1 "
S/P(R)/A/SUR(1)	Steel with a rinsed phosphate, anodic electrocoat and surfacer
S/P/A/SUR(1)	Steel with an unrinsed phosphate, anodic electrocoat and surfacer
S/P(R)/C1/SUR(1)	Steel with a rinsed phosphate, cathodic 1 electrocoat and surfacer
S/P/C1/SUR(1)	Steel with an unrinsed phosphate, cathodic 1 electrocoat and surfacer
F/S A(R)(1)	Steel with a rinsed phosphate, anodic electrocoat surfacer and topcoat
F/S A(1)	Steel with an unrinsed phosphate, anodic electrocoat surfacer and topcoat
F/S C1(R)(1)	Steel with a rinsed phosphate, cathodic 1 electrocoat surfacer and topcoat
F/S C1(1)	Steel with an unrinsed phosphate, cathodic 1 electrocoat, surfacer and topcoat

F/S - full system
On photographs the topcoat is designated TC.

TABLE 4.1B

SYMBOL	SPECIMEN
1	Granodine 902
1/A	Granodine 902 with anodic electrocoat
1/C2	Granodine 902 with cathodic 2 electrocoat
2	Granodine 2500
2/A	Granodine 2500 with anodic electrocoat
2/C2	Granodine 2500 with cathodic 2 electrocoat
3	Granodine 2000
3/A	Granodine 2000 with anodic electrocoat
3/C2	Granodine 2000 with cathodic 2 electrocoat
4	Granodine 16

cathodic 2 electrocoat applied directly to the steel, again with no further coats. These are also shown on table 4.1A. The exact formulations of the paint coats are not given due to industrial secrecy.

Another series of tests used various phosphates with anodic or cathodic 2 electrocoats. These are given in table 4.1B. The various phosphates are all zinc phosphates, but of various coating weights. G902, G2500, G2000 and G16 have coating weights of 1.8,1.9,2.0 and 2.3gm^{-2} respectively. The G16S phosphate,above has a coating weight of 2.6gm^{-2}. Conventional tests, carried out by I.C.I. paints division indicate that Granodine 16 gives similar corrosion resistance to Granodine 16S, that Granodine 902 is similar to Granodine 2000, and that Granodine 2500 gives a coat with very little resistance.

4.2 Experimental proceedure.

4.2.1 Tensile testing.

The painted panels were cut, using a guillotine, into tensile specimens with dimensions 152mm by 13mm by 0.7mm, and were stored in a dessicator in the dark. For tensile testing the specimens were cleaned with methanol then held in Instron tensile testing machine friction grips to give a gauge length of 80mm. The tests were performed at room temperature ($23\mp3^{o}C$) and at a relative humidity of $40\mp10\%$, with a strain rate of $4 \times 10^{-4} sec^{-1}$.

The acoustic emission was detected and analysed using the system shown in figure 4.2A. The transducer was P.Z.T. with a

resonant frequency of 150kHz. (Dunegan Endevco D140 BDE). This was coupled to the specimen through a thin layer (~0·2 mm) of vacuum grease and held in place with a constant load spring clip. P.V.C. tape was used to prevent the clip earthing the transducer to the specimen.

The transducer output was amplified by a Tek 105 preamplifier with a nominal gain of 40dB, then fed into a Tek 105 totaliser, to record the ringdown counts, and a Dunegan Endevco distribution analyser (920 and 921 units) to monitor the events and amplitude distribution. The outputs were recorded on an Omniscribe chart recorder, and the amplitude distibutions at the end of the tests on a 25000 A4 Bryans XY recorder. In some cases the amplitude distributions were recorded at pre-failure strains. A Telequipment D83 oscilloscope was incorporated into the equipment to allow the transducer output to be viewed directly. The gain of the Tek was 93dB and the threshold of the Dunegan Endevco equipment was 24dB for all tests.

4.2.2 Watersoaking tests.

Painted strips (152mm by 13mm by 0.7mm) were immersed in distilled water at 40∓3°C for 96 hours (as recommended by S.M.M.T. 1956). As the strips were cut by guillotining it was necessary to prevent water entering the interface along the edge. Initially this was done by painting with chlorinated rubber paint, but this was found to contribute to the acoustic emission and was difficult to remove. Instead a thin layer of Vaseline was applied along the edge, which was removed with methanol prior to

testing. Surplus water was removed by wiping with a tissue. The specimens were tensile tested, as described above, within ten minutes of their removal from the water bath.

4.2.3 Other tests.

Several conventional tests have been performed on the paint films.

Glass transition temperatures were determined by measuring the hardness at a series of temperatures. This was done by placing a $2cm^2$ piece of painted steel plate on a stage which could be heated. At a series of temperatures from 5 to 90°C a loaded needle was allowed to indent the paint film and the penetration depth measured. These depths were of the order of 3µm (Monk and Wright,1965).

A comparison of the adhesion of the paints was made using a cross hatch technique. A grid of ten lines 0.5mm apart was scored through the paint, Sellotape was attached and then pulled off rapidly. The damage sustained by the various paints during the test gave a measure of the adhesion.

The times for the paint films to dry after immersion were measured using a capacitance technique, as described in section 2.4.2. The paint films were immersed in distilled water at room temperature for 48 hours. On removal surplus water was wiped off and the capacitance of the paint measured at 5, 60 and 120 minutes after soaking (sometimes more frequently) with the sample being stored in a dessicator between measurements. The time to dry was then determined by extrapolating to the capacitance of a

paint film which had not been immersed.

4.2.4 Photography and microstructure.

Several paint specimens were photographed during tensile testing. This was done using a cold flashlight and a Leica camera.

The microstructure of the coatings were examined in a Cambridge Stereoscan 600 scanning electron microscope. To study the specimens in cross section, specimens were pulled to various strains and then mounted in araldite, MY753 resin and HY956 hardener, in the proportion of 4 to 1 by weight. The whole was then slit into sections perpendicular to the tensile axis, using a carborundum blade. Several sections were slit parallel to the tensile axis. The slit sections were remounted to facilitate grinding and polishing. They were polished on a low nap cloth, using Hyprez lapping fluid and diamond paste to 1μm.

FIGURE 4.1A

Steel treatment. At each stage several panels. were put aside for testing.

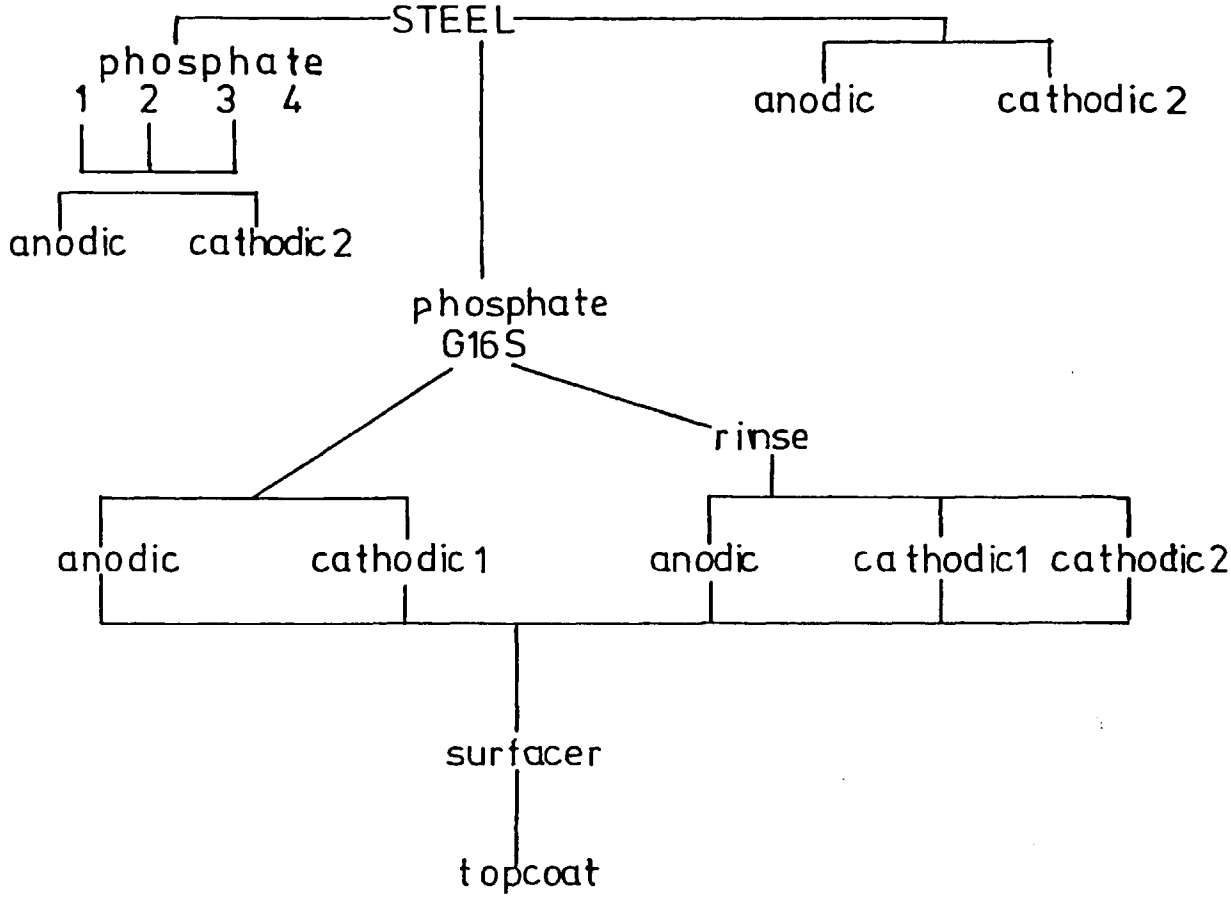

Chapter 5. Results.

5.1 Mechanical properties of the steel.

Most of the specimens were on a substrate of nominally the same steel. There was, however, some variability in its mechanical properties. Typically the 0.2% proof stress was $0{\cdot}2 \rightarrow 0{\cdot}251 GNm^{-2}$, the U.T.S. was $\cdot 23 \rightarrow \cdot 31 GNm^{-2}$ and the %strain to failure 36 → 56%.

An interesting feature of the results was that, although the uncoated steel showed no Luders region during testing, once a coating was applied a distinct Luders region was observed with prominant bands. If the coating was ground off then the steel substrate still gave Luders bands. An uncoated specimen of the steel that had been aged at the coating temperature (of ~ 200°C) for the coating time (of ~ 15min) was found to show no Luders region on testing.

Several of the specimens, namely the various phosphates and S/A and S/C2, had a steel substrate from a different batch, as mentioned in section 4.1. This showed no Luders bands at any time.

5.2 Reproducibility of the acoustic emission.

Trends in the acoustic emission with strain were quite reproducible, with the peaks in the acoustic emission occurring at

strains which were generally repeatable to ~ ∓5%strain.

Although the trends were repeatable, the numbers of events and ringdown counts were less so, often ∓30% and sometimes ∓50% with the reproducibility of the tests after the specimens had been soaked being particuarly bad. For clarity the ringdown count rate vs. strain curves shown are those of typical specimens, as are the amplitude distributions. However the events vs. strain curves give an indication of the scatter, as the curves presented are the maximum and minimum for each system; thus the other samples of the system lie within the band shown.

5.3 Acoustic emission from tensile tests on steel, phosphated steel, and electrocoated steel.

The event and ringdown count data are summarised in table 5A, and a graphical representation is given in figure 5.3I.

There is little difference between the rinsed and unrinsed samples of each system, except that the rinsed systems seem to show less scatter, so these will be discussed together.

A. Events.

1) The effect of phosphating and anodic electrocoating.

Figure 5.3A shows the events vs. strain curves for steel, phosphated steel and electrocoated steel. As there are such large differences between the systems the events are plotted on a logarithmic scale.

a) Steel.

This shows far fewer events than any of the other systems, with much of the emission occurring in the first 3% of strain. The steel gave less than a total of 200 events to fracture in each case.

A steel that had the coating ground off gave similar acoustic emission to the untreated steel, but with emission almost exclusively in the Luders region.

b) Phosphated steel.

S/P and S/P(R) gave a large number of events in the first 10% of strain, and then were quiet, giving in total ~ 6000 events to fracture.

c) Electrocoated and phosphated steel.

Systems with an anodic electrocoat, S/P/A and S/P(R)/A gave a large number of events in the first 5% of strain, though less than the same system with no electrocoat (S/P and S/P(R)), then became quiet until just prior to fracture, when there was another burst of events, giving in total ~ 2000 events.

2) The effect of various electrocoats.

Figure 5.3B shows the events vs. strain curves for the various electrocoats that were tested. Again the events are on a logarithmic scale and there is little difference between the rinsed and unrinsed samples.

Unlike the system with an anodic electrocoat, described above, the systems with the addition of the cathodic electrocoats gave more emission to failure than those that were only phosphated.

Systems with the cathodic 2 electrocoat, S/P/C2 and

S/P(R)/C2, gave slightly fewer events in the first 10% of strain than S/P and S/P(R), then continued to rise more slowly to ~ 28% strain when there was a dramatic increase to failure. This gave in total ~ 15,000 events.

With the cathodic 1 electrocoat, S/P/C1 and S/P(R)/C1 the systems gave a very large number of events in the first 5% of strain, many more than any of the other systems. S/P/C1 and S/P(R)/C1 then continued to emit, though less frequently, to fracture, giving in total ~ 40,000 events.

3) The effect of omitting the phosphate.

Figure 5.3C shows the events vs. strain curves for the systems which were electrocoated with no phosphate layer, together with the curves for the same electrocoats with a phosphate layer, which are included for comparison. Again the events are on a logarithmic scale.

With the anodic coat, S/A, there are a large number of events in the first 3% of strain, more than the system with an anodic coat and a phosphate layer (S/P/A) but still less than the system with only a phosphate coat (S/P). After 5% strain the system became quiet, giving ~ 2000 events in total.

The system with the cathodic 2 electrocoat, S/C2, gave about the same number of events as S/P/C2 in the first 10% of strain and then became quiet until just prior to failure when there was another slight increase in the emission rate. In total this gave ~ 5,000 events, fewer than S/P/C2.

It is striking that when no phosphate layer is present the anodic and cathodic 2 electrocoats give similar shapes of curves

and numbers of events.

B. Ringdown counts.

Figures 5.3D and E show the typical ringdown count rate vs. strain curves. In general the peaks in the ringdown count rate occurred at the same strains as the increases in the events, discussed above. It should be noted that the ringdown count data are not all plotted on the same scale. For all systems the strain at failure is indicated by an arrow on the ringdown count rate curves.

1) The effect of phosphating and anodic electrocoating.

Typical ringdown count rate vs. strain curves for these systems are shown in figure 5.3D.

a) Steel.

This shows a small peak at ~ 7% strain, and a second, higher peak as it fails. The second peak is not expected from the events vs. strain data of figure 5.3A. The steel gives, in total ~ 1,500 ringdown counts to failure.

b) Phosphated steel.

S/P and S/P(R) each show a single broad peak centred at about 7% strain and extending from 0 → 20% strain. They gave ~ 15,000 ringdown counts in total, considerably more than the non-phosphated steel.

c) Phosphated steel with an anodic electrocoat.

Systems with an anodic electrocoat, S/P/A and S/P(R)/A, show two quite narrow peaks, one at low strains (~ 5%) and the second

just prior to failure. In total they gave ~ 150,000 ringdown counts.

2) The effect of various electrocoats.

Figure 5.3E shows typical ringdown count vs. strain curves for the systems with various electrocoats.

Systems with a cathodic 2 electrocoat, S/P/C2 and S/P(R)/C2, gave a small peak at low strains (0 → 8%), then a larger broad peak at high strains, giving ~ 1,000,000 ringdown counts in total, many more than the system with an anodic electrocoat.

Systems with a cathodic 1 electrocoat, S/P/C1 and S/P(R)/C1, gave about the same total number of ringdown counts as those with the cathodic 2 coat (~ 1,000,000) but in this case the counts appear ed as a narrow peak at low strains, followed by a very broad (10 → 40% strain) peak, the second giving a greater number of ringdown counts than the first.

3) The effect of omitting the phosphate layer.

The typical ringdown count rate vs. strain curves for these systems are also shown in figure 5.3E.

The system with an anodic electrocoat, S/A, has a narrow peak at low strains, and a second peak on failure. This is similar to the same system with a phosphate coat (S/P/A) as described above. S/A, however, gave fewer counts, 100,000 to failure.

The system with a cathodic 2 electrocoat, S/C2, has a narrow peak at low strains, then a second, smaller peak as it fails. This is similar to the behaviour of the system with an anodic

electrocoat (S/A), but gives many more counts ~ 400,000 in total. This is considerably fewer than the cathodic 2 electrocoat coated onto phosphate, the difference being mainly that there are fewer counts at high strains for S/C2.

C. Amplitude distribution for the whole test.

1) The effect of phosphating and anodic electrocoating.

Typical amplitude distributions are shown in figure 5.3F. These have various scales for events.

a) Steel.

With so few events the amplitude distribution is difficult to interpret but appears to be a single peak centred at about 26dB.

b) Phosphated steel.

Both S/P and S/P(R) have single peaks at about 26dB, and very few events with amplitudes above 45dB.

c) Phosphated and electrocoated steel.

Systems with an anodic electrocoat, S/P/A and S/P(R)/A, give a series of three or four peaks of decreasing intensities. The 26dB peak appears to rise more slowly than when only a phosphate layer is present, and there are events to very much higher amplitudes, ie. to 75dB, in contrast to 45dB for S/P and S/P(R).

2) The effect of various electrocoats.

Typical amplitude distributions are shown in figure 5.3G. Again the scale for events differs between specimens.

Systems with a cathodic electrocoat (S/P/C1, S/P(R)/C1,

S/P/C2 and S/P(R)/C2) show three or four peaks, in similar positions to those seen when an anodic electrocoat is present. Again there are events at higher amplitudes, ie. up to 70dB. In the cathodic 1 coat the 33dB peak appears to be higher than the other peaks.

3) The effect of omitting the phosphate layer.

Typical amplitude distributions are shown in figure 5.3H.

Both the anodic, S/A, and the cathodic, S/C2, electrocoated systems have three or four peaks of decreasing intensities, very similar to S/P/A and S/P/C2. With all the events having amplitudes below ~ 70dB.

5.4. Acoustic emission during tensile testing of systems coated on one side only.

As discussed in section 4.1, specimens were electrocoated on both sides but the surfacer and topcoat were applied to only one side. For this series of tests the additional electrocoat and phosphate layer were removed from one side to prevent extraneous effects in the comparison of systems as further coats were added.

As in section 5.3, there was little difference between the rinsed and unrinsed specimens, as before they will be discussed together. The ringdown count rate and event data for these systems are summarised in table 5A and figures 5.4G and H.

A. Events.

The maximum and minimum event vs. strain curves are shown in

figures 5.4A and B. The events are on a logarithmic scale.

1) The effect of additional coats on a system with an anodic electrocoat.

a) Phosphated steel with an anodic electrocoat.

S/P/A(1) and S/P(R)/A(1) gave a large number of events in the first 5% of strain and then became quiet until just prior to failure, giving in total ~ 2000 events, the same as previously reported for the system with both sides coated, S/P/A.

b) Phosphated steel with an anodic electrocoat and a surfacer.

S/P/A/SUR(1) and S/P(R)/A/SUR(1) also gave a large number of events in the first 5% of strain, then became quiet until just prior to failure, giving ~ 400 events in total, considerably quieter than the system with no surfacer, although the shape of the curves are similar.

c) Full system with an anodic electrocoat.

In a similar manner to S/P/A(1) and S/P(R)/A/SUR(1), the full systems with an anodic electrocoat, F/S A(1) and F/S A(R)(1) gave a large number of events in the first 5% of strain, became quiet and then began emitting again at ~ 40% strain. This gives a total of ~ 200 events, quieter than the system with no topcoat.

2) The effect of additional coats on a system with a cathodic 1 electrocoat.

The differences as further coats are added to a cathodic 1 electrocoat are very much greater than the differences when the electrocoat was anodic, described in the previous section. The

events vs. strain curves are shown in figure 5.4B.

d) Phosphated steel with a cathodic 1 electrocoat.

S/P/C1(1) gave a large number of events to about 3% strain then continued to rise, but more slowly to fracture, giving ~ 20,000 events in total.

S/P(R)/C1(1) behaved in a similar manner, but giving ~ 30,000 events. This behaviour is similar to that of the system coated on both sides (section 5.3) although there are fewer events.

e) Phosphated steel with a cathodic 1 electrocoat and a surfacer.

S/P/C1/SUR(1) and S/P(R)/C1/SUR(1) gave a large number of events in the first 8% of strain, then became quiet, increasing to failure from about 36% strain. These gave ~ 1,200 events in total, considerably quieter than the same system without a surfacer.

f) Full systems with a cathodic 1 electrocoat.

F/S C1(1) and F/S C1(R)(1) gave a large number of events to ~ 3% strain, then became quiet, increasing to failure from ~ 28% strain and giving ~ 600 events in total. This is quieter than the system without a topcoat, but gave more events than the full system with an anodic electrocoat.

B. Ringdown count rate.

Typical ringdown count rate vs. strain curves are shown in figures 5.4C and D. The scale for ringdown counts varies between specimens. The strains at which the specimen failed is indicated by an arrow on these curves. Again there is generally good

agreement between emission rate as measured by event and ringdown counting.

1) The effect of additional coats on the system with an anodic electrocoat.

The ringdown count rate vs. strain curves are shown in figure 5.4C.

a) Phosphated steel with an anodic electrocoat.

S/P/A(1) and S/P(R)/A(1) each gave two fairly broad peaks (each covering a range of ~ 10% strain) the first at low strains and the second just prior to failure. This gave, in total, ~ 100,000 ringdown counts, again similar to the system with a coat on both sides (section 5.3).

b)Phosphated steel with an anodic electrcoat and a surfacer.

S/P/A/SUR(1) and S/P(R)/A/SUR(1) showed two narrow peaks. The first at ~ 5% strain and the second, higher peak just prior to failure. Both peaks were associated with less counts than the corresponding peaks in S/P/A and S/P(R)/A and gave ~ 4000 ringdown counts.

c) Full system with an anodic electrocoat.

F/S A(1) and F/S A(R)(1) gave quite broad peaks at low strains (~ 0 → 10% strain). F/S A(1) gave a second, higher peak at failure, whereas F/S A(R)(1) gave a second peak at ~ 35% strain. In total both gave ~ 50,000 ringdown counts, considerably more than the same system without a topcoat, but less than when only an electrocoat was present.

2) The effect of additional coats on a system with a cathodic 1

electrocoat.

As with the events data there were more variations as coats were added to the cathodic 1 than when added to the anodic electrocoat. The ringdown count vs. strain curves are shown in figure 5.4D.

d) Phosphated steel with a cathodic 1 electrocoat.

S/P/C1(1) gave a quite broad peak at low strains followed by a peak extending from 10% strain to failure. This gave in total ~ 500,000 ringdown counts, less counts than when the coating was present on both sides (section 5.3) but similar in all other respects.

S/P(R)/C1(1), however, gave only one broad peak (0 → 30% strain) with ~ 1,000,000 ringdown counts in total. Although this was the same number of counts as when both sides were coated the strain dependance was different to S/P(R)/C1 which exhibited two peaks (figure 5.3E).

e) Phosphated steel with a cathodic 1 electrocoat and a surfacer.

S/P/C1/SUR(1) and S/P(R)/C1/SUR(1) each gave a fairly broad peak at low strains and a second broad peak, representing many more ringdown counts, at ~ 35% strain. In total these gave ~ 150,000 counts, considerably less than the system without a surfacer, but more than the anodic electrocoat with a surfacer (S/P/A/SUR(1)).

f) Full system with a cathodic 1 electrocoat.

F/S C1(1) and F/S C1(R)(1) also gave quite broad peaks at low strains. Each had a second, narrow peak representing more

ringdown counts than the first, at ~ 30% strain in F/S C1(1) and ~ 25% strain in F/S C1(R)(1). In total each gave ~ 200,000 ringdown counts, less than the system with only an electrocoat, but more than the same system without a topcoat. More, also, than the full system with an anodic electrocoat (F/S A(1)).

C. Amplitude distributions for the whole test.

These are shown in figures 5.4E and F. The scale for events is different for the various specimens.

1) The effect of additional coats on a system with an anodic electrocoat.

These distributions are shown in figure 5.4E.

a) Phosphated steel with an anodic electrocoat.

S/P/A(1) and S/P(R)/A(1) gave a series of peaks of decreasing intensities, very similar to S/P/A of section 5.3, and amplitudes of up to ~ 80dB.

b) Phosphated steel with an anodic electrocoat and a surfacer.

S/P/A/SUR(1) and S/P(R)/A/SUR(1) each gave a series of peaks, the first with a much greater intensity than the others. Again events had amplitudes of up to ~ 80dB.

c) Full system with an anodic electrocoat.

F/S A(1) and F/S A(R)(1) gave distributions quite similar to those of the systems with no topcoat, that is there was only one prominent peak, that at about 26dB. In this case the events have amplitudes up to ~ 85dB.

2) The effect of additional coats on a system with a cathodic 1 electrocoat.

These distributions are shown in figure 5.4F.

d) Phosphated steel with a cathodic 1 electrocoat.

S/P/C1(1) and S/P(R)/C1(1) gave a series of three or four peaks with the highest at ~ 36dB and events up to ~ 70dB. This is similar to the system with both sides coated (S/P/C1), except that the third (46dB) peak is very much higher (particularly for S/P(R)/C1(1)).

e) Phosphated steel with a cathodic 1 electrocoat and a surfacer.

S/P/C1/SUR(1) and S/P(R)/C1/SUR(1) gave, in a similar manner to the system with an anodic coat and a surfacer, a 26dB peak very much higher than the others and events up to ~ 80dB. In this case,though, there also appears to be a broad peak centred ~ 60dB from ~ 40 → 80dB.

f) Full systems with a cathodic 1 electrocoat.

F/S C1(1) and F/S C1(R)(1) show a very pronounced peak at ~ 26dB and events up to ~ 100dB. The distributions are similar to the system with an anodic coat (F/S A(1)) but with more higher amplitude events.

5.5 Acoustic emission during tensile testing of specimens coated with the full system on one side and up to the electrocoat on the other.

As in the preceding sections, there was little difference

between the rinsed and unrinsed specimens with the same coatings, so these will be discussed together. The event and ringdown count data are summarised in table 5A and in figure 5.5D.

A. Events.

The events vs. strain curves for these systems are shown in figure 5.5A. The events are on a logarithmic scale.

1) Systems with an anodic electrocoat.

F/S A and F/S A(R) gave a large number of events in the first 5% of strain, then became quiet, with another sharp increase at ~ 30% strain. This gave in total ~ 2,500 events, about the same as S/P/A of section 5.3.

2) Systems with a cathodic 1 electrocoat.

F/S C1 and F/S C1(R) gave a large number of events to ~ 25% strain and then became quiet. This behaviour is quite different to S/P/C1 of section 5.3, resembling more that of F/S C1(1) (section 5.4). In total F/S C1 and F/S C1(R) gave ~ 15,000 events, considerably quieter than S/P/C1, though noisier than F/S C1.

B. Ringdown counts.

The ringdown counts vs. strain curves are shown in figure 5.5B. The peaks in the ringdown count rate curves reflect the increases in events, as described above. The strains at which the specimens failed are marked by arrows on the strain axes. The scale for ringdown counts varies between specimens.

1) Systems with an anodic electrocoat.

F/S A and F/S A(R) each gave a fairly broad peak (0 → 10% strain) at low strains and a second, higher peak at ~ 30% strain. In total they gave ~ 250,000 ringdown counts, more than S/P/A (section 5.3).

2) Systems with a cathodic 1 electrocoat.

F/S C1 and F/S C1(R) each gave a rather small peak at ~ 2% strain and a very broad (10 → 35% strain) and higher second peak. This gave in total ~ 1,000,000 ringdown counts, approximately the same as S/P/C1 of section 5.3, though here the low strain peak represented fewer counts.

C. Amplitude distributions for the whole test.

These are shown in figure 5.5C. The scale for events varies between specimens.

1) Systems with an anodic electrocoat.

F/S A and F/S A(R) gave a series of three or four peaks of decreasing intensities, with events of amplitudes up to ~ 85dB. This is similar to S/P/A of section 5.3, but with events at higher amplitudes.

2) Systems with a cathodic 1 electrocoat.

F/S C1 and F/S C1(R) gave a series of three or four peaks, all of approximately equal heights, with events of amplitudes up to ~ 85dB, higher amplitudes than S/P/C1 of section 5.3.

5.6 .... Acoustic emission during tensile testing of systems after immersion.

The systems tested after immersion were electrocoated on both sides, but the surfacer and topcoat were applied on one side only. As in the previous sections there was little difference between results for rinsed and unrinsed phosphate coats, though there seemed to be less scatter when the specimens had been rinsed. There was one notable exception to this, the full system with the cathodic 1 electrocoat gave very different results when the phosphate was rinsed to when it was left unrinsed. The rinsed and unrinsed results will though, be discussed together. Ringdown count and event data are summarised in table 5A and figure 5.6G.

A. Events.

The events vs. strain curves are shown in figures 5.6A and B. Again the events are on a logarithmic scale.

1) Systems with an anodic electrocoat.

S/P/A and S/P(R)/A gave a large number of events in the first 5% of strain then continued to emit, though more slowly, to fracture. This gave in total ~ 500 events, quieter than the same system when dry (figure 5.3A).

F/S A and F/S A(R) gave a large number of events in the first 2% of strain, then became quieter until ~ 24% strain, when there was a sudden increase in the events. They then became quiet, having given in total ~ 5,000 events. This was more events

than the same system dry (section 5.5) and the second burst of events occurred at lower strains.

2) Systems with a cathodic 1 electrocoat.

S/P/C1 and S/P(R)/C1 gave a large number of events in the first 5% of strain (though less than when dry, section 5.3); they then continued to emit, more slowly to fracture, giving ~ 30,000 events in total. As with the anodic coat, this was quieter than when dry.

For full systems with a cathodic 1 electrocoat there was a dramatic difference between the specimens containing rinsed and unrinsed phosphates. Each gave a large number of events in the first 5% of strain and then became quiet, but F/S C1 gave ~ 13,000 events, about the same as the system when dry, whereas F/S C1(R) gave far fewer events, ~ 6,000, considerably quieter than the dry system.

B. Ringdown count rate.

The ringdon count rate vs. strain curves for these systems are shown in figure 5.6C and D. Peaks in these curves correspond to the increases in the events in figure 5.6A and B. The ringdown count scale differs between specimens and the strain at failure is indicated by an arrow.

1) Systems with an anodic electrocoat.

S/P/A and S/P(R)/A gave two narrow peaks, one at ~ 3% strain and the second, slightly higher at failure. In total this gave ~ 50,000 ringdown counts, fewer than the system when dry.

F/S A and F/S A(R) each gave a peak from ~ 0 + 7% strain and a second, very much higher peak at ~ 20 + 40% strain. This gave in total ~ 400,000 ringdown counts, more than when dry, and with the second peak at slightly lower strains.

2) Systems with a cathodic 1 electrocoat.

S/P/C1 and S/P(R)/C1 gave two peaks. The first at ~ 2% strain and the second, very much bigger ~ 8% + fail. This gave in total ~ 2,000,000 ringdown counts, considerably more than the same system when dry, and with the second peak at very much lower strains.

F/S C1 and F/S C1(R) each had only one, broad, peak at ~ 0 + 20% strain, as opposed to the dry where there were two distinct peaks. In total F/S C1 gave ~ 1,000,000 counts, the same as when dry, whereas F/S C1(R) was considerably quieter with only ~ 500,000 counts.

C. Amplitude distributions for the whole test.

These are shown in figure 5.6E and F. The scale for events varies between specimens.

1) Systems with an anodic electrocoat.

All the amplitude distributions show a series of three or four peaks, with the first two (26 and 33dB) being higher than the others. When no surfacer or topcoat was present, S/P/A and S/P(R)/A, there were very few events above ~ 55dB. F/S A and F/S A(R), however had events up to ~ 85dB. Systems S/P/A and S/P(R)/A differ from the dry in having fewer events of high

amplitude, and F/S A and F/S A(R) differ from the dry in having higher second and third peaks (33 and 46dB)

2) Systems with a cathodic 1 electrocoat.

All show a series of three or four peaks and events with amplitudes up to ~ 80dB. For S/P/Cl and S/P(R)/Cl the second and third (33 and 46dB) peaks are slightly higher than the other peaks. They differ from the dry in having higher third and fourth (54dB) peaks. F/S Cl and F/S Cl(R) have the 26dB peak as the highest, this is different to the dry , where the peaks are all about the same height.

5.7.... Acoustic emission during tensile testing of systems with various phosphate coats.

The various phosphate coats are described in table 4.1B. The phosphate used in the preceding work will be refered to as G16S. The data for events and ringdown counts for these systems is summarised in table 5A and figure 5.7J.

A... Events.

Events vs. strain curves are shown in figures 5.7A,B and C. The numbers of events are fairly similar in figures 5.7A and B, so it has been possible to keep a normal scale in these instances, unlike the preceding events vs. strain curves, where the events were plotted on a logarithmic scale.

1) Steel with various phosphate coats.

All the phosphates studied gave most of the events in the first 10% of strain, then became quiet, though phosphate 4 seemed in one case to have continued to emit slightly. Phosphate 1 was the quietest, giving only ~ 200 events in total, about the same as the untreated steel (section 5.3). Phosphate 2 gave ~ 1,500 events and phosphate 4 ~ 2,000 events. Phosphate 3 gave ~ 5,000 events. The G16S phosphate (section 5.3) showed similar behaviour to phosphate 3, and gave ~ 6,000 events in total.

2) Phosphated steel with an anodic electrocoat.

All the phosphates gave a similar shape of curve when an anodic electrocoat was present. This was, as described in section 5.3, with a large number of events in the first 5% of strain, then becoming quiet until just prior to failure.

1/A was the quietest, giving ~ 700 events in total, 2/A and 3/A were approximately the same, giving ~ 1,500 events and G16S/A (S/P/A, above) gave the most events, ~ 2,000.

3) Phosphated steel with a cathodic 2 electrocoat.

All these gave very many more events than the systems with an anodic electrocoat. In all cases a large number of events were monitored in the first 5% of strain, followed by a period of less activity. There was, in each system, a further rapid increase in events before failure. This occurred just before failure for 1/C2, at ~ 30% strain for 2/C2 and at ~ 22% strain for 3/C2. For G16S/C2 (S/P/C2) this occurred at ~ 35% strain.

As was the case when an anodic electrocoat was present, the

system with phosphate 1, 1/C2, was the quietest, giving ~ 3,000 events in total. 2/C2 gave ~ 5,000 and 3/C2 ~ 11,000 events. G16S/C2 gave the most events, ~ 15,000.

B. Ringdown count rate.

Typical ringdown count rate vs. strain curves are shown in figures 5.7D and E. Curves for the G16S phosphate are repeated for comparison. In general peaks in the ringdown count rate reflect increases in the events. The scale for ringdown counts varies between specimens, and the strain at failure is indicated by an arrow.

1) Steel with a phosphate coat.

The ringdown count rate vs. strain curves for these systems are shown in figure 5.7D.

In all the systems there is a peak at low strains centred at ~ 5% strain and ranging from ~ 0 → 20% strain. These are in direct agreement with the events vs. strain curves, but there are also further peaks, at failure for phosphates 1 and 4, and a very small peak at ~ 20% strain for phosphate 2 (this 20% peak was present for all the samples of phosphate 2 tested).

Phosphate 1 was the quietest, giving ~ 5,000 counts to failure. Phosphates 2 and 4 gave ~ 10,000 counts, G16S gave ~ 15,000 counts and phosphate 3 gave 20,000 counts.

2) Phosphated steel with an anodic electrocoat.

The ringdown count rate vs. strain curves are shown in figure 5.7E. All the systems behaved in a similar manner, with a

peak at low strains and a second, higher peak at failure. For 1/A and G16/A the first peak was very narrow (extending ~ 2% strain), for 2/A it ranged 0 → 10% strain and for 3/A from 0 → 15% strain.

As before the system with phosphate 1 (1/A) was the quietest giving ~ 20,000 counts; 2/A and 3/A gave ~ 100,000 counts and G16S/A gave ~ 150,000 ringdown counts.

3) Phosphated steel with a cathodic 2 electrocoat.

Typical ringdown count vs. strain curves are shown in figure 5.7E.

Again each system showed two peaks, one at low strains, which was narrow (extending over ~ 4% strain) for 1/C2 and 3/C2 and broader (0 → 10% strain) for 2/C2 and G16S/C2. The second peak was higher in all cases but the strain at which it occurred depended on the phosphate. For 1/C2 and G16S/C2 the second peak was at ~ 30 → 40% strain, for 2/C2 ~ 30 → 35% strain and for 3/C2 ~ 20 → 30% strain.

In this case 2/C2 and 3/C2 gave ~ 100,000 ringdown counts in total, 1/C2 gave more, ~ 200,000 and G16S/C2 gave ~ 1,000,000 counts.

C. Amplitude distributions for the whole test.

Typical amplitude distributions are shown in figures 5.7G, H and I. Again the scale for events varies between specimens.

1) Steel with phosphate coats.

The distributions are shown in figure 5.7G. All the systems appear to have one peak centred at ~ 26dB and possibly a second

at ~ 33dB. In no case are there many events above ~ 40dB, except possibly phosphates 3 and G16S which have few events above ~ 45dB.

2) Phosphated steel with an anodic electrocoat.

Typical distributions are shown in figure 5.7H.

1/A gave a very high peak at ~ 26dB, then possibly one or two other peaks, with few events above ~ 60dB.

2/A, 3/A and G16S/A gave a series of three or four peaks, with the intensities of the first two very much higher than the others. 2/A gave few events above ~ 65dB and 3/A and G16S/A few above ~ 75dB.

3) Phosphated steel with a cathodic 2 electrocoat.

Typical amplitude distributions are shown in figure 5.7I. All the systems gave a series of three or four peaks of decreasing intensities and events up to ~ 80dB, except 1/C2 which gave few events above ~ 65dB.

5.8 Amplitude distributions at pre-failure strains for several systems.

As described in the preceding sections, many of the systems studied showed two distinct regions of acoustic emission activity, which appear as two peaks in the ringdown count rate vs. strain curves. In order to investigate this further the amplitude distribution was recorded during the test, encompassing the first area of high activity, for several

systems.

1) Phosphated steel.

Figure 5.8A shows the amplitude distribution at failure for S/P. The shaded area represents the distribution monitored at 15% strain. The two distributions do not differ significantly.

2) Phosphated and electrocoated steel.

Typical amplitude distributions at failure for S/P/A and S/P(R)/A are shown in figure 5.8B, with the distribution at ~ 8% strain shaded. At 8% strain the events are mainly about 26dB and above 60dB. Between 8% strain and failure there are very few events above 60dB and a further distinct peak, at 33dB appears.

Figure 5.8C shows typical amplitude distributions for S/P/C1 and S/P(R)/C1, recorded at failure. The shaded regions represent the distribution at 10% strain for S/P/C1 and at 5% strain for S/P(R)/C1. The low strain distributions are very similar to those at failure, with three peaks, the second appearing to be the highest. There are however, few events with amplitudes above 50dB occuring at higher strains.

The phosphated and electrocoated steels, coated on one side only, showed similar trends to those described here.

3) Phosphated steel with an electrocoat and a surfacer.

Figure 5.8D shows typical amplitude distributions at failure for S/P/A/SUR(1) and S/P(R)/A/SUR(1) with the distributions at 10% strain shaded. In both cases at 10% strain there is a peak at 26dB and some high amplitude events. Between 10% strain and

failure a large number of events occur at 26dB, and some at 33dB.

Typical amplitude distributions at failure for S/P/C1/SUR(1) and S/P(R)/C1/SUR(1) are also shown in figure 5.8D, with the distributions at 10% strain shaded. In both cases the 10% strain distribution shows a distinct peak at 26dB and a second, broader peak at ~ 70dB. Between 10% strain and failure the events had amplitudes mainly between 26 and 70dB.

4) Full systems.

Figure 5.8E shows typical amplitude distributions from the whole test, with those taken at 15 and 10% strain shaded for F/S A(1) and F/S A(R)(1) respectively. At low strains there is a peak at about 26dB and several high amplitude events. There is little difference between these distributions and those at failure.

Figure 5.8E also shows typical amplitude distributions at failure for F/S C1(1) and F/S C1(R)(1), with the distributions at ~ 10% shaded. Again the low strain distribution shows a peak at ~ 26dB, but few other events with amplitudes below ~ 70dB. Between 10% strain and failure the events are mainly below 70dB.

5.9 Pulse width measurements of the acoustic emission during tensile testing.

For several tests it was possible to include in the acoustic emission equipment a Dunegan Endevco 922 unit, which was used to monitor the duration of each acoustic emission event. The durations varied between 0 and 30 μs. As the dead time of the

system used was set at 1000μs the pulses fell well within the envelope.

5.10 Glass transition temperatures of the paint coats.

The indentation depth vs. temperature curves for the electrocoats and topcoat are shown in figure 5.10A. The glass transition temperature is taken as the temperature where the slope of the curve changes, and is thus ~ 40°C for the anodic electrocoat, ~ 70°C for the cathodic 1 electrocoat and ~ 45°C for the topcoat. The cathodic 2 electrocoat had a glass transition temperature of greater than 90°C, too high to be measured with the apparatus available. Thus, at room temperature, at which the acoustic emission tests were performed, the coatings can be classed, in order of brittleness:

C2 > C1 > TC > A

Tests were also carried out on coatsfollowing their immersion in water. Specimens were taken from the waterbath, surface water removed and they were placed in the apparatus. The results are represented by the shaded symbols on figure 5.10A. The apparatus was humidity controlled and employed a heated stage which meant that the water was quickly lost, hence the lack of wet results at higher temperatures. The results indicated only that water acted to plasticise the anodic coat, but had little effect on either of the cathodic coats.

5.11 Water content of the paint films as they dry after immersion.

Figure 5.11A shows the % of water, by volume, contained in the paint films. The data for the full systems show that F/S A lost the excess water, picked up during the 48 hour soak, within 50 minutes, and that F/S C1 took considerably longer than two hours, the length of the test. Although not as complete, the data for the electrocoats show the same trends, S/P/A losing the water within 50 minutes and S/P/C1 taking very much longer times.

The results also suggest that systems with the cathodic 1 electrocoat took up more water initially than those with the anodic.

5.12 Adhesion of the paint films.

Typical results from the cross hatch tests are shown in figure 5.12A. These demonstrate that the anodic and cathodic 2 electrocoats suffered some loss of adhesion, the cathodic 2 electrocoat suffering adhesion loss in the first 5% of strain similar to that of the anodic coat in the first 10%. The cathodic 1 electrocoat suffered a very great loss of adhesion at low strains, when a phosphate coat was present. The cathodic 2 electrocoat shows slightly worse adhesion loss at ~ 3% strain than does the anodic at ~ 10% strain.

Cross hatch tests of S/A and S/C2 indicated a similar loss of adhesion during the first 3% of strain to S/P/C2.

The technique was not able to detect any adhesion loss, even after ~ 10% strain when a topcoat was present.

Tensile adhesion tests, using araldite to glue the paint to

plates (of dimensions 10mm x 10mm x 80mm) which were then pulled apart in a tensile test, were attempted. Unfortunately, in all cases the araldite failed before the paint coat.

5.13 Observations made during tensile testing.

Typically the specimens failed as shown in figures 5.13A and B. Damage was visible on S/P/C1 and S/P(R)/C1 from ~ 5% strain, on S/P(R)/C2 from ~ 15% strain and on S/P/A and S/P(R)/A only just prior to failure. On the full systems damage was visible from ~ 24% strain on F/S C1 and F/S C1(R) and just prior to failure on F/S A and F/S A(R).

This type of cracking, a diamond shaped area, which comes away and then cracks across, perpendicular to the tensile axis, although not commonly found in paint testing has been observed on other occassions (Strivens,1980).

When photographs were taken regularly throughout a test the specimens were found to give less events than otherwise, though there were no differences visible in the amount of damage occurring.

5.14 Scanning electron microscope and microprobe examination.

The surface of the G16S phosphate is composed of hopeite needles on a phosphophyllite surface, as shown in figure 5.14A. The other types of phosphates studied seem to have a similar type of structure, as can be seen in figure 5.14C. The structure of the phosphophyllite and the size and distribution of the needles

depend on the type of phosphate. A comparison of the phosphates based on this is given in table 5.14A.

Globular particles such as those in figure 5.14C have been seen on several occassions. These are probably rust beginning to form, and have been seen most frequently on the unrinsed phosphate (S/P).

S/P and S/P(R) have been examined at both 5% strain and after failure has occurred. Typical areas after fracture are shown in figure 5.14B, and show that near where the final fracture occurred there are very few needles remaining on the surface, a small distance away from the fracture there are a large number of cracked needles, and at large distances from the fracture the needles appear in tact. Examination of specimens at ~ 5% strain indicated that at low strains there are cracked needles and areas where few needles remain.

The various other phosphates have also been examined after testing, at ~ 10mm from where the final fracture took place, to eliminate any effects due to local necking. Phosphate 3 had very few needles or platelets present, and those remaining were cracked; phosphate 2 had many needles missing, though there were some areas where the coating appeared in tact but with cracked needles and platelets; phosphate 4 had a number of cracked needles attached to the surface and phosphate 1 had several bare areas, but generally appeared better preserved than any of the other phosphates and no cracked needles were seen.

In several cases the electrocoat was removed after testing and the interface was examined using a microprobe. Zinc was detected on both the electrocoat back and, in smaller quantities

TABLE 5.14A

Phosphate	No. needles	Needle'length	Distribution	Phosphophyllite
G16S	many	20-40μm	even	some platelets
G16 (4)	many	~40μm	even	some platelets
G902 (1)	several	20-30μm	even	flat
G2500 (2)	many	30-40μm	even	some platelets
G2000 (3)	few	~20μm	uneven	many platelets

on the substrate from which the coat had been removed. It is assumed that the zinc was present as zinc phosphate. Scanning electron microscopy of the same areas showed that there were some needles present on the electrocoat back. A large amount of cracking of the electrocoat was seen. A large number of the finishes have been studied in cross section, with sections taken perpendicular to the tensile axis. Finishes that had not been tested are shown in figures 5.14D and E. No phosphate coat is distinguishable in the scanning electron microscope, but microprobe work (figure 5.14F) demonstrated the existance of a pronounced phosphate layer under each electrocoat. The microscopy of the untested specimens of the full systems (figure 5.14E) demonstrate considerable damage. This is mainly along the electrocoat/surfacer interface and within the surfacer coat. Cracking rarely extended from the steel through to the outer surface of the system. The systems with only an electrocoat showed marked damage about the interface between the electrocoat and the substrate, but little other damage.

Examination of S/P(R)/A and S/P(R)/Cl at 3% and 10% strain, as shown in figure 5.14G, indicated that the in the low strain region damage occurs within the electrocoat in the form of minute cracks, usually running perpendicular to the coating, but sometimes going across it. From low strains in S/P(R)/Cl and near to failure in S/P(R)/A gross adhesion failure was seen, in the form of the paint coat coming away from the substrate. This is shown in figure 5.14H. At each strain studied all the finishes showed marked variation through the sample. Figure 5.14I shows a circular crack near the surface, seen on several occassions when

examining the full systems.

Several systems have also been examined along sections taken parallel to the tensile axis. These are very similar to the sections taken perpendicular, with the damage as minute cracks, though there appears to be less damage along the coating/substrate interface.

TABLE 5A.

TENSILE TESTS (5.3)

SYSTEM	TOTAL EVENTS	TOTAL COUNTS	STRAIN PEAK 1	STRAIN PEAK 2
S	200	2000	5%	At fail
S/P	6000	15000	6%	-
S/P/A	2000	150000	3%	At fail
S/P/C1	40000	1000000	2%	25%
S/P/C2	15000	1000000	4%	34%
S/A	2000	100000	4%	At fail
S/C2	5000	400000	2%	At fail
TENSILE TESTS, COATING ON ONE SIDE ONLY (5.4)				
S/P/A	2000	100000	5%	38%
S/P/A/SUR	400	4000	6%	44%
F/S A(1)	200	50000	4%	At fail
F/S A(R)(1)	200	50000	4%	26%
S/P/C1(1)	20000	500000	5%	22%
S/P(R)/C1(1)	30000	1000000	12%	-
S/P/C1/SUR(1)	1200	150000	3%	35%
F/S C1(1)	600	200000	4%	32%
F/S C1(R)(1)	600	200000	4%	26%
TENSILE TESTS,TO FULL SYSTEM ON ONE SIDE, TO ELECTROCOAT ON OTHER (5.5)				
F/S A	2500	250000	4%	30%
F/S C1	15000	1000000	2%	24%
TENSILE TESTS, AFTER IMMERSION (5.6)				
S/P/A	500	50000	1%	At fail
S/P/C1	30000	2000000	1%	7%
F/S A	5000	400000	3%	30%
F/S C1	13000	1000000	8%	-
F/S C1(R)	6000	500000	6%	-
TENSILE TESTS, VARIOUS PHOSPHATES (5.7)				
1	200	5000	2%	30%
2	1500	10000	6%	18%
3	5000	20000	4%	-
4	2000	10000	3%	40%
1/A	700	20000	2%	At fail
2/A	1500	100000	4%	At fail
3/A	1500	100000	4%	At fail
1/C2	3000	200000	2%	40%
2/C2	5000	100000	2%	34%
3/C2	11000	100000	2%	24%

FIGURE 5.3A.

The events vs. strain curves for S, S/P, S/P(R), S/P/A and S/P(R)/A. The curves shown are the maximum and minimum found for these systems, to give an indication of the scatter; and the events are on a logarithmic scale.

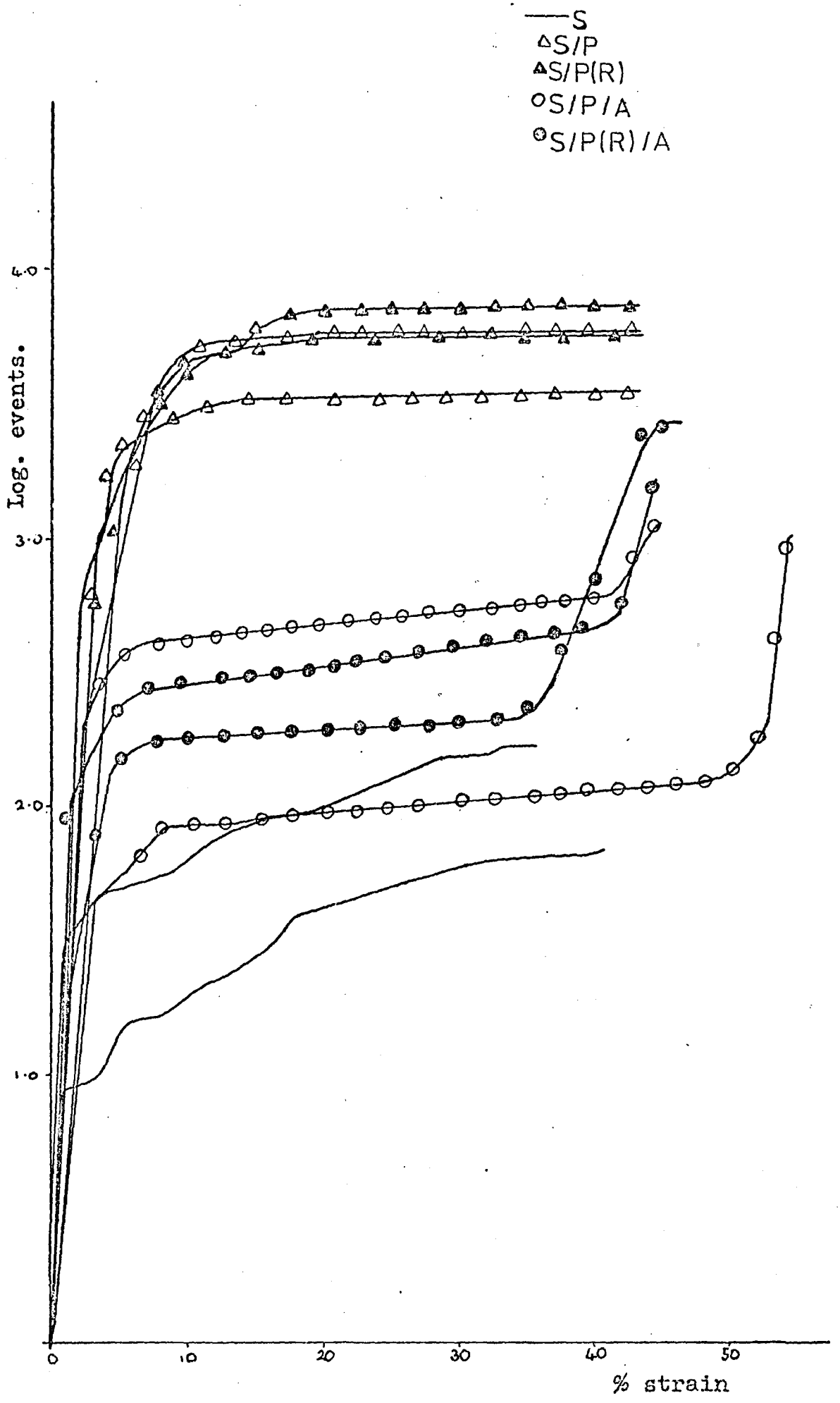
S
S/P
S/P(R)
S/P/A
S/P(R)/A
Log. events.
4·0
3·0
2·0
1·0
0
10
20
30
40
50
% strain

FIGURE 5.3B

The events vs. strain curves for S/P/C1, S/P(R)/C1, S/P/C2 and S/P(R)/C2, showing the differences between the electrocoats. The events are on a logarithmic scale.

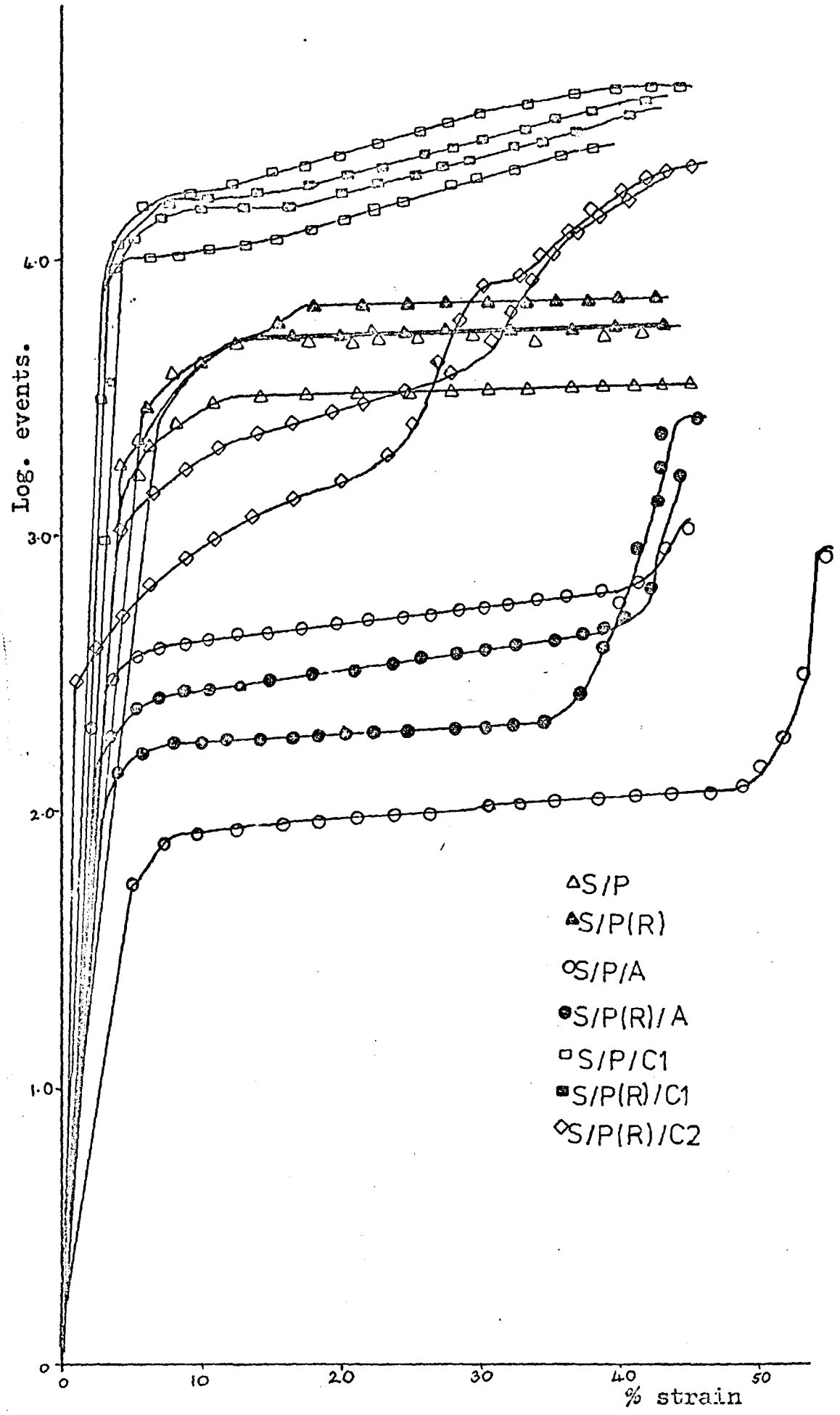
Log. events.
4·0
3·0
2·0
1·0
0
0
10
20
30
40
50
% strain
△S/P
▲S/P(R)
○S/P/A
●S/P(R)/A
□S/P/C1
■S/P(R)/C1
◇S/P(R)/C2

FIGURE 5.3C

The events vs. strain curves for S/A and S/C2, with the curves for S/P/A and S/P/C2 repeated for comparison, showing the effect of omitting the phosphate layer. The events are on a logarithmic scale.

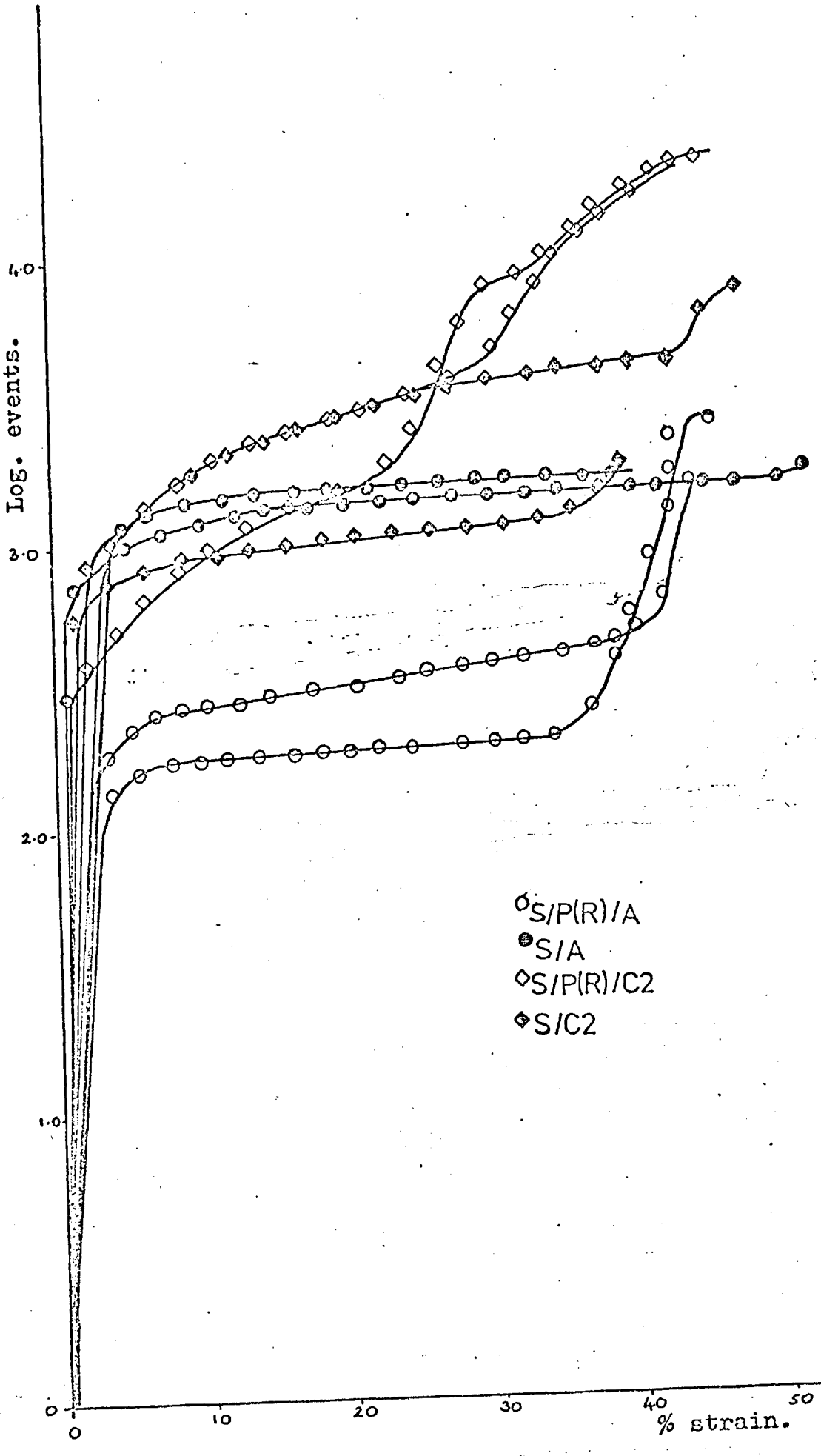
Log. events.
4.0
3.0
2.0
1.0
0
0
10
20
30
40
50
% strain.
S/P(R)/A
S/A
S/P(R)/C2
S/C2

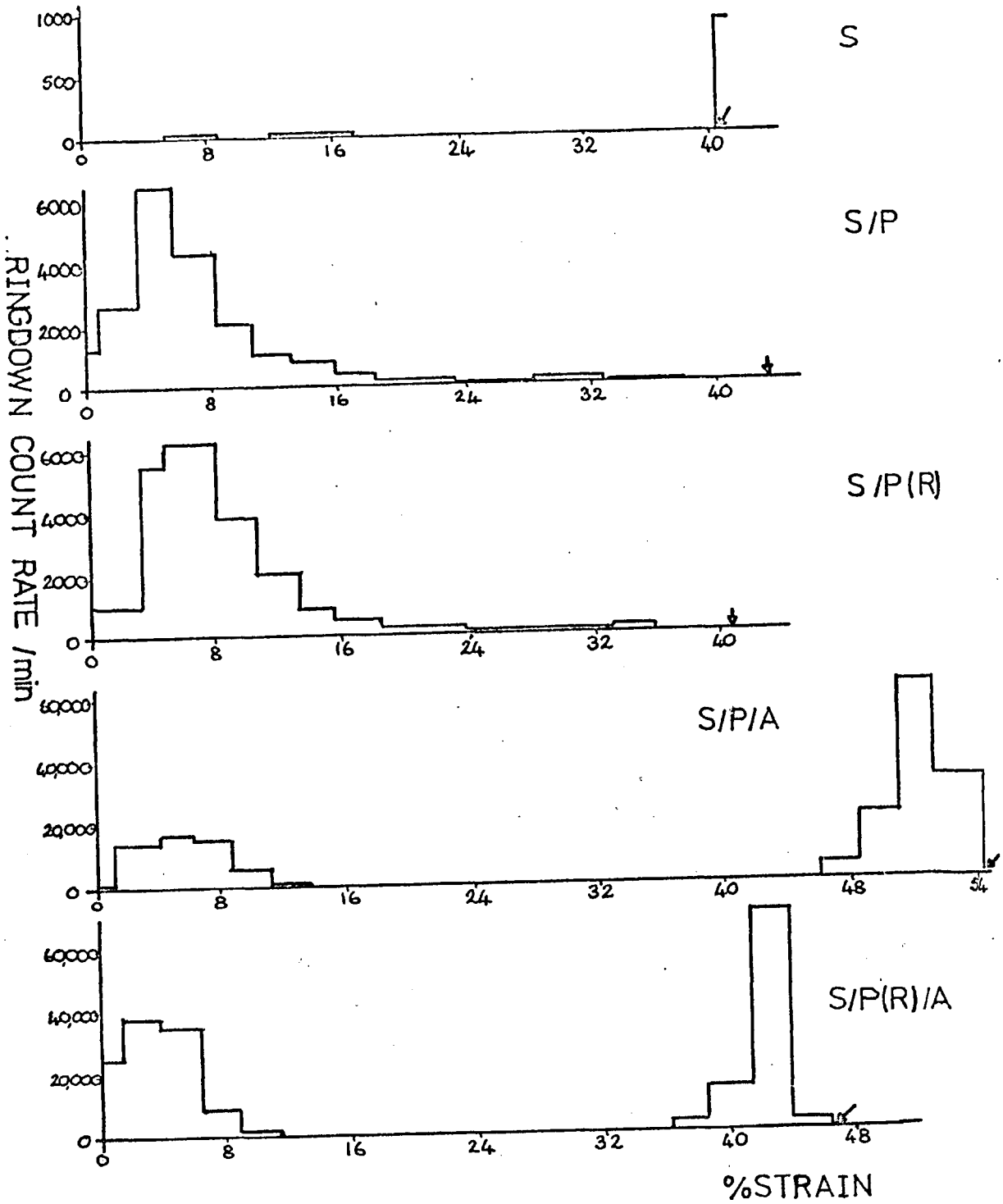

Figure 5.3D.
The ringdown count rate vs. strain curves for steel, phosphated steel and phosphated steel with an anodic electrocoat.

FIGURE 5.3E.

Ringdown count vs. strain curves for S/P/A, S/P/C1, S/P/C2 S/A and S/C2, showing the emission from the different electrocoats.

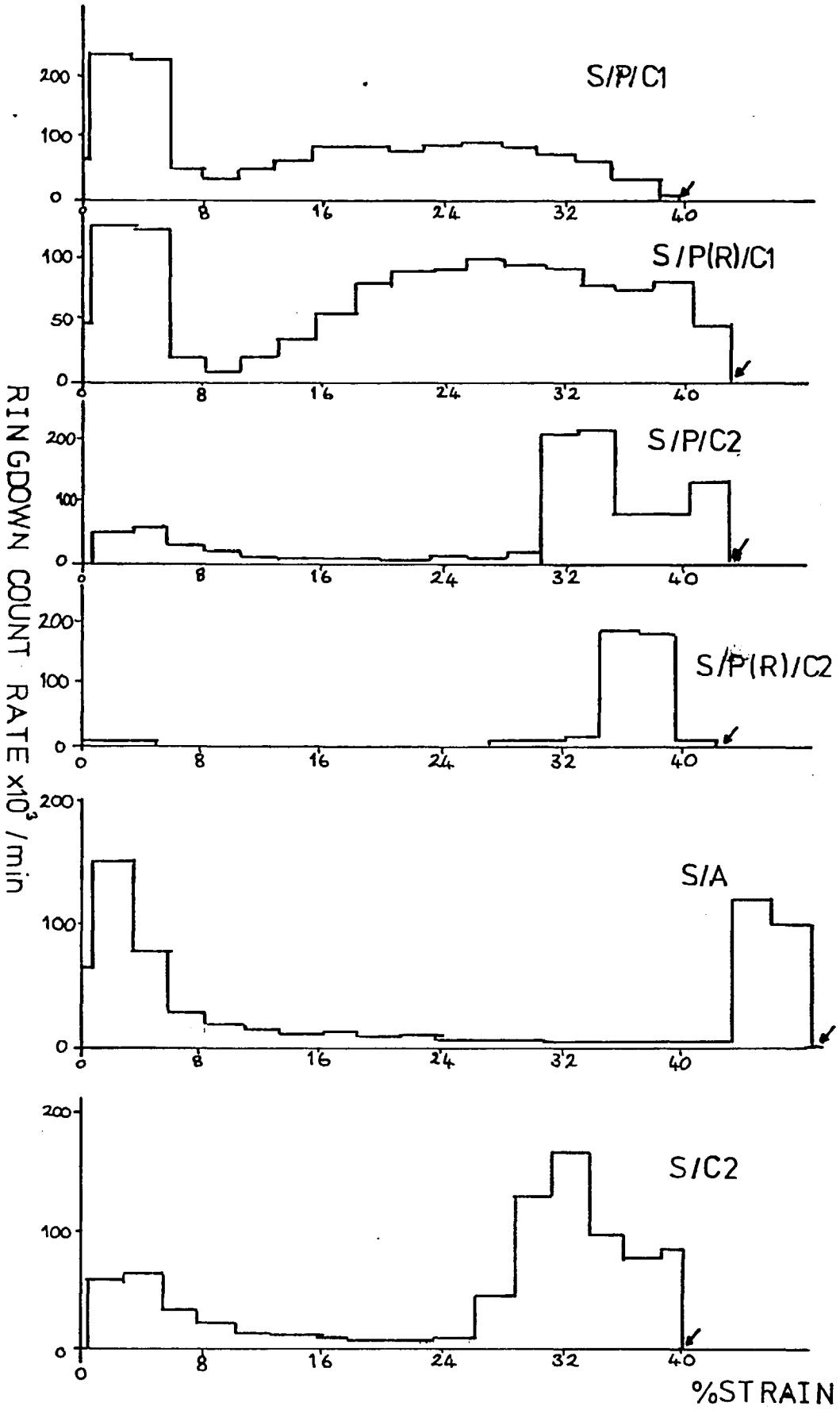
S/P/C1
S/P(R)/C1
S/P/C2
S/P(R)/C2
S/A
S/C2
RINGDOWN COUNT RATE x10³/min
%STRAIN
0
8
16
24
32
40
100
200
50

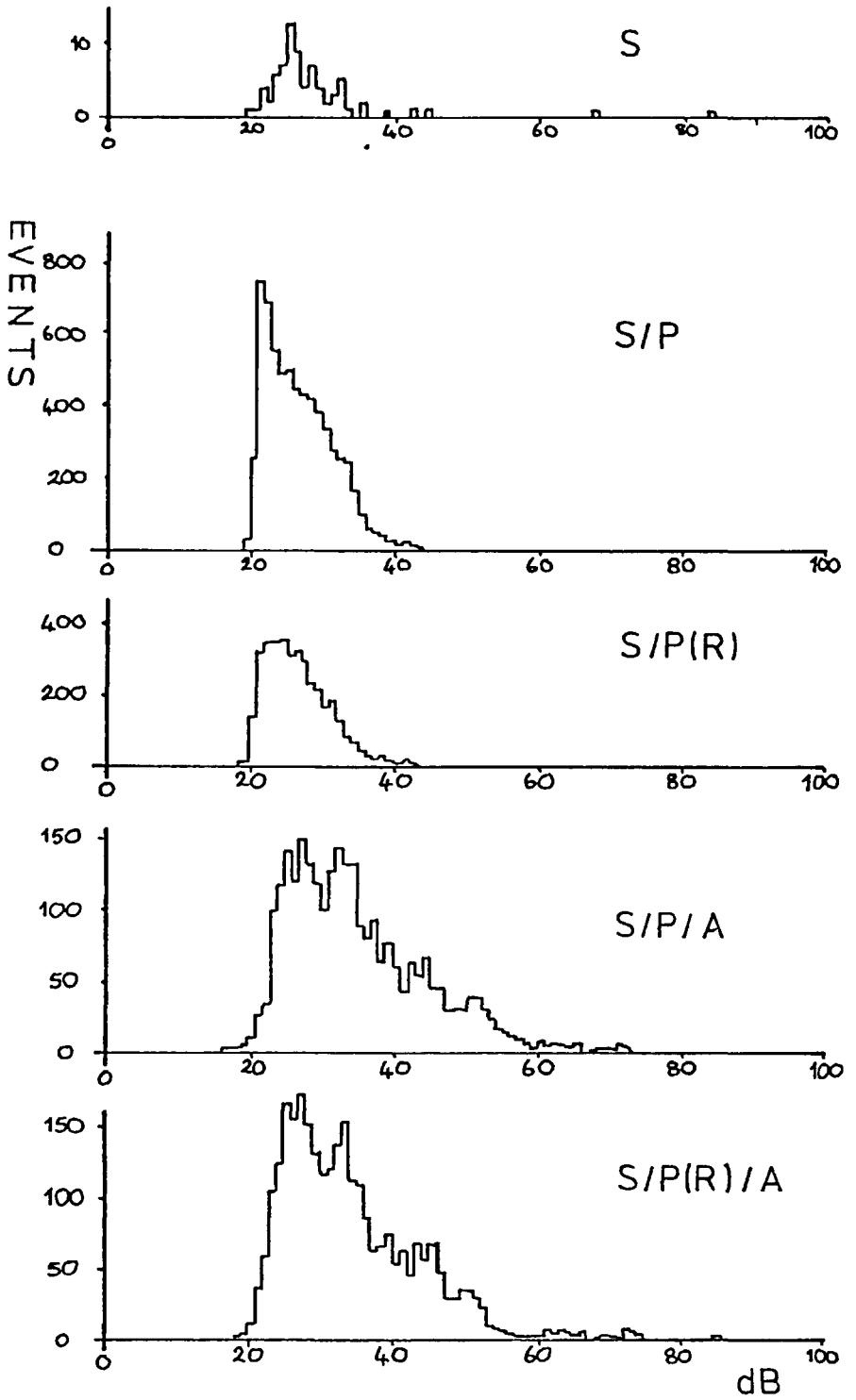

FIGURE 5·3F

Amplitude distributions for steel, phosphated steel and anodically coated steel.

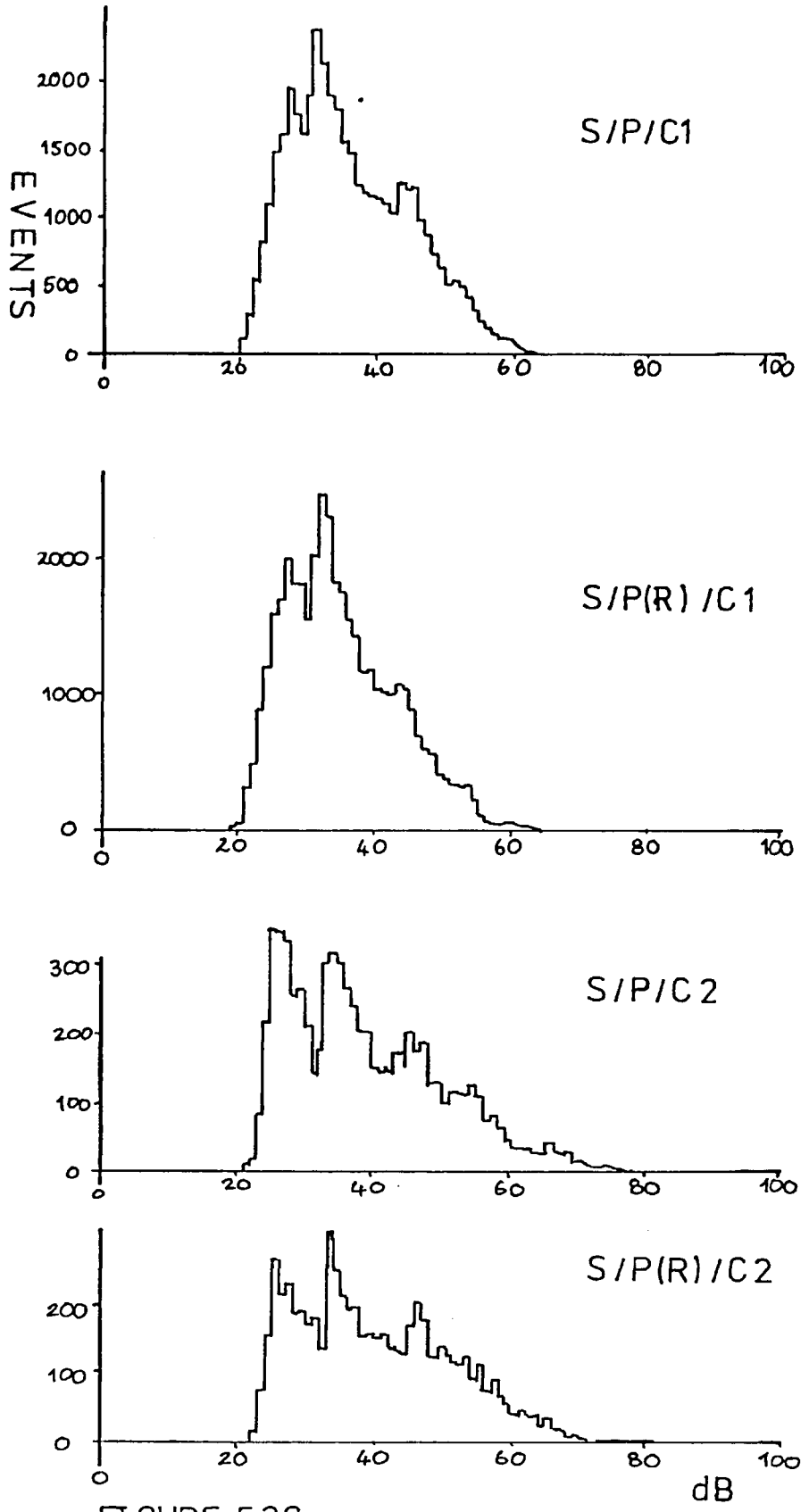

FIGURE 5·3G

Amplitude distributions for the systems with cathodic electrocoats.

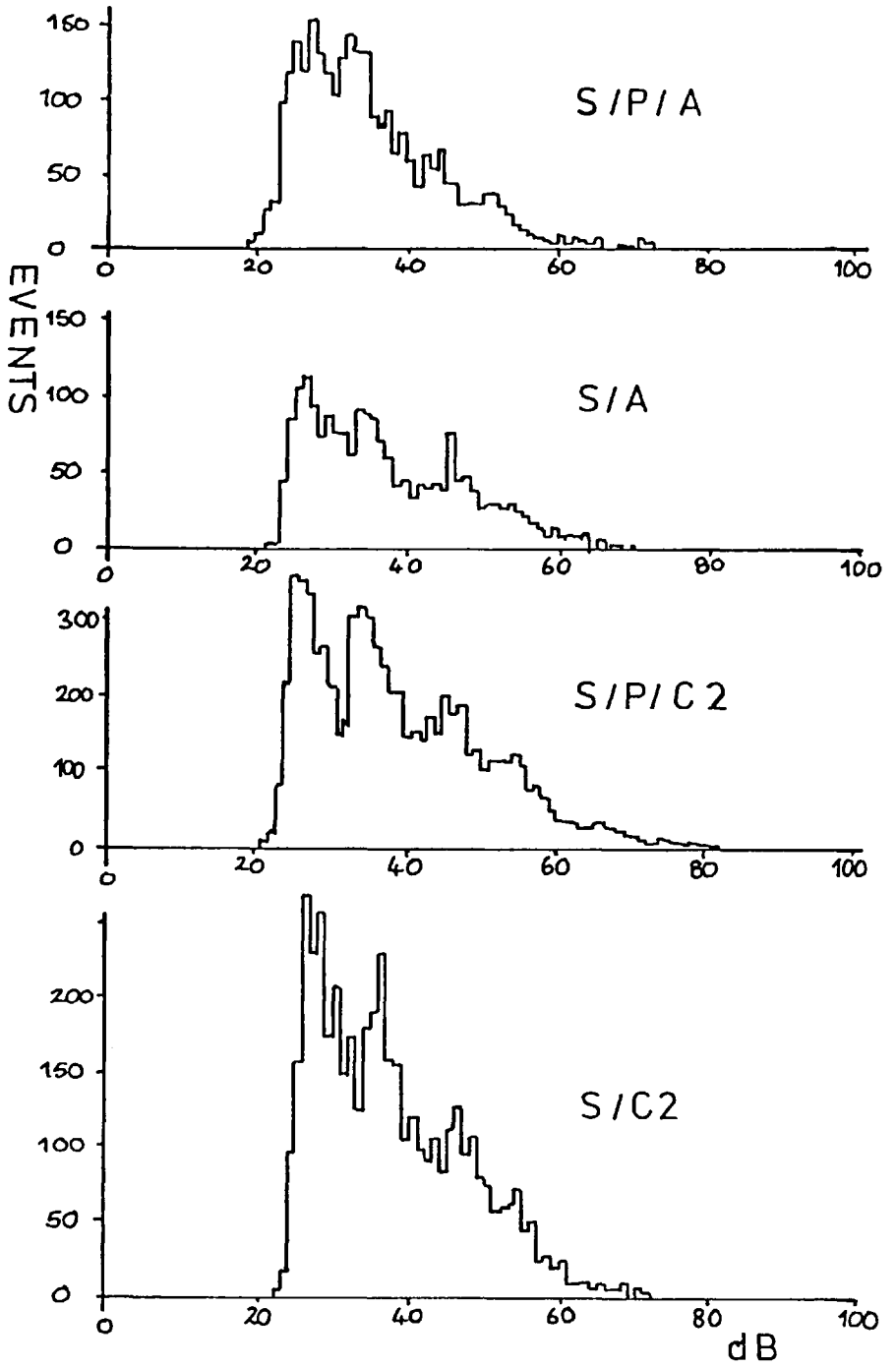

FIGURE 53H

Typical amplitude distributions showing the effect of omitting the phosphate layer.

FIGURE 5.3I

Histograms showing the differences in the total number of events and ringdown counts to failure between the steel, phosphated steel and electrocoated steel. They also show the differences between the electrocoats, and the effect of omitting the phosphate coat.

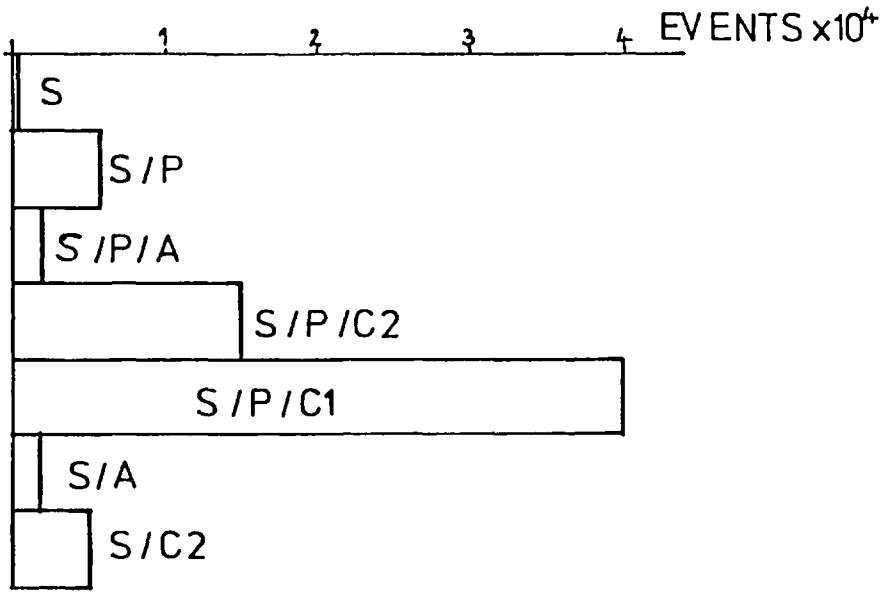
1
2
3
4
EVENTS x10⁴
S
S/P
S/P/A
S/P/C2
S/P/C1
S/A
S/C2

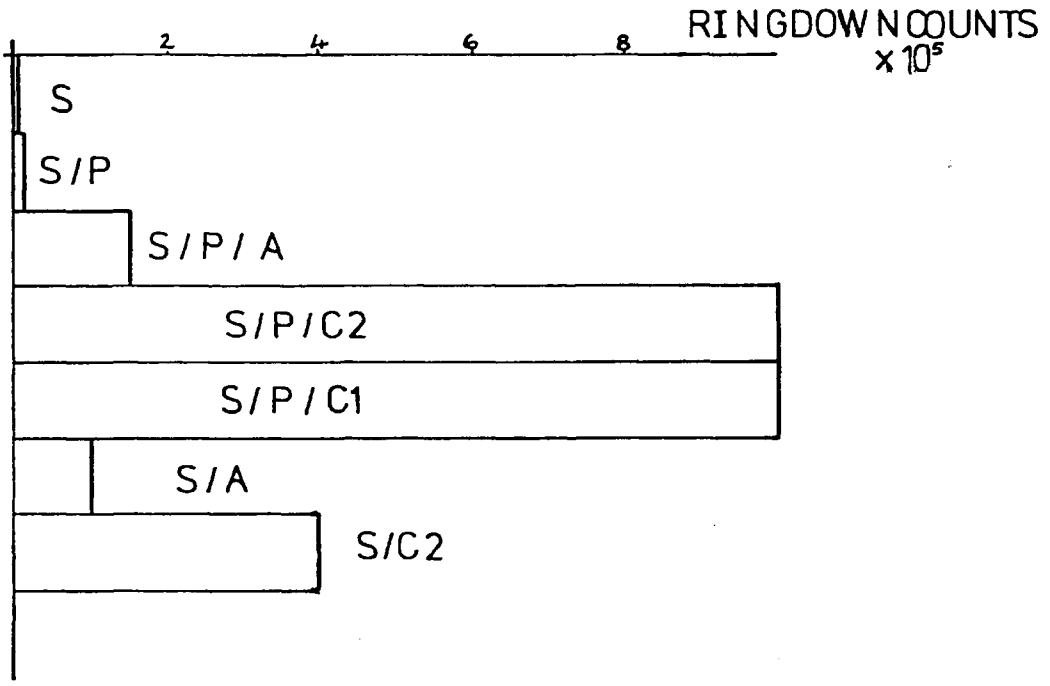
2
4
6
8
RINGDOWN COUNTS
x10⁵
S
S/P
S/P/A
S/P/C2
S/P/C1
S/A
S/C2

FIGURE 5.4A

The events vs. strain curves for S/P/A(1), S/P(R)/A(1), S/P/A/SUR(1), S/P(R)/A/SUR(1), F/S A(1) and F/S A(R)(1) showing the effect of additional coats on the anodic electrocoat. The events are on a logarithmic scale.

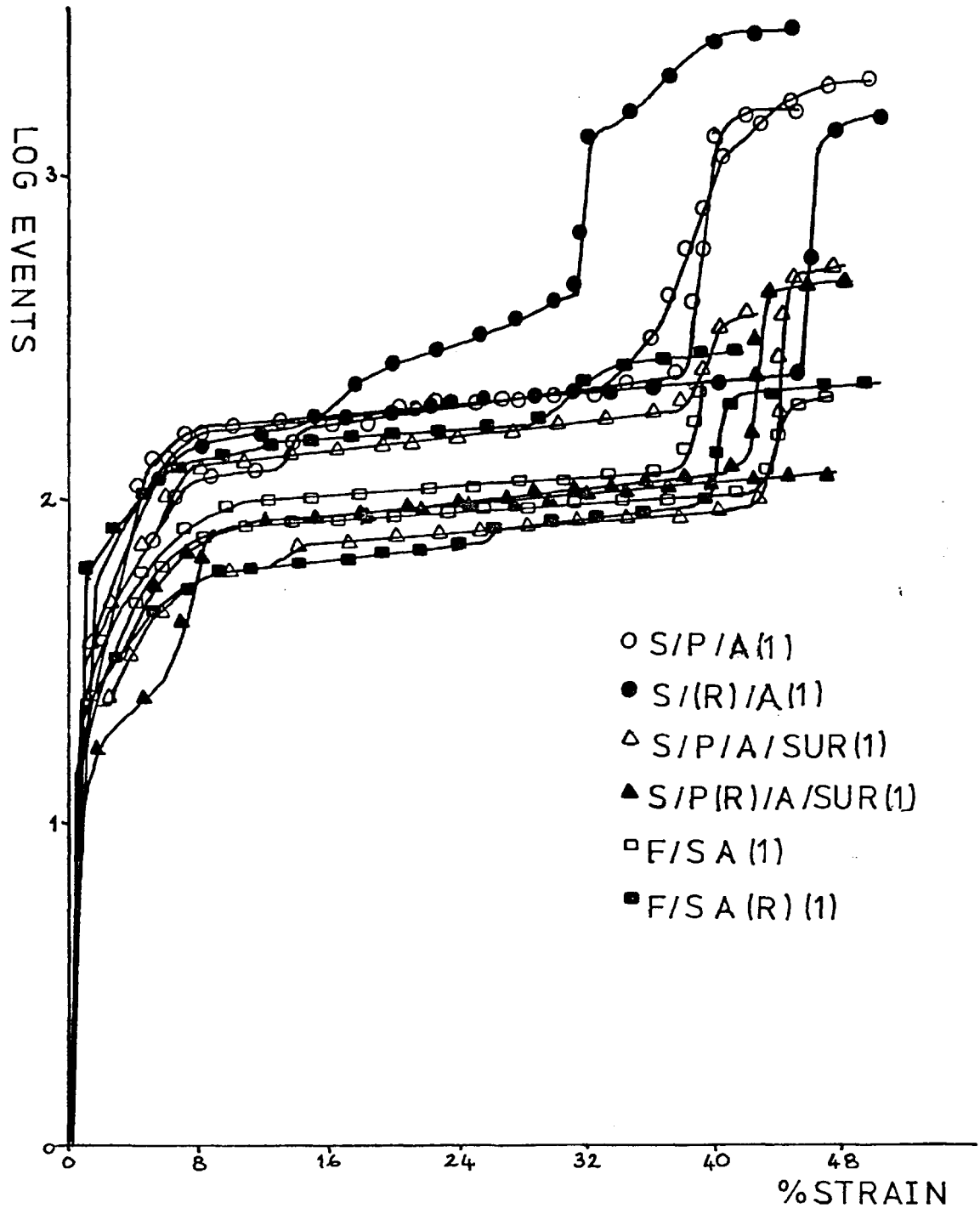
LOG EVENTS
3
2
1
0
0
8
16
24
32
40
48
%STRAIN
S/P/A(1)
S/(R)/A(1)
S/P/A/SUR(1)
S/P(R)/A/SUR(1)
F/S A (1)
F/S A (R) (1)

FIGURE 5.4B

The events vs. strain curves for S/P/Cl(1), S/P(R)/Cl(1), S/P/Cl/SUR(1), S/P(R)/Cl/SUR(1), F/S Cl(1) and F/S Cl(R)(1), showing the effect as further coats are added to the cathodic 1 electrocoat. The events are on a logarithmic scale.

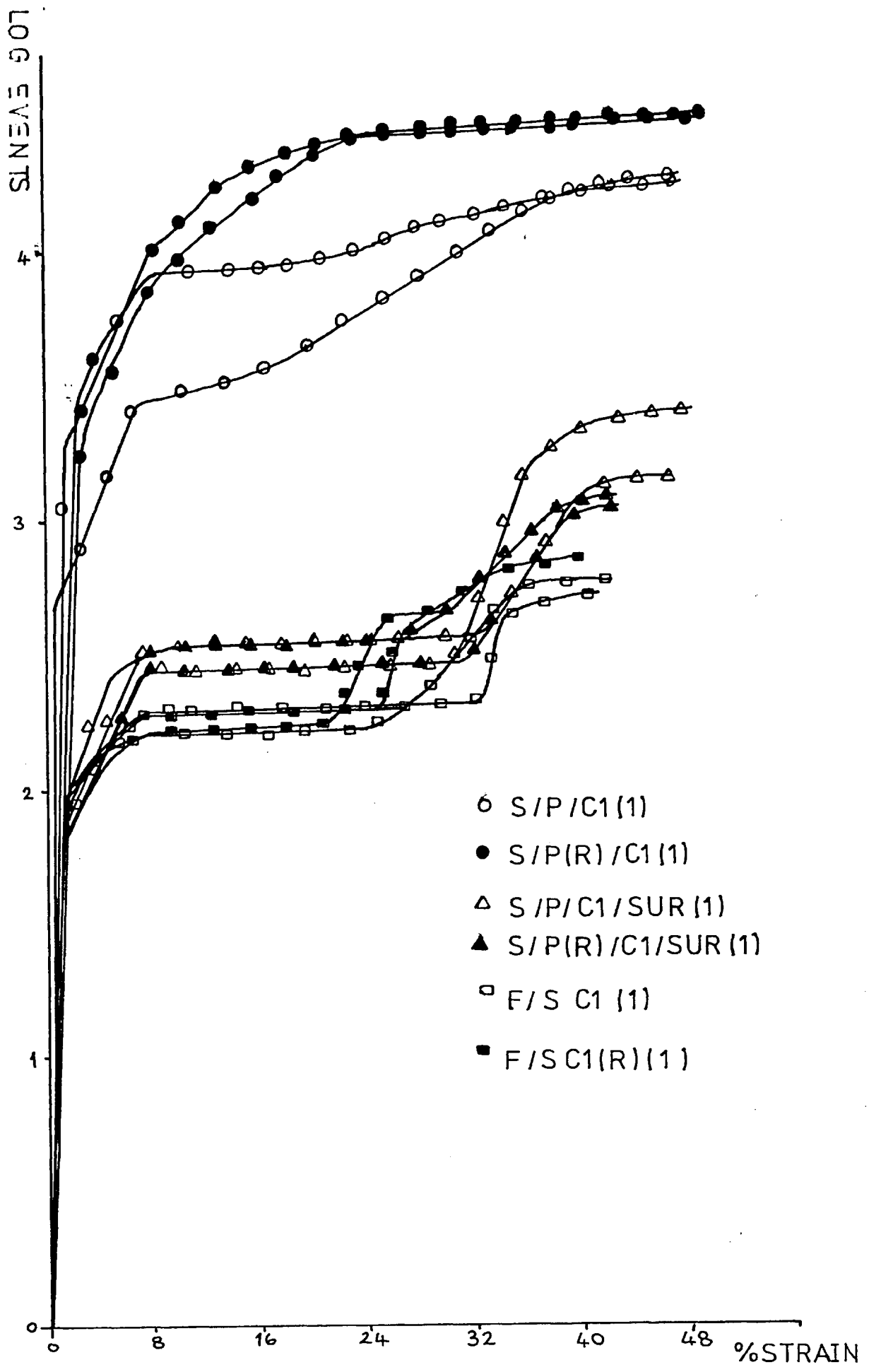
LOG EVENTS
4
3
2
1
0
0
8
16
24
32
40
48
%STRAIN
S/P/C1(1)
S/P(R)/C1(1)
S/P/C1/SUR(1)
S/P(R)/C1/SUR(1)
F/S C1 (1)
F/S C1(R)(1)

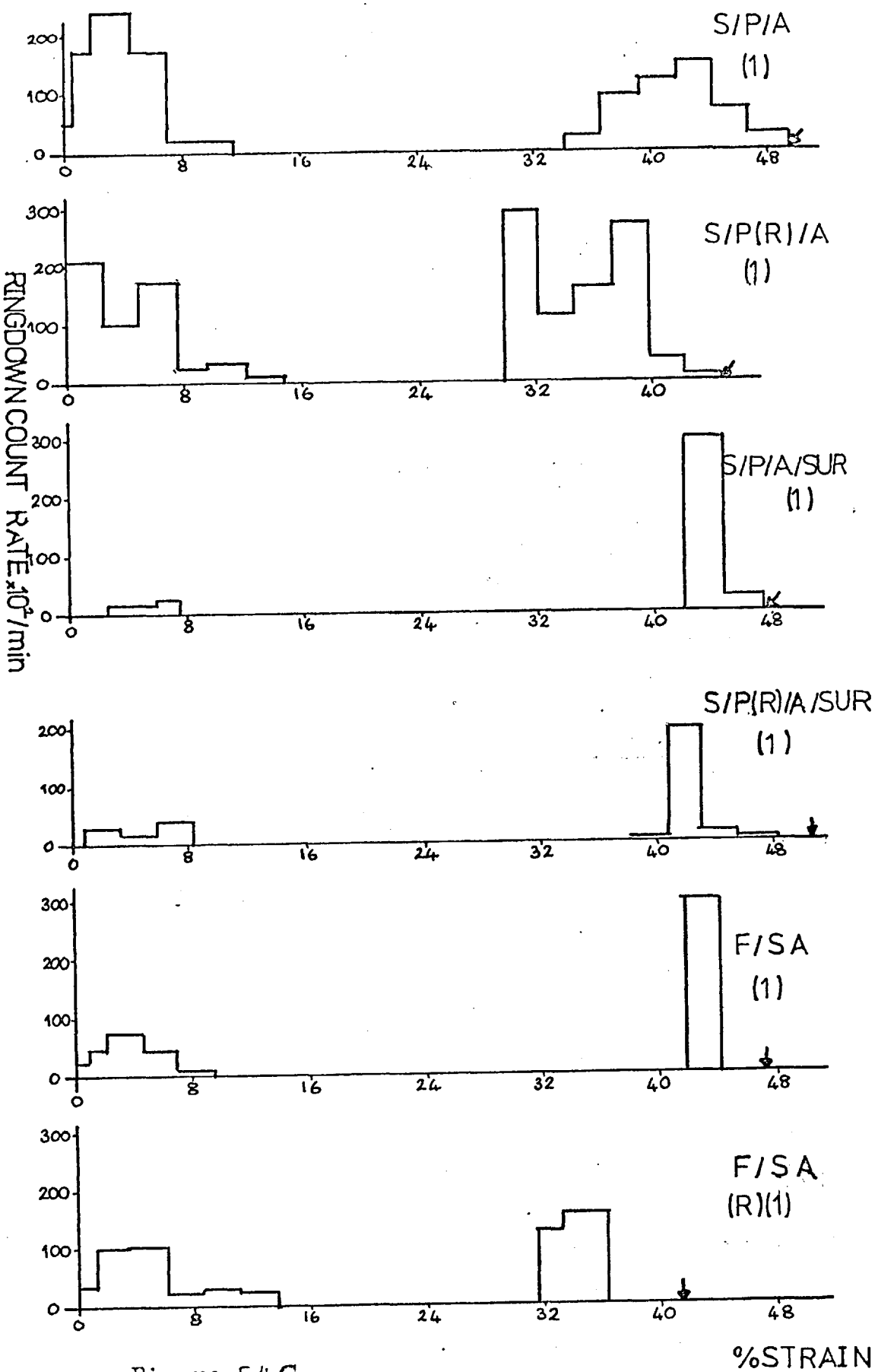

Figure 5.4 C.

The ringdown count rate vs. strain curves showing the differences in acoustic emission as further coats are added to the anodic electrocoat.

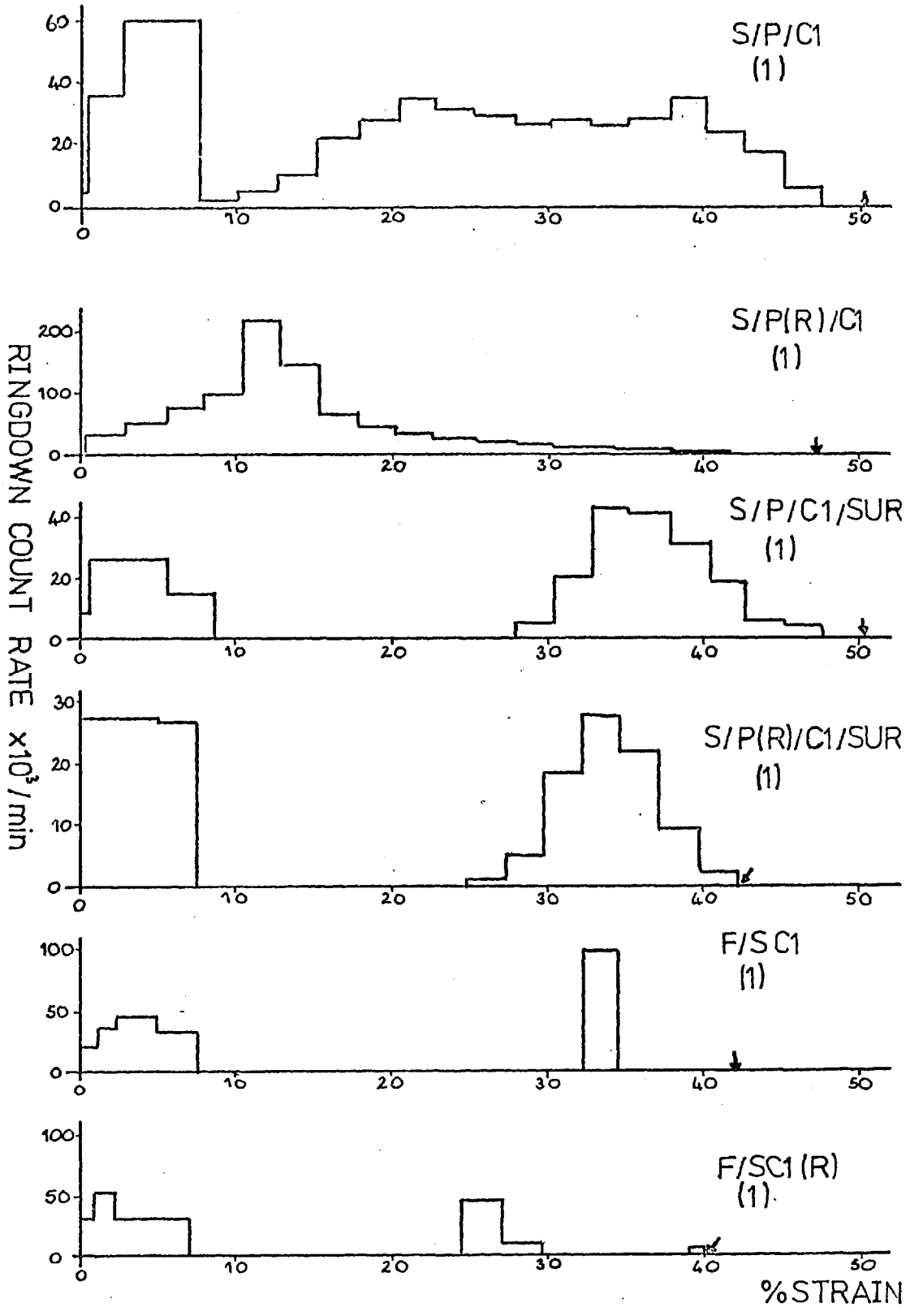

Figure 5.4D.

The ringdown count rate vs. strain curves, showing differences in the acoustic emission as further coats are added to the cathodic 1 electro-coat.

FIGURE 5.4E

The amplitude distributions, showing the effect of the addition of further coats to the anodic electrocoat.

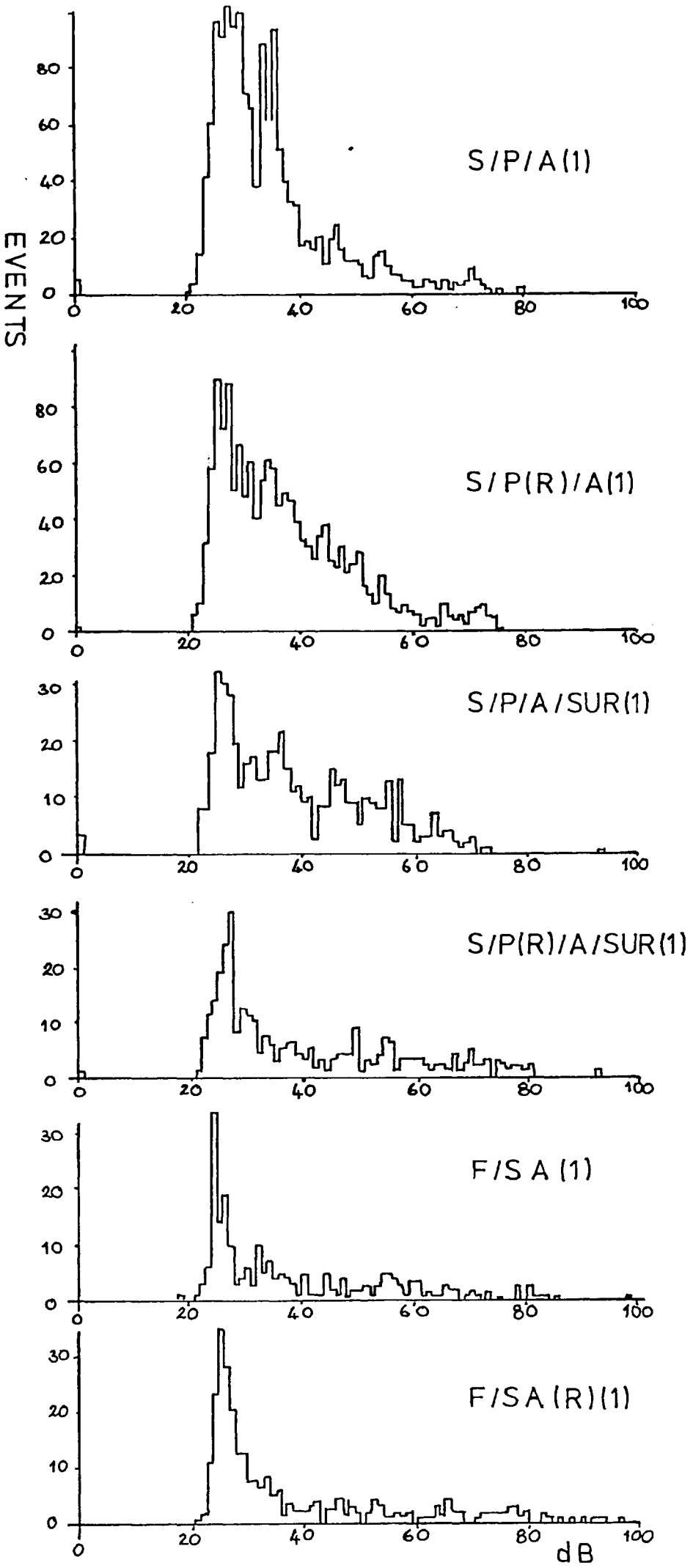
EVENTS
S/P/A(1)
S/P(R)/A(1)
S/P/A/SUR(1)
S/P(R)/A/SUR(1)
F/S A (1)
F/S A (R)(1)
dB

FIGURE 5.4F

Amplitude distributions showing the effect of the addition of further coats to the cathodic 1 electrocoat.

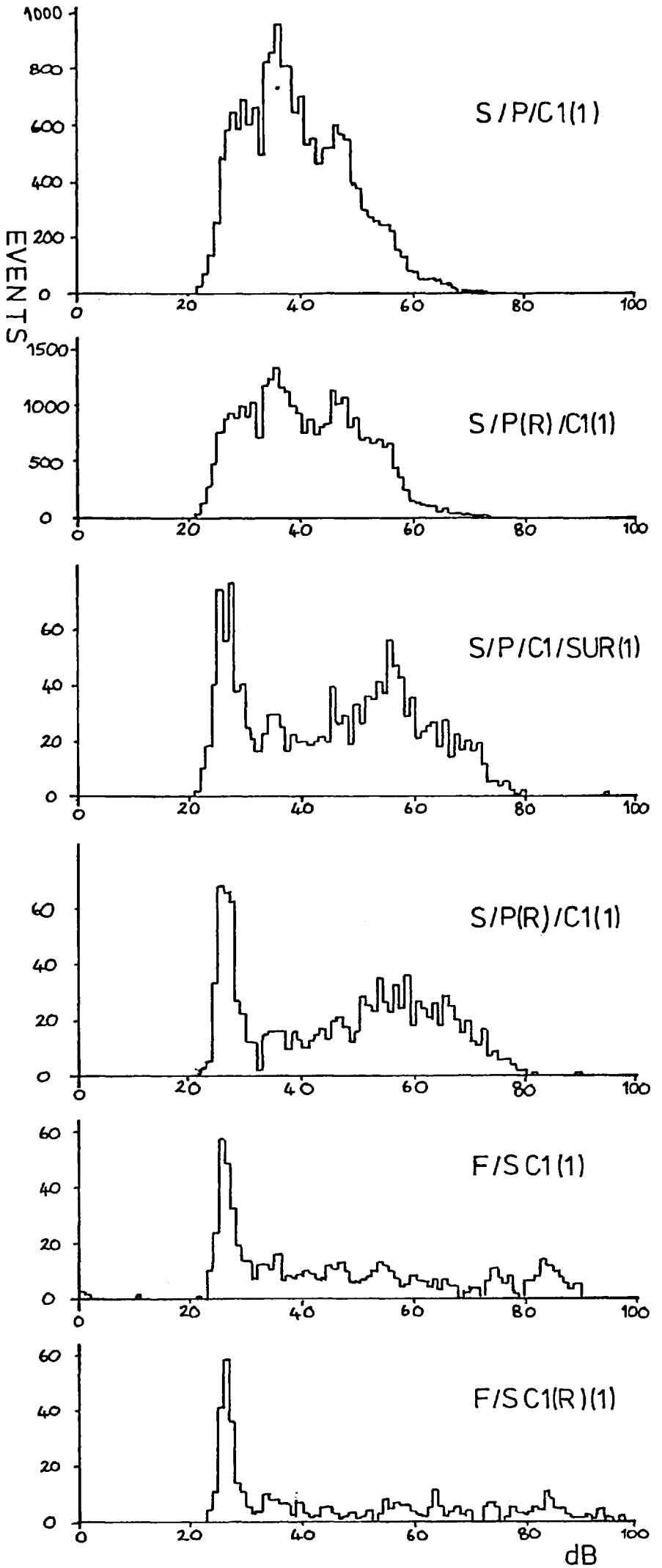
EVENTS
S/P/C1(1)
S/P(R)/C1(1)
S/P/C1/SUR(1)
S/P(R)/C1(1)
F/S C1(1)
F/S C1(R)(1)
dB

FIGURE 5.4G

Histograms showing the differences in the total number of events and ringdown counts to failure as further coats are added to the anodic electrocoat.

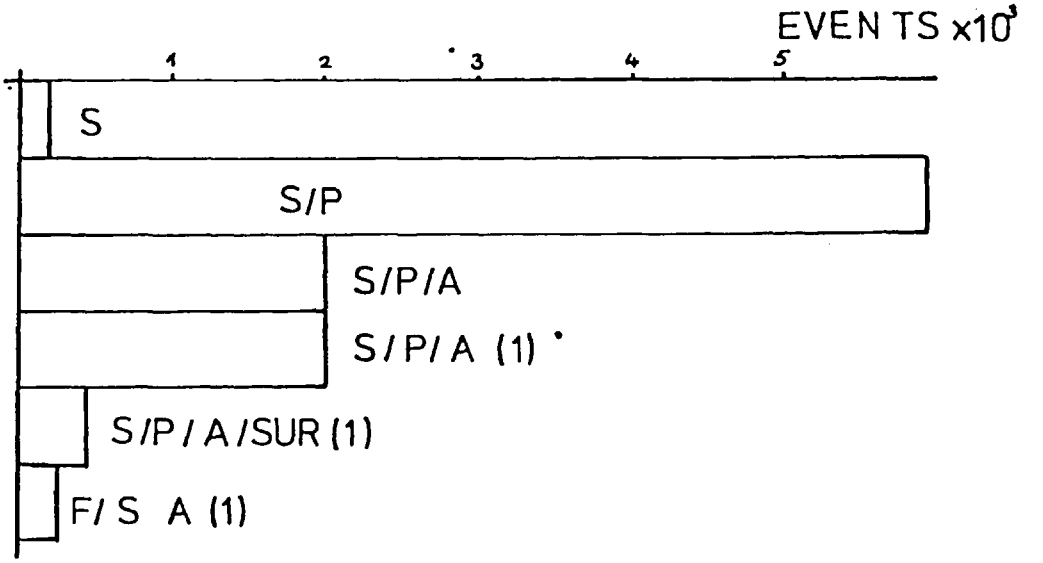
EVENTS x10³
1
2
3
4
5
S
S/P
S/P/A
S/P/A (1)
S/P/A/SUR (1)
F/S A (1)

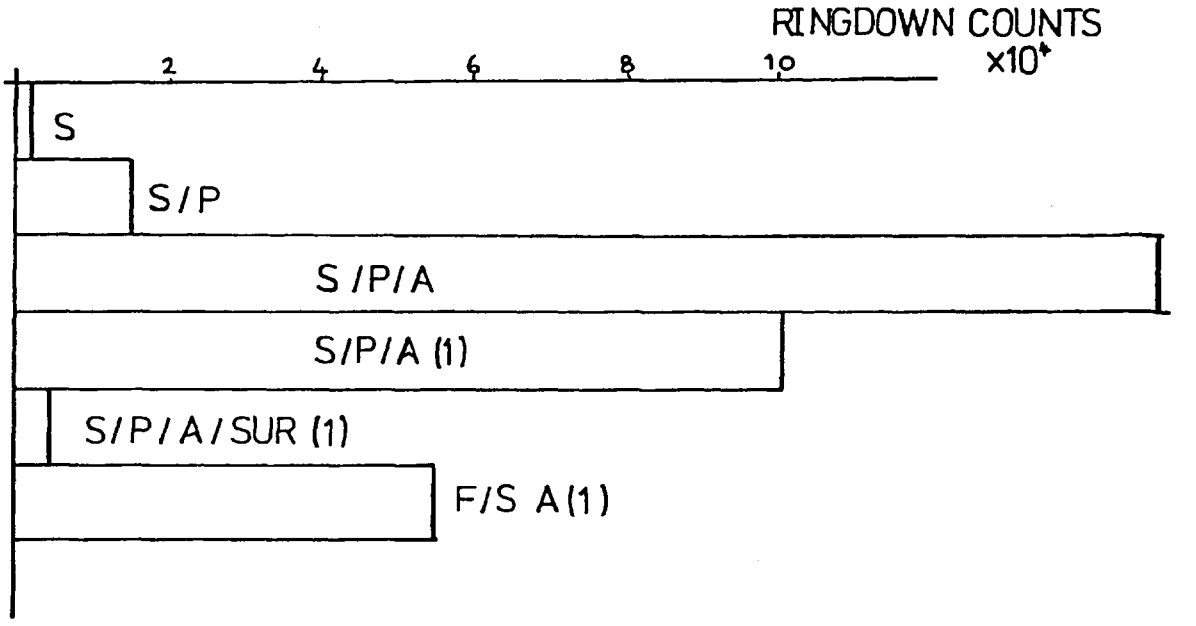
RINGDOWN COUNTS
x10⁴
2
4
6
8
10
S
S/P
S/P/A
S/P/A (1)
S/P/A/SUR (1)
F/S A (1)

FIGURE 5.4H

Histograms showing the differences in the total number of events and ringdown counts to failure as further coats are added to the cathodic 1 electrocoat.

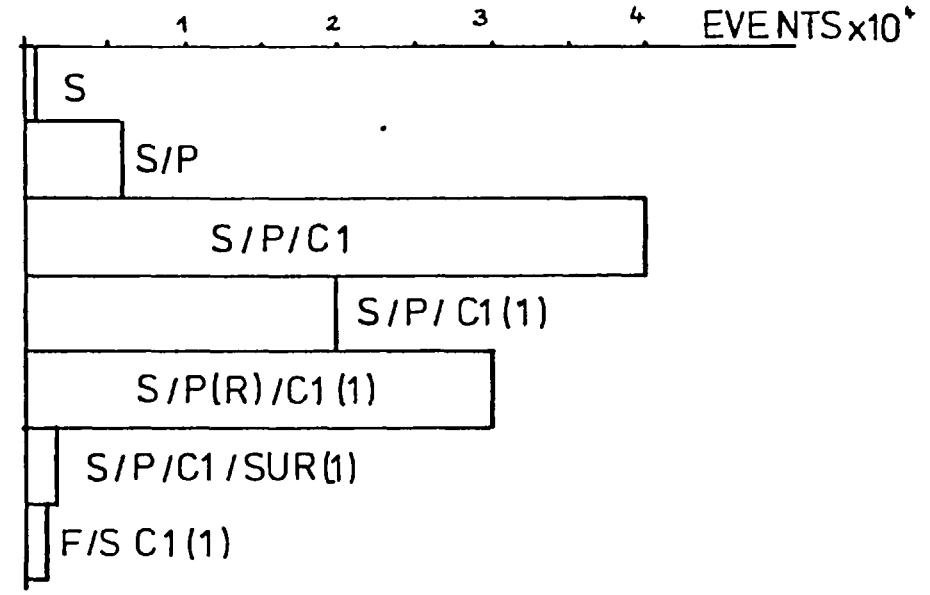
1
2
3
4
EVENTS x10⁴
S
S/P
S/P/C1
S/P/C1(1)
S/P(R)/C1(1)
S/P/C1/SUR(1)
F/S C1(1)

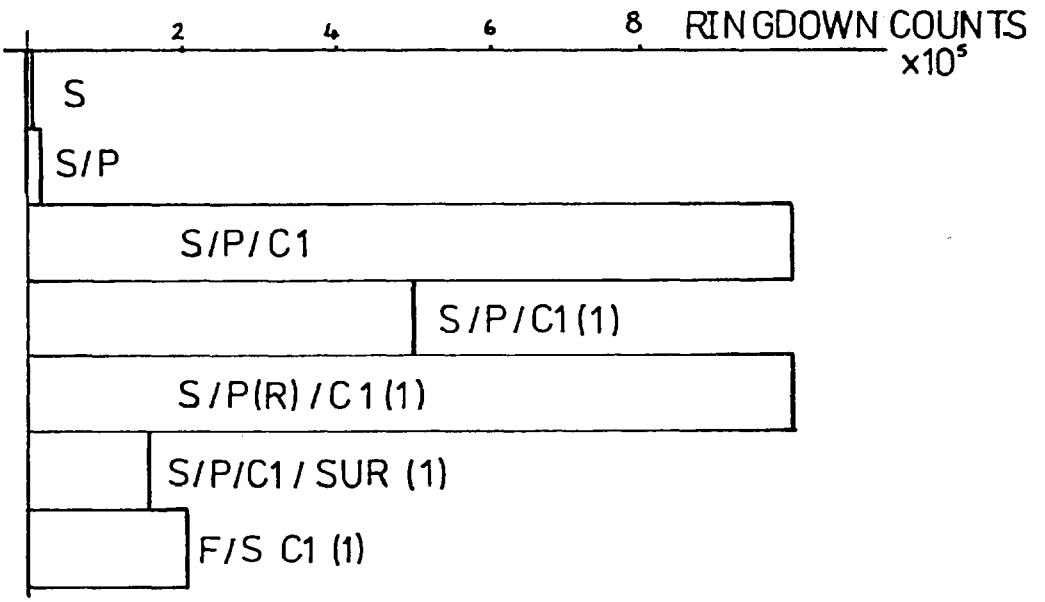
2
4
6
8
RINGDOWN COUNTS
x10⁵
S
S/P
S/P/C1
S/P/C1(1)
S/P(R)/C1(1)
S/P/C1/SUR (1)
F/S C1 (1)

FIGURE 5.5A

The events vs. strain curves for F/S A, F/S A(R), F/S C1 and F/S C1(R). For comparison with the same systems after immersion (section 5.6).

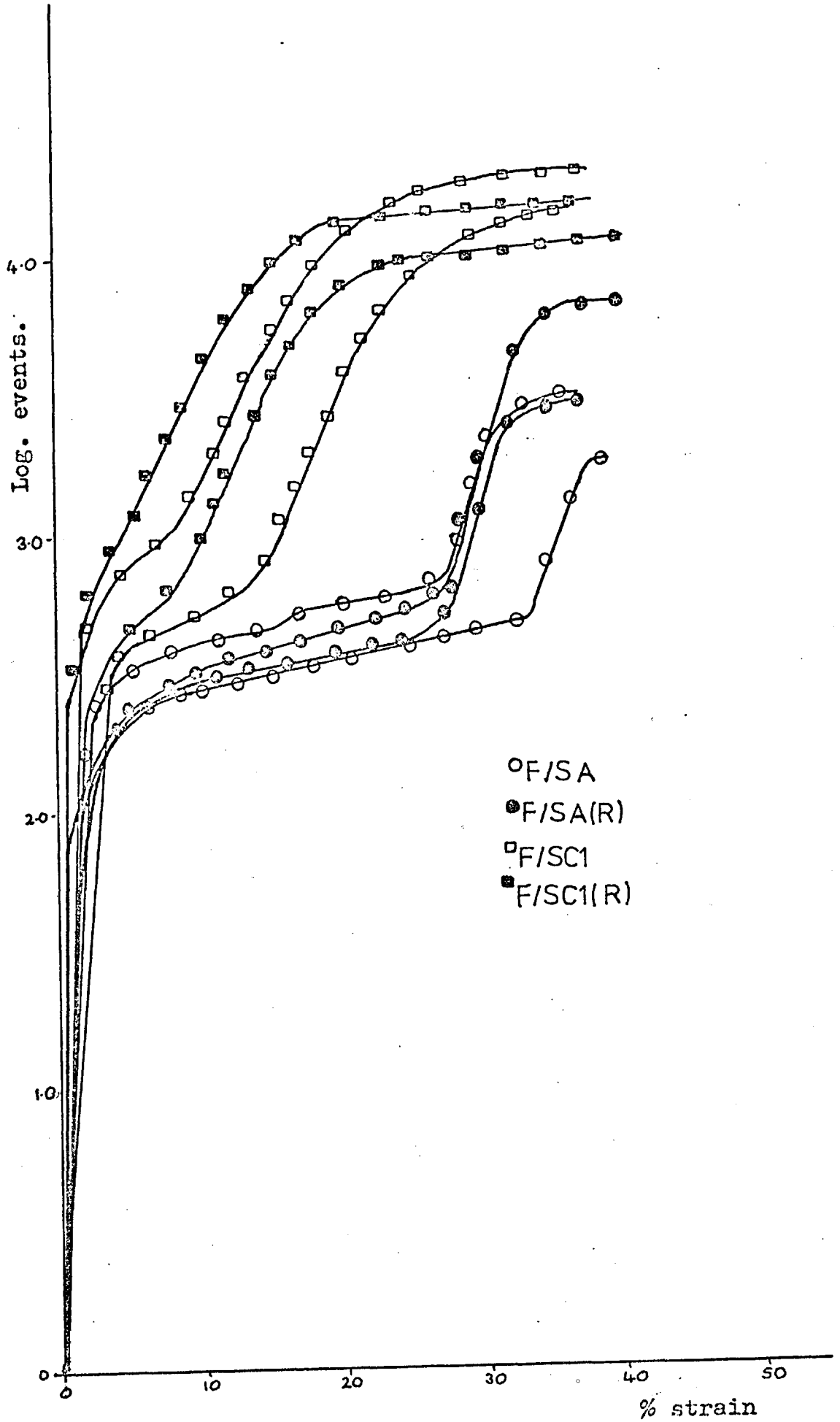
Log. events.
4·0
3·0
2·0
1·0
0
0
10
20
30
40
50
% strain
○F/SA
●F/SA(R)
□F/SC1
■F/SC1(R)

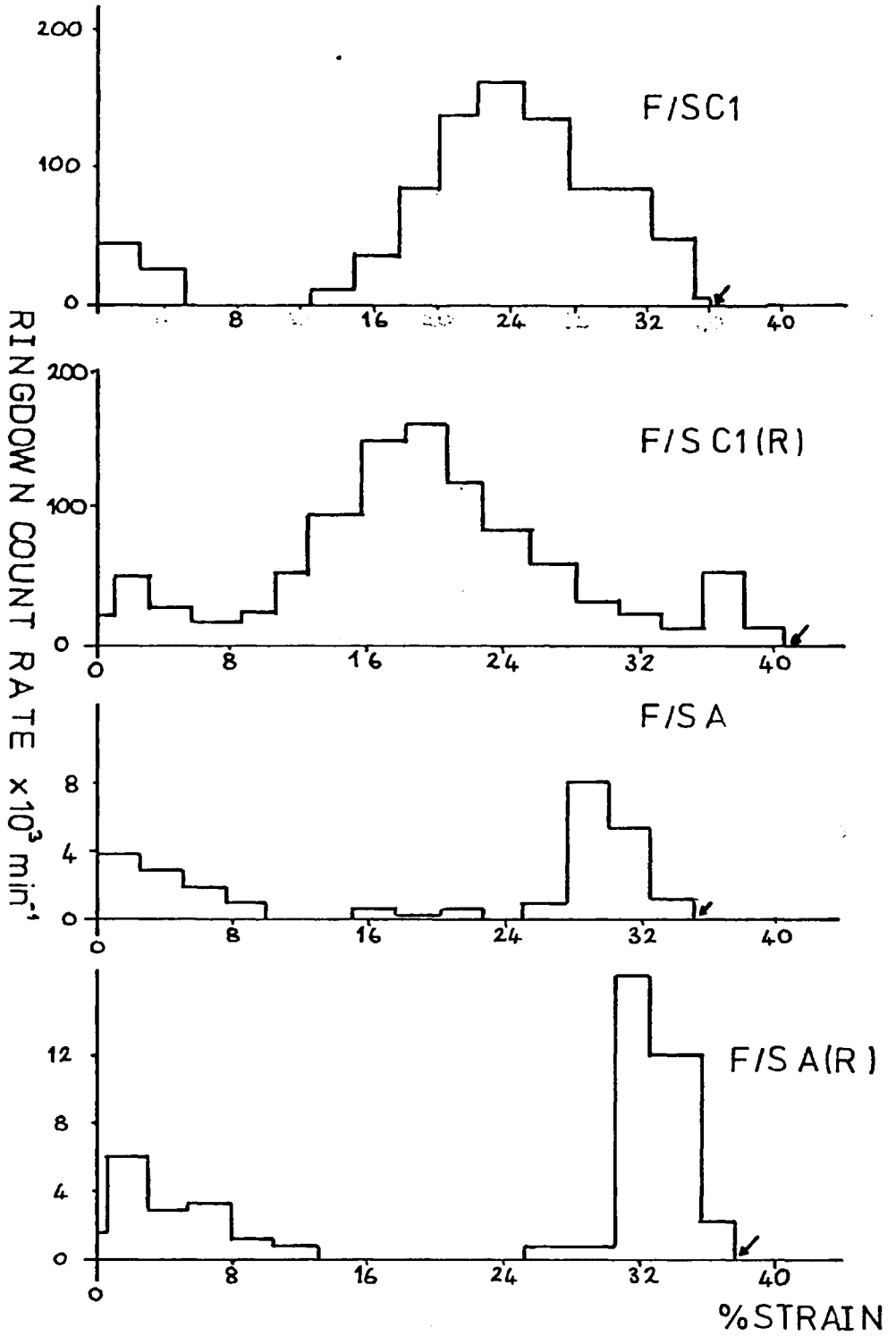

FIGURE 5.5B

Ringdown count rate vs strain curves for systems electrocoated on both sides and with surfacer and topcoat on one side.

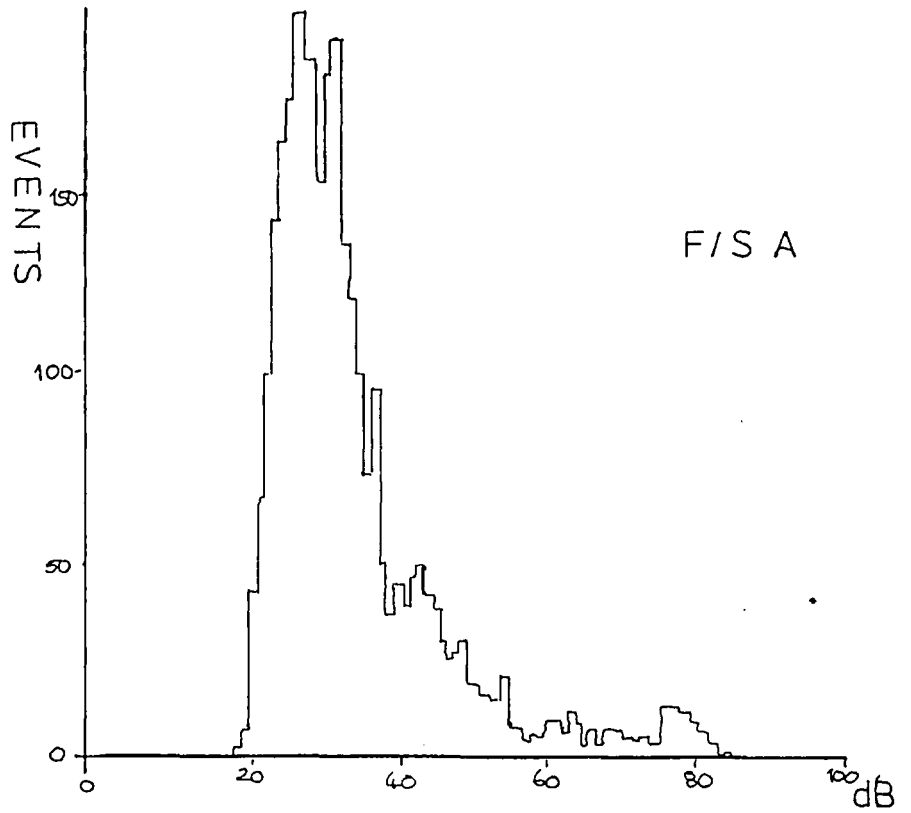

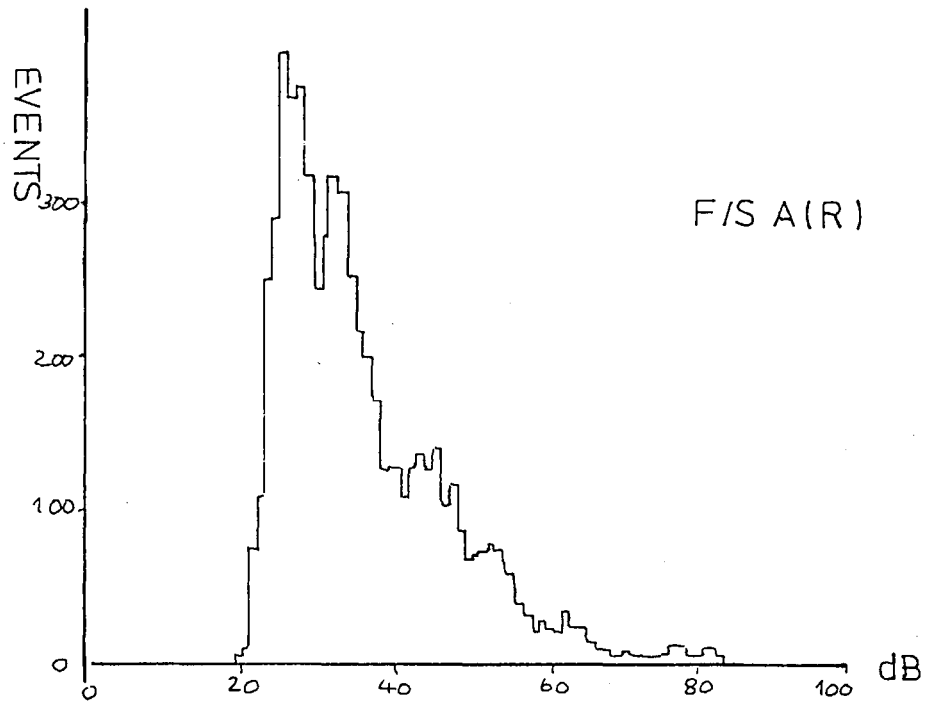

FIGURE 5.5.C
Amplitude distributions full systems on one side to electrocoat on other.

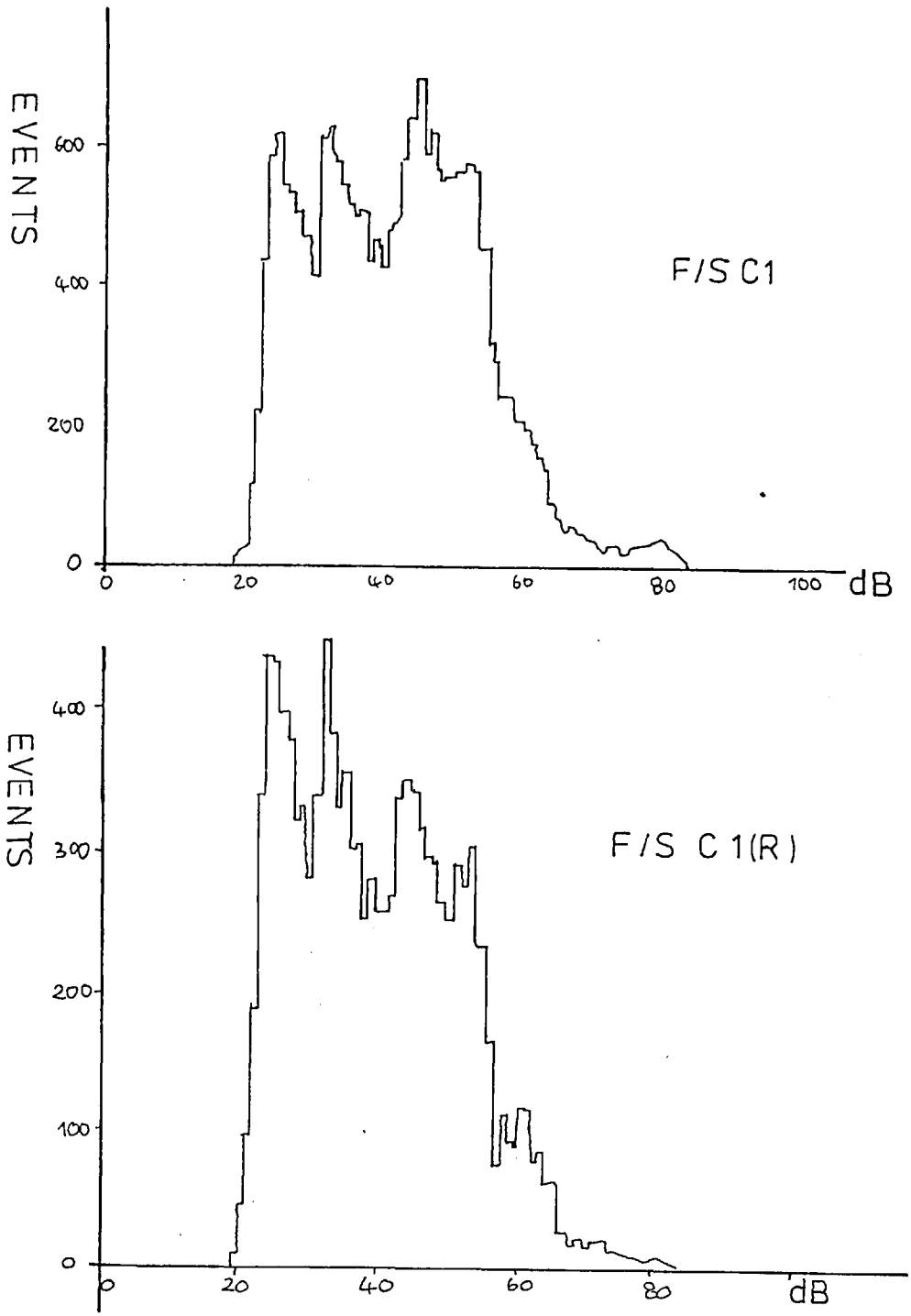

FIGURE 5.5 C contd.

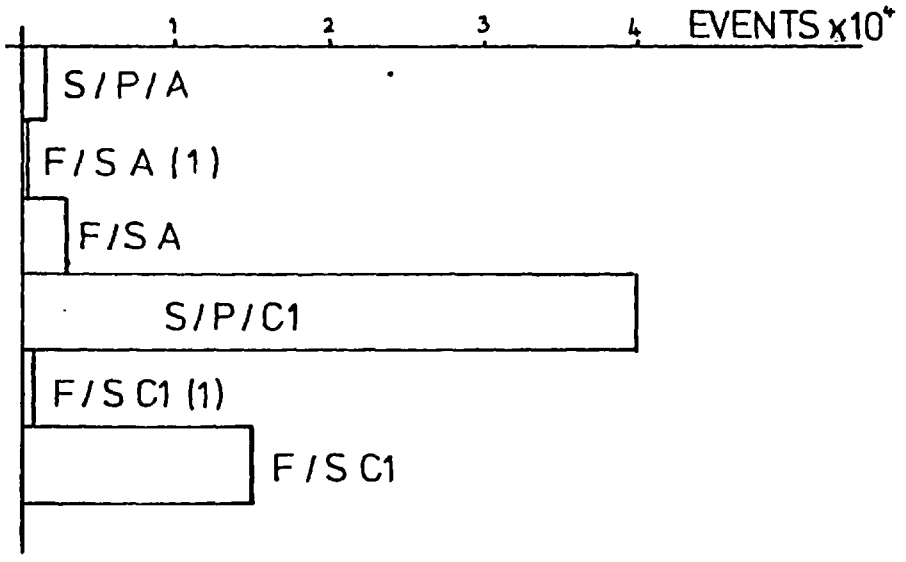

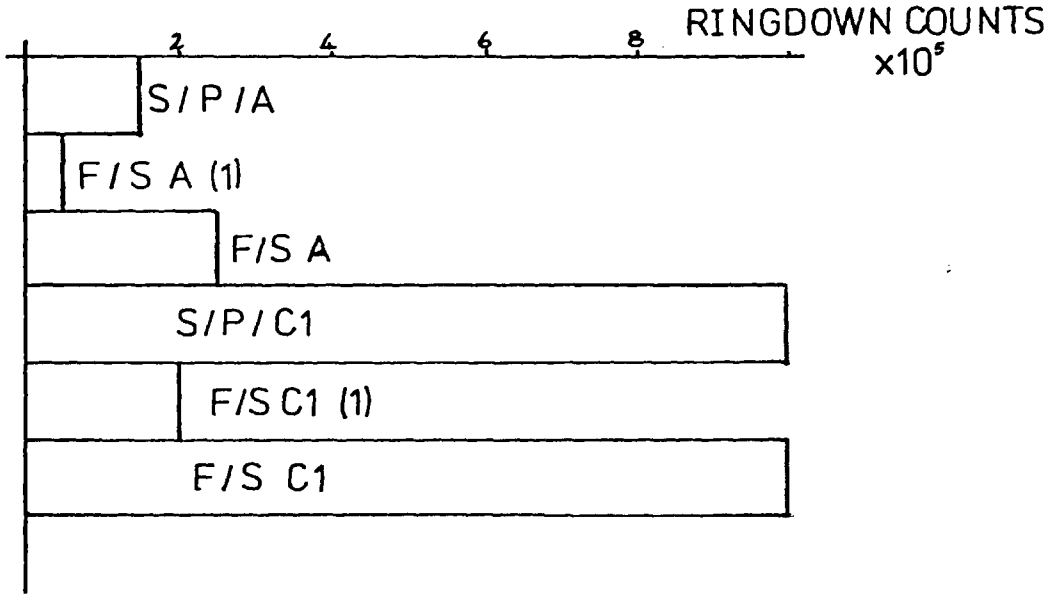

FIGURE 5·5 D

Histogram showing differences in total events and counts between systems with coats on one or both sides.

FIGURE 5.6A

The events vs. strain curves showing the effect of immersion prior to testing on the acoustic emission of the systems containing an anodic electrocoat. The events are on a logarithmic scale.

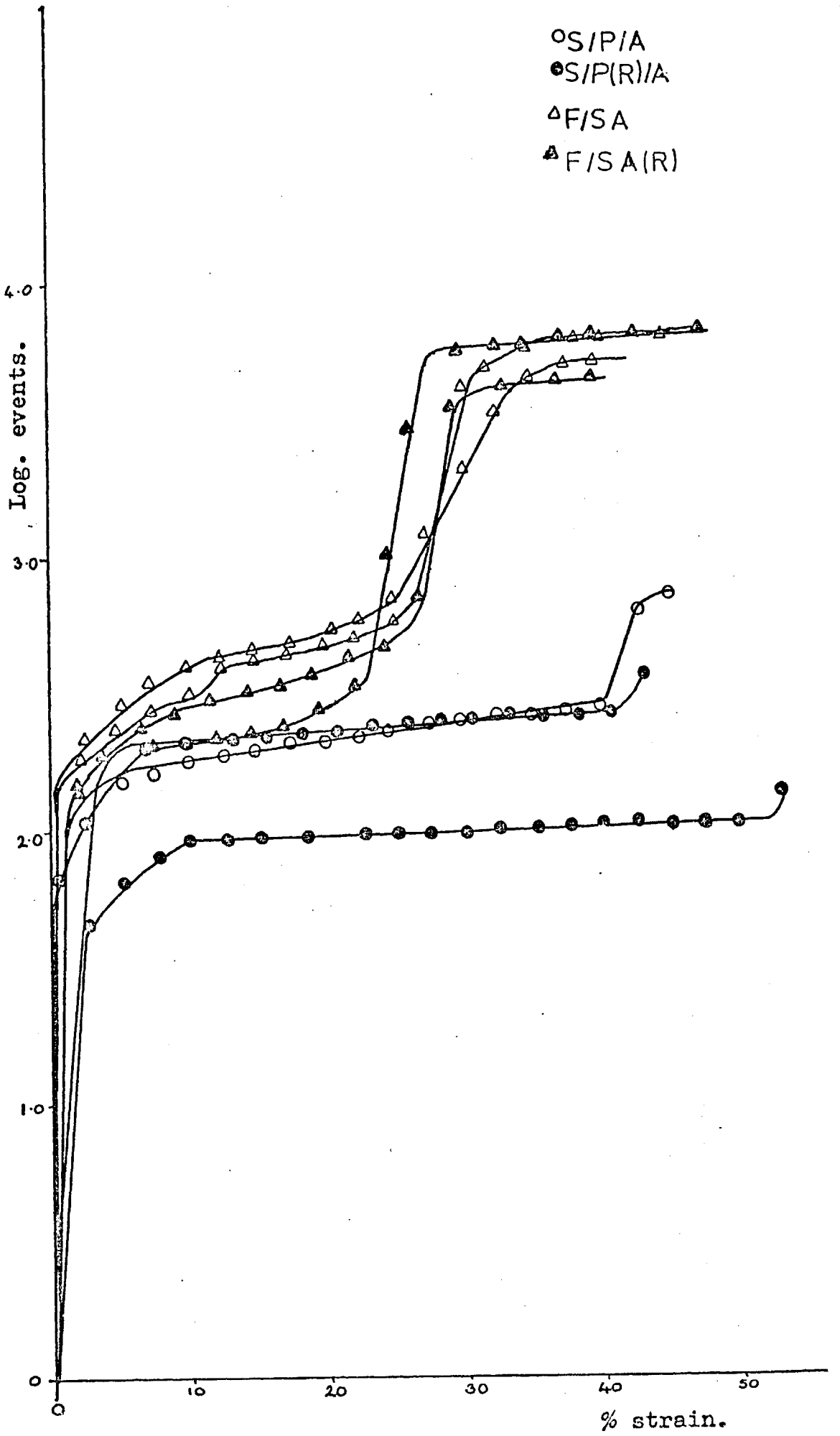
○S/P/A
●S/P(R)/A
△F/SA
▲F/SA(R)
Log. events.
4·0
3·0
2·0
1·0
0
0
10
20
30
40
50
% strain.

FIGURE 5.6B

The events vs. strain curves for S/P/Cl and F/S Cl showing the effect of immersion prior to testing on the systems containing the cathodic 1 electrocoat.

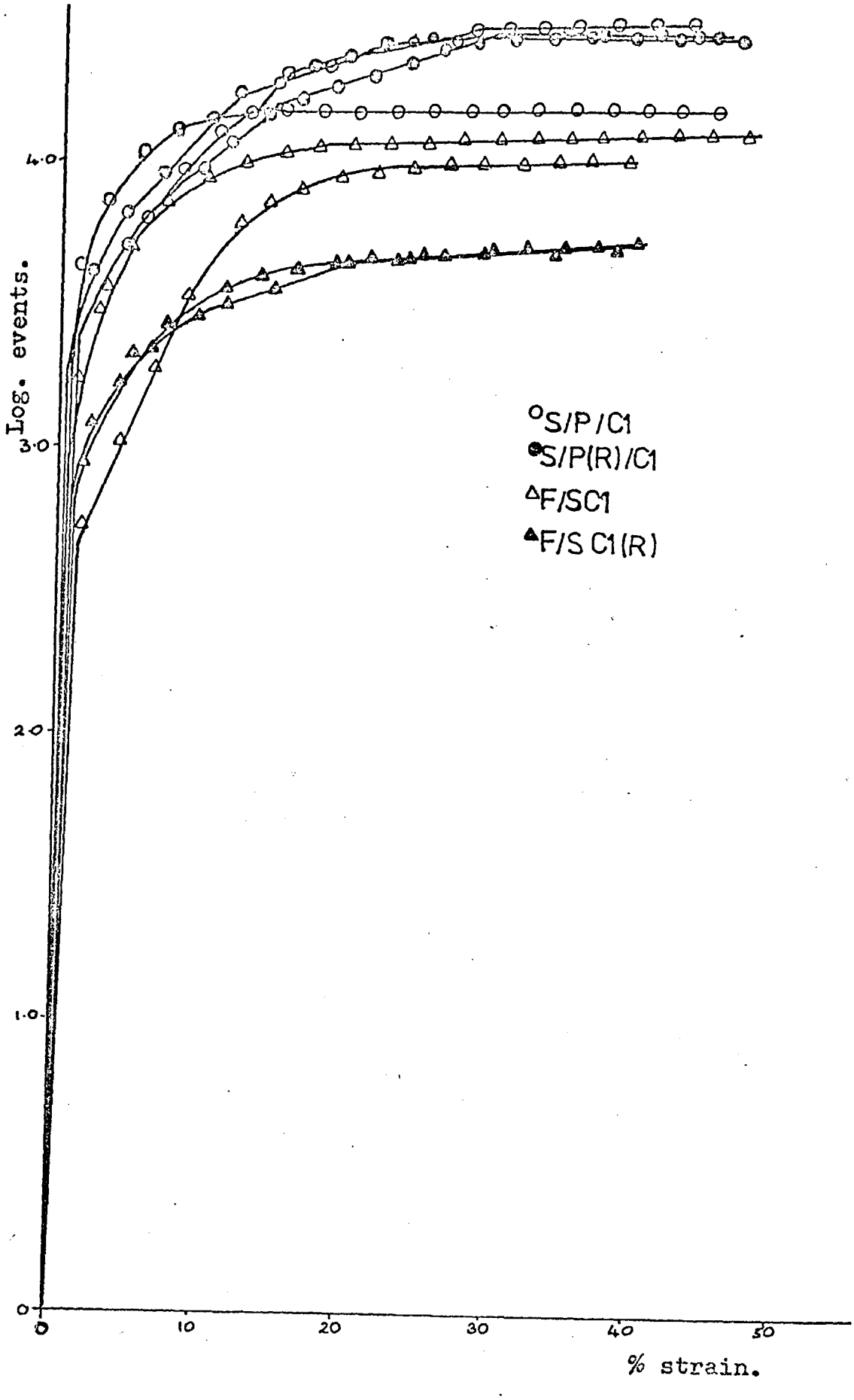
Log. events.
4·0
3·0
2·0
1·0
0
0
10
20
30
40
50
% strain.
°S/P/C1
•S/P(R)/C1
△F/SC1
▲F/S C1(R)

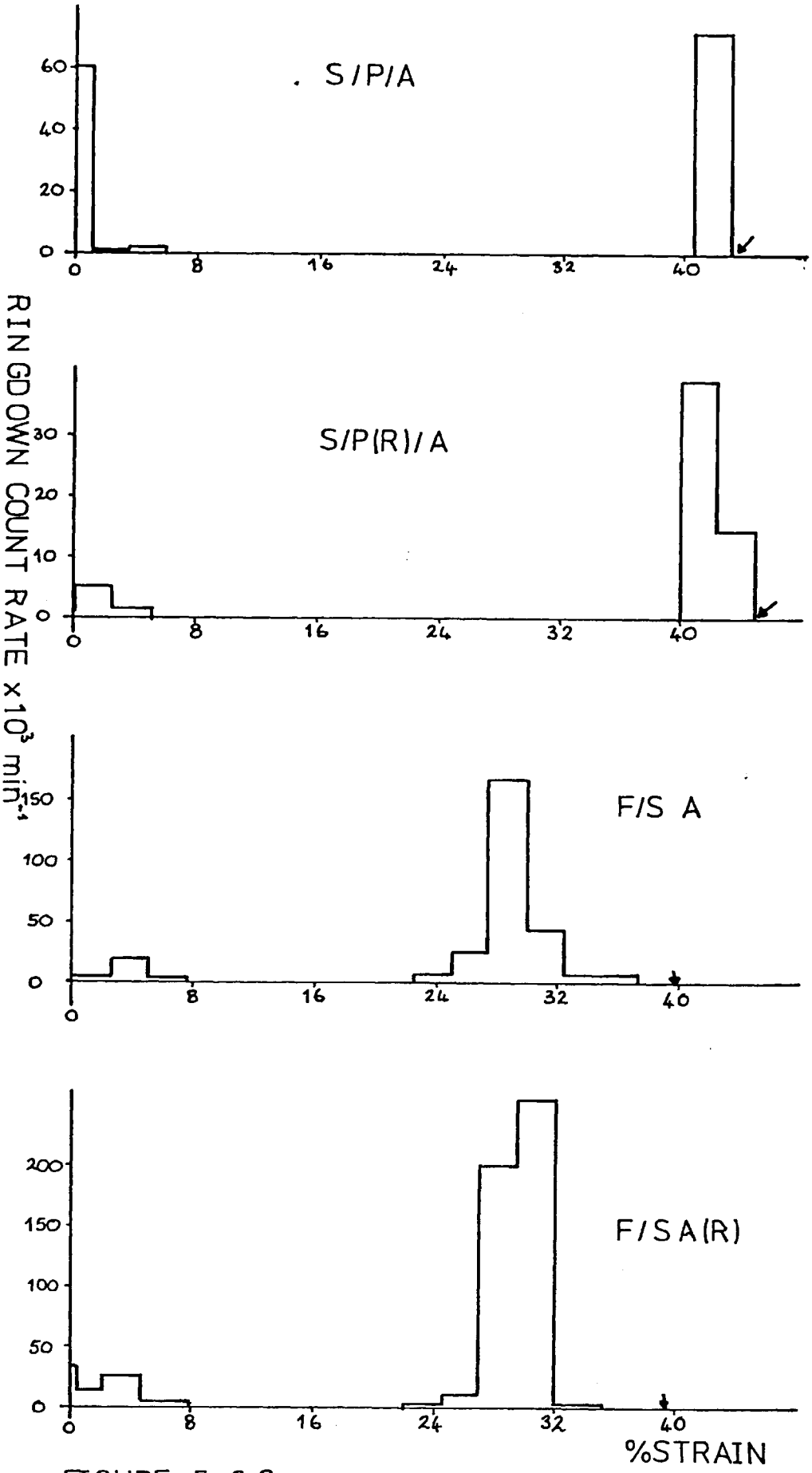

FIGURE 5.6 C

Ringdown count vs strain curves for the systems with anodic electrocoats after immersion.

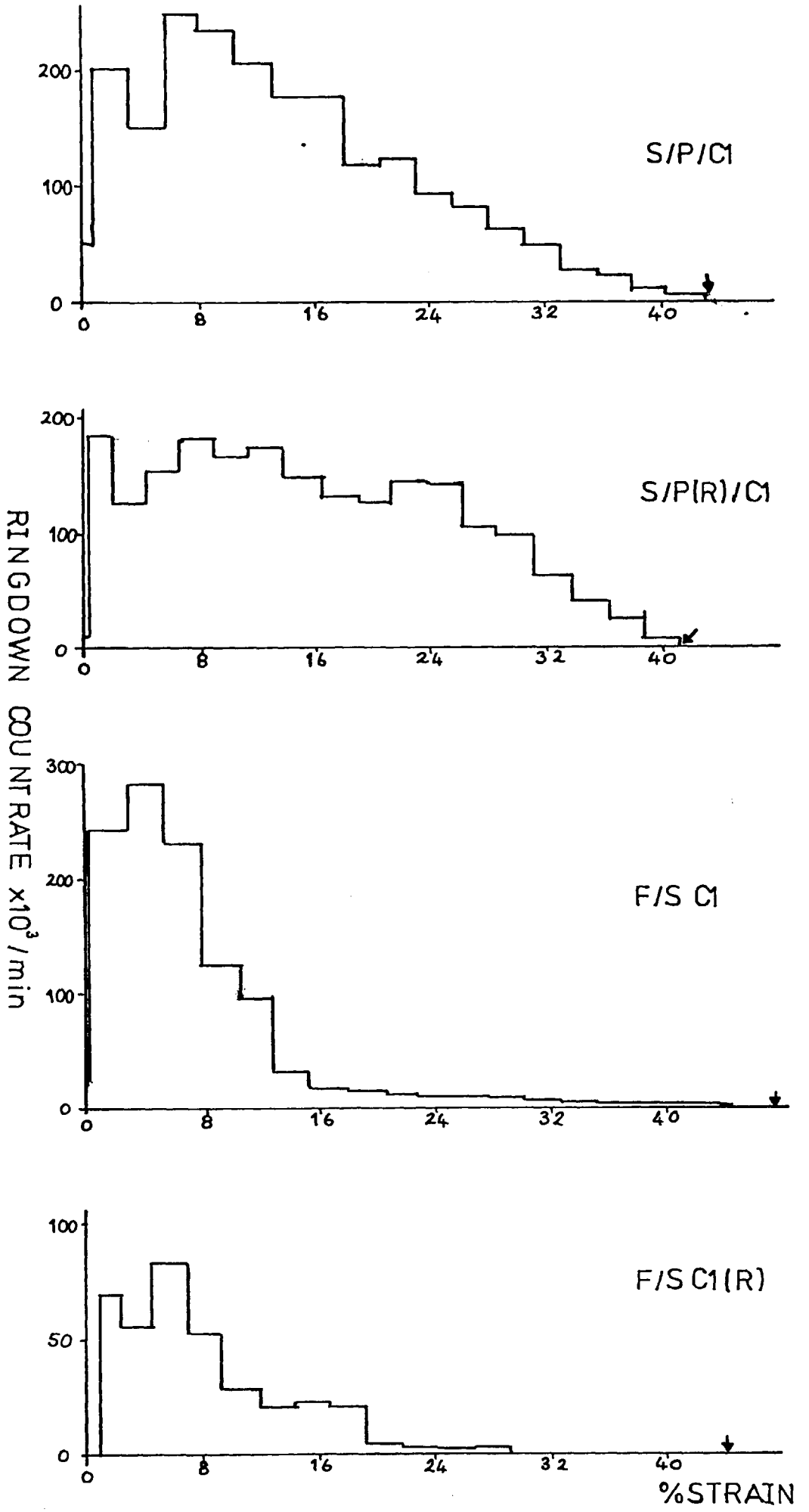

FIGURE 5·6D
Ringdown count rate curves for systems with a cathodic 1 electrocoat after immersion.

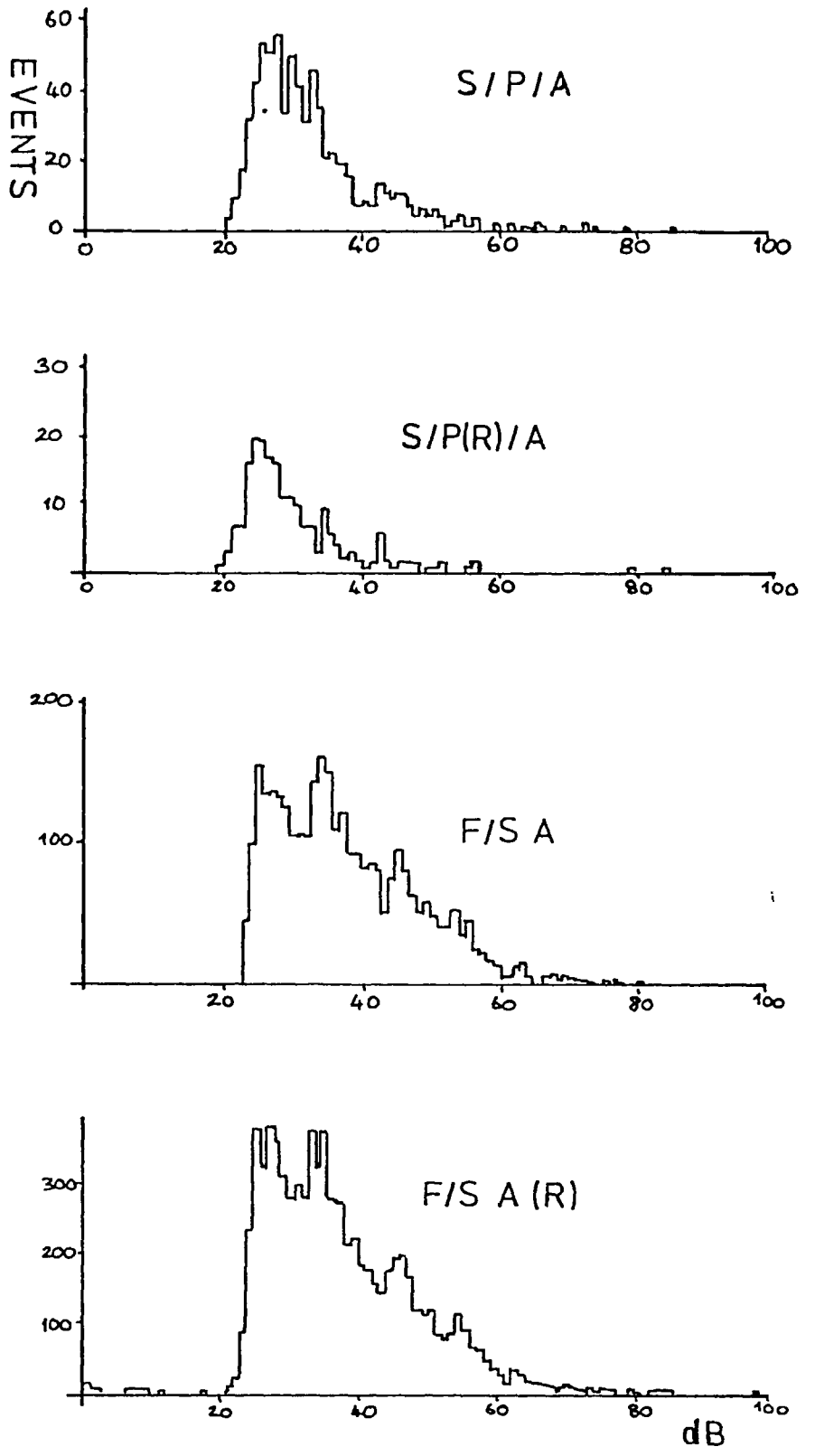

FIGURE 5·6E

Typical amplitude distributions for systems with an anodic electrocoat after immersion.

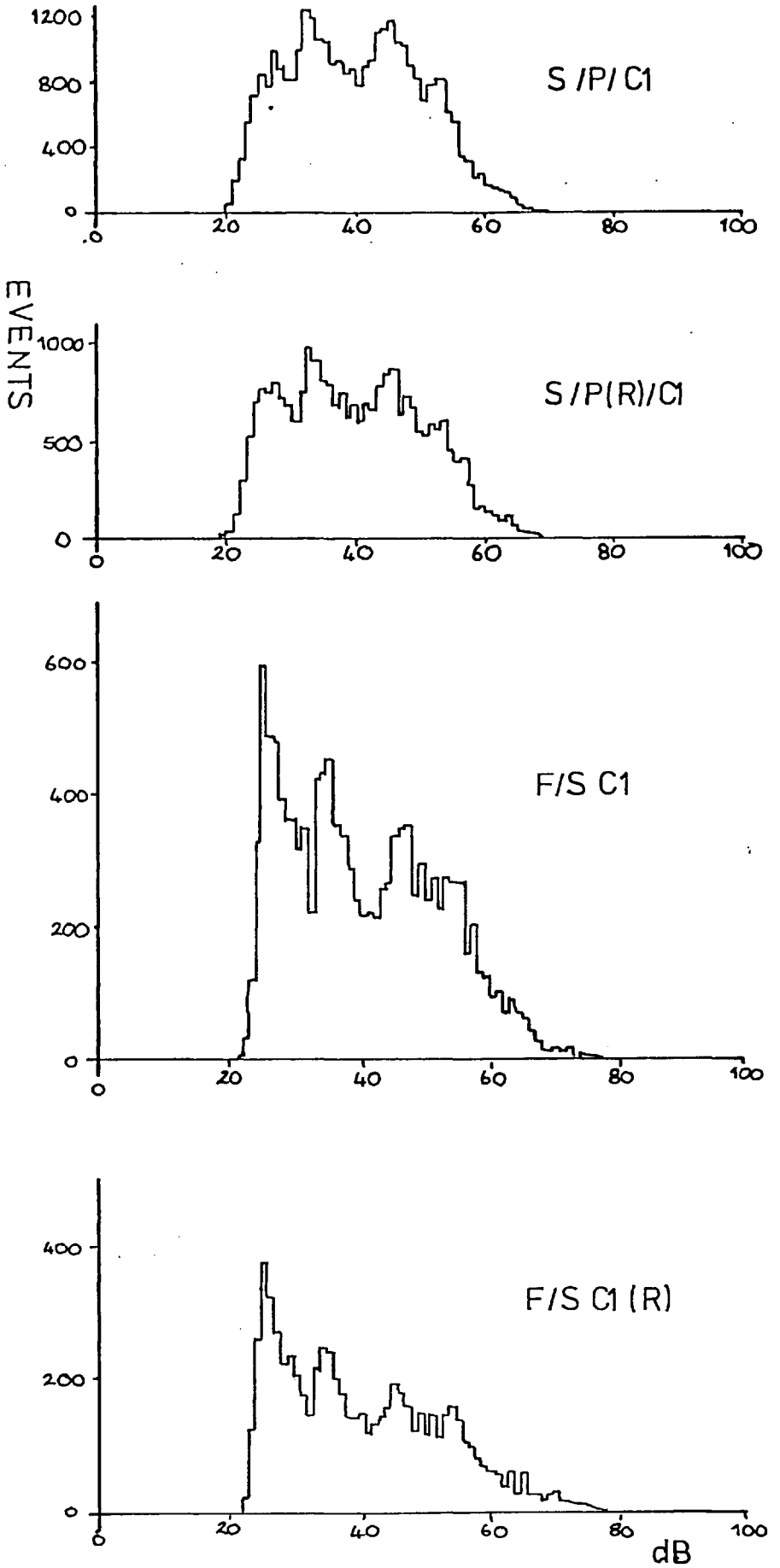

FIGURE 5·6F

Typical amplitude distributions for systems with a cathodic coat after immersion.

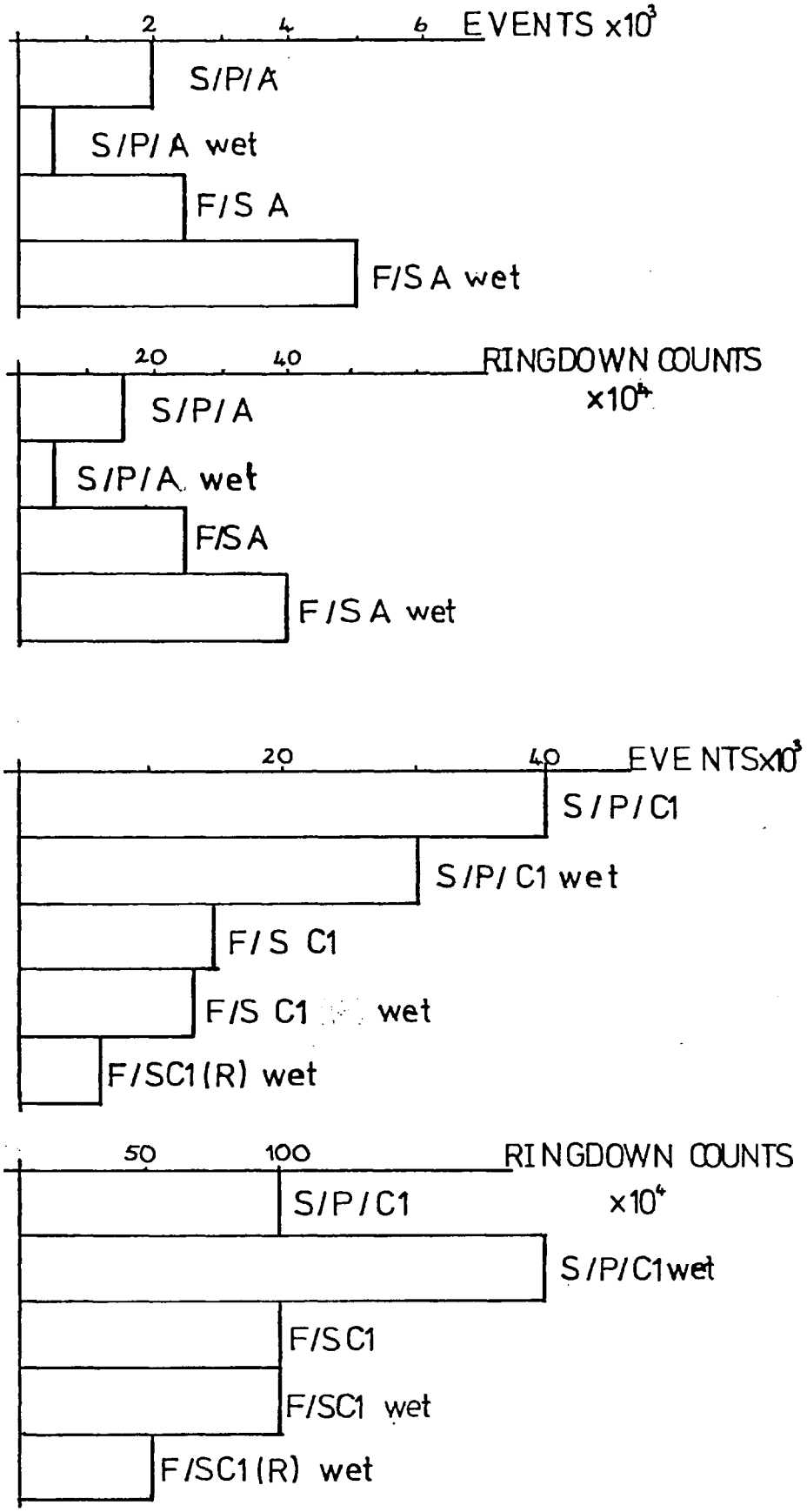

FIGURE 5 6G Histograms showing differences in total events and counts between wet and dry systems.

FIGURE5.7A

The events vs. strain curves showing the differences between the various phosphates. The events are not on a logarithmic scale in this case.

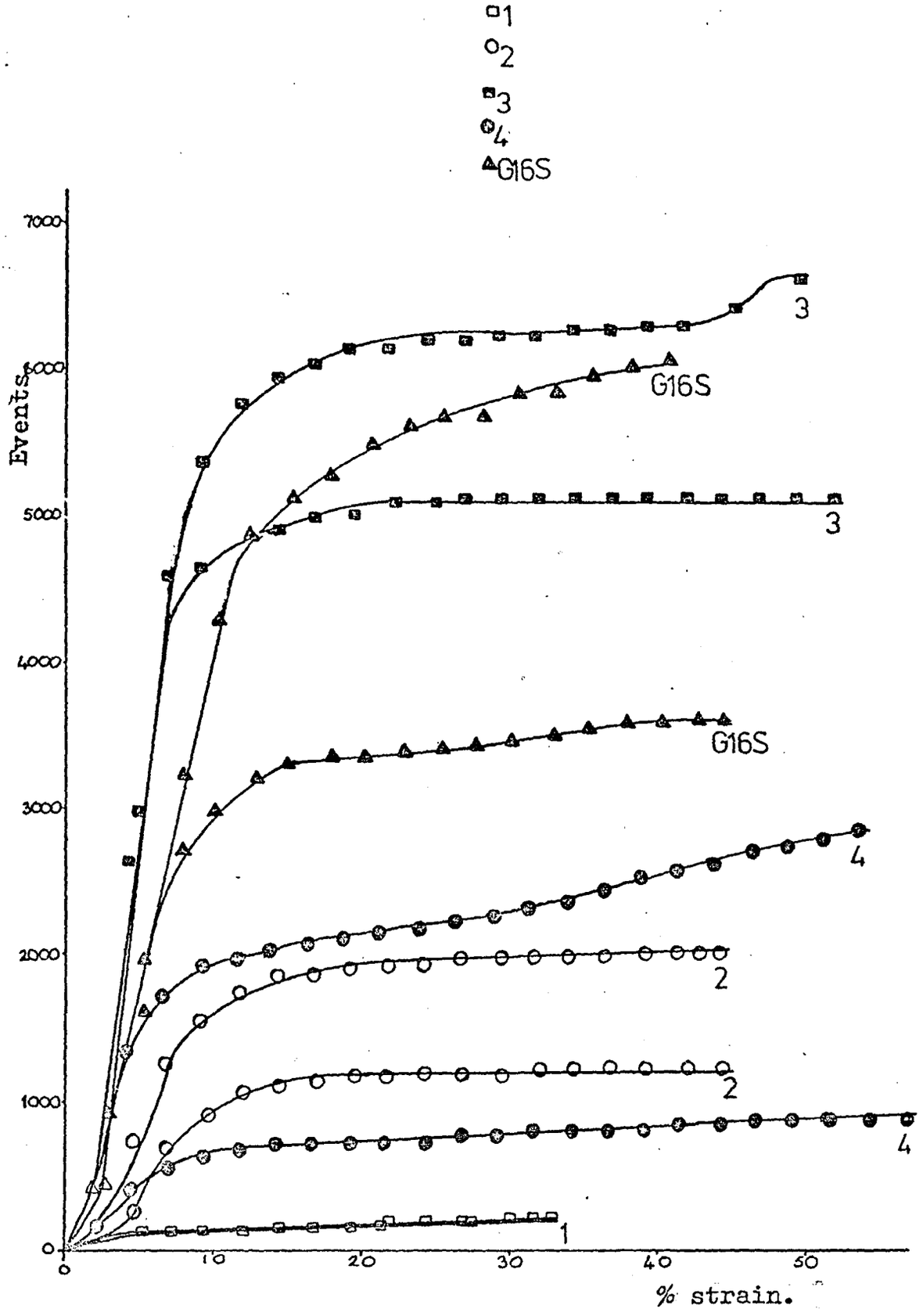

Figure 5.7A Events vs. strain curves for the various phosphate coats.

FIGURE 5.7B

The events vs. strain curves showing the differences between the various phosphates with an anodic electrocoat. The events are not on a logarithmic scale in this case.

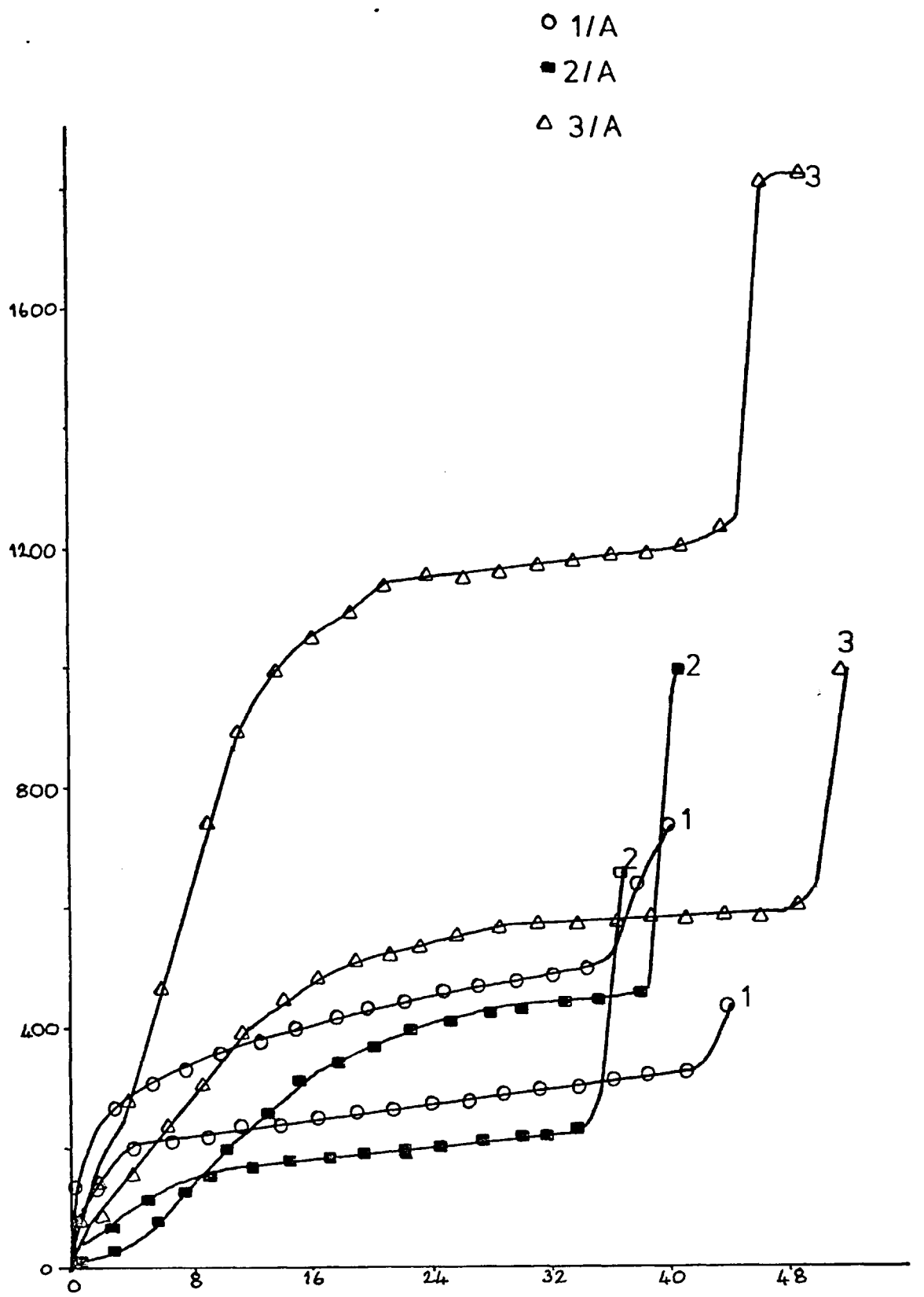
1/A
2/A
3/A
1600
1200
800
400
0
0
8
16
24
32
40
48
1
2
3
1
2
3

FIGURE 5.7C

The events vs. strain curves showing the differences between the various phosphates with a cathodic 2 electrocoat. The events are on a logarithmic scale.

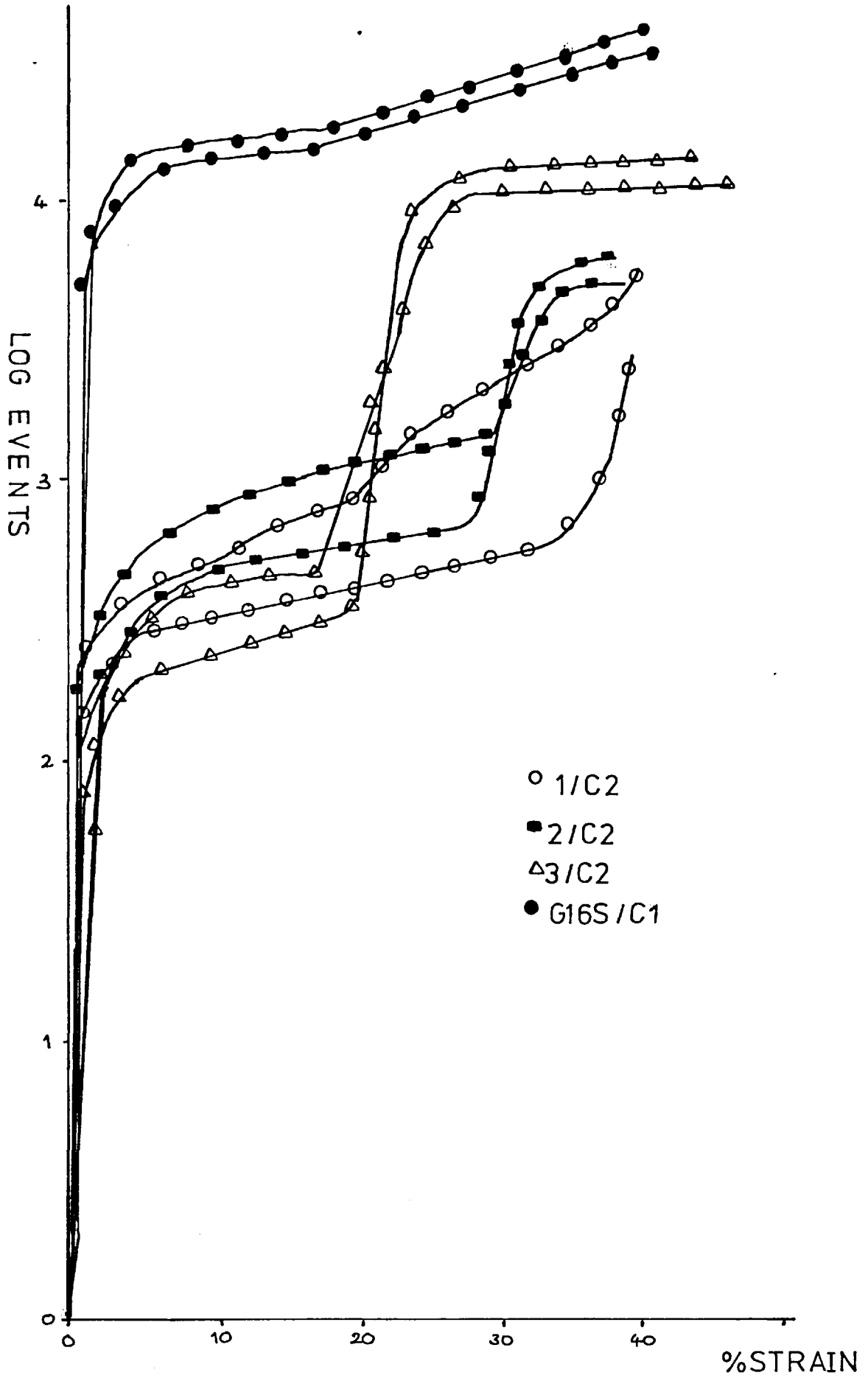
LOG EVENTS
0
1
2
3
4
0
10
20
30
40
%STRAIN
1/C2
2/C2
3/C2
G16S/C1

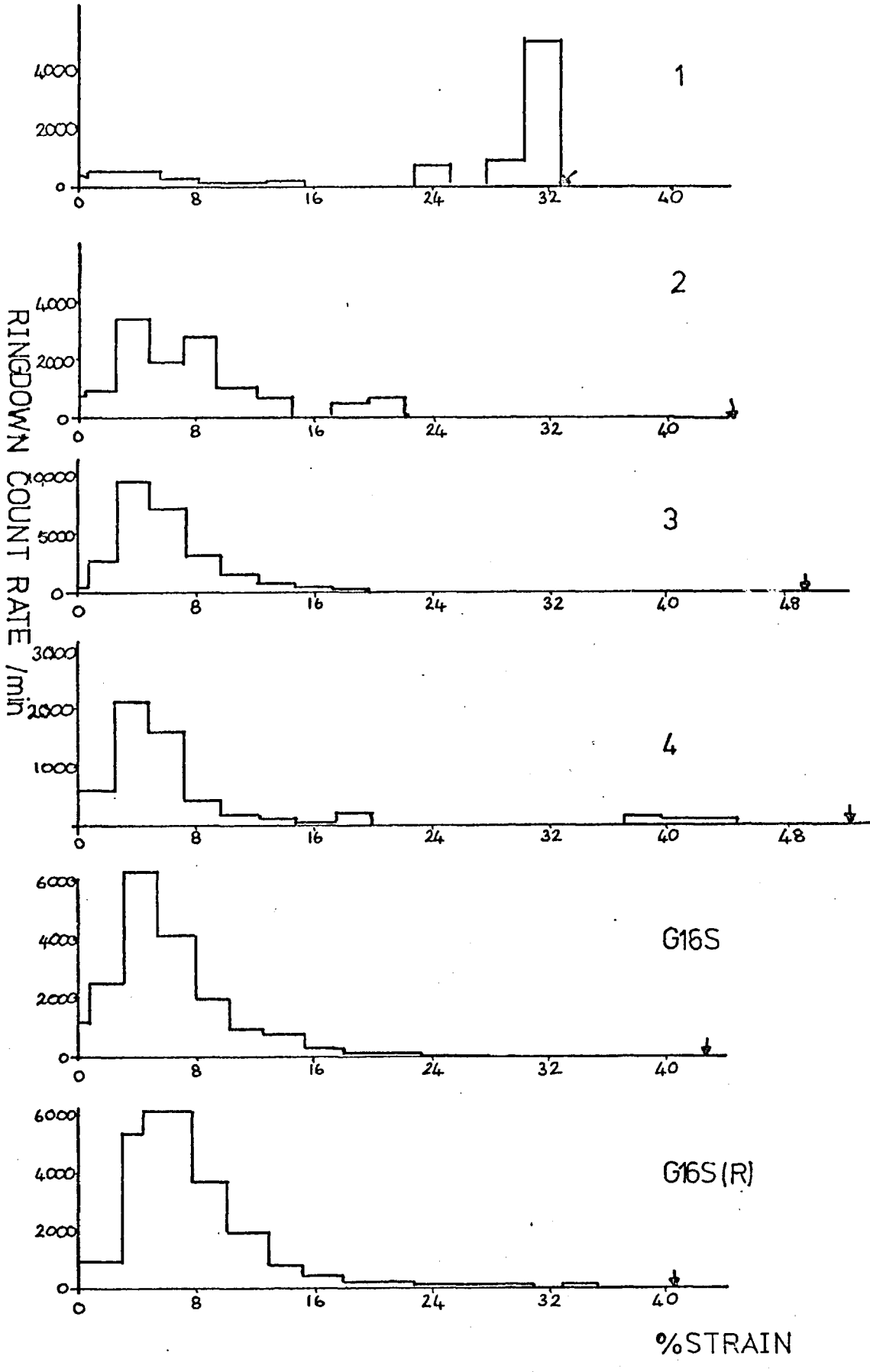

Figure 5.7D.

The ringdown count rate vs. strain curves showing the differences in acoustic emission between the various phosphates.

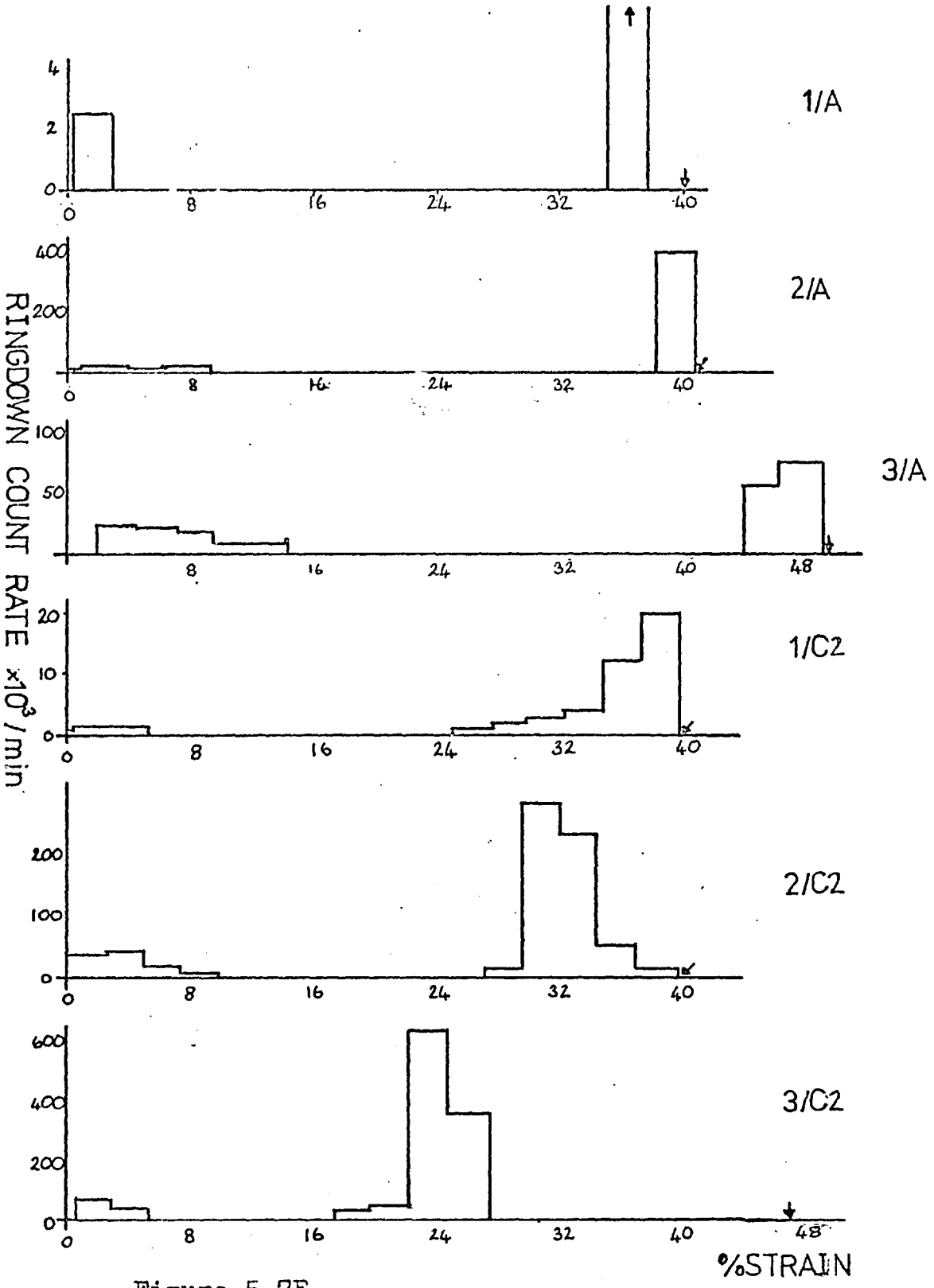

Figure 5.7E.

The ringdown count rate vs. strain curves showing differences in the acoustic emission between anodic and cathodic 2 electrocoats on the various phosphates.

FIGURE 5.7G

The amplitude distributions for the various phosphates.

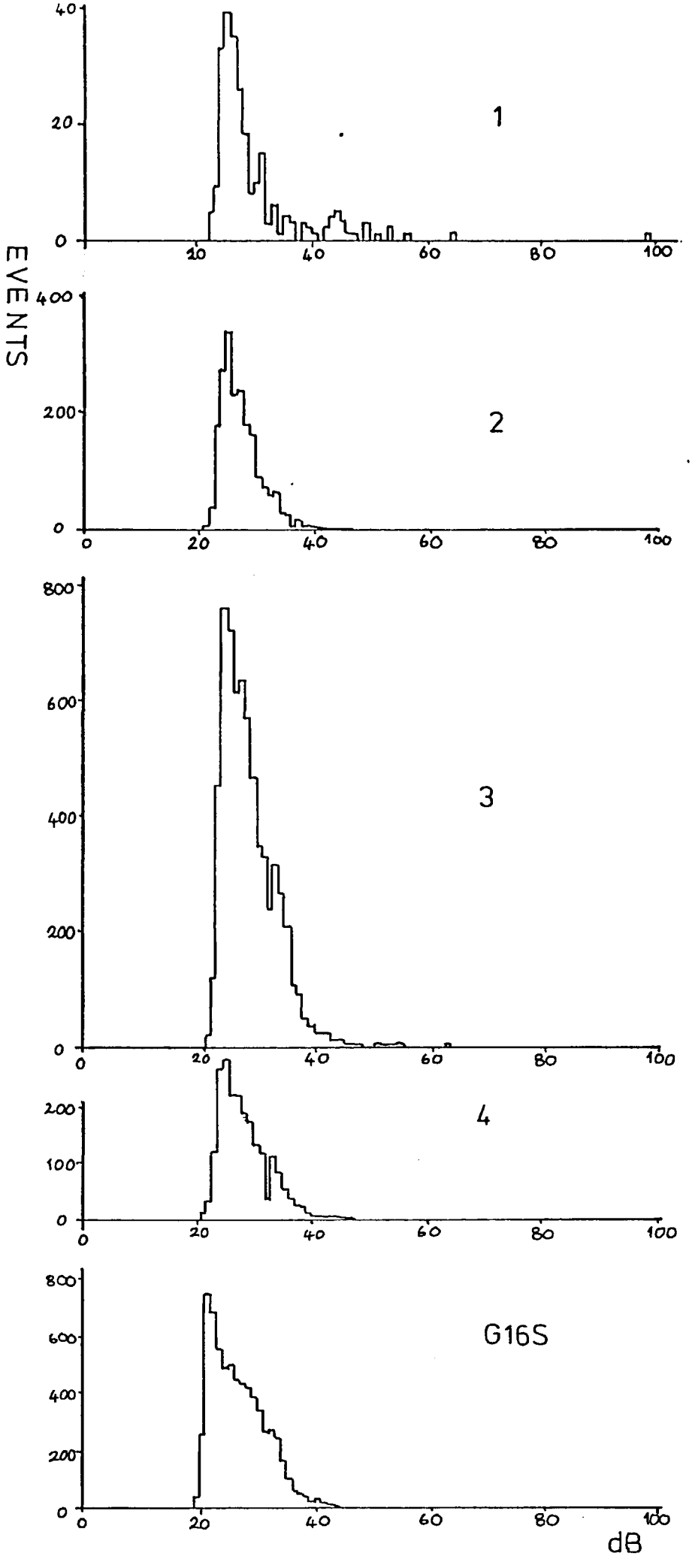
EVENTS
1
2
3
4
G16S
dB
0
20
40
60
80
100
200
400
600
800

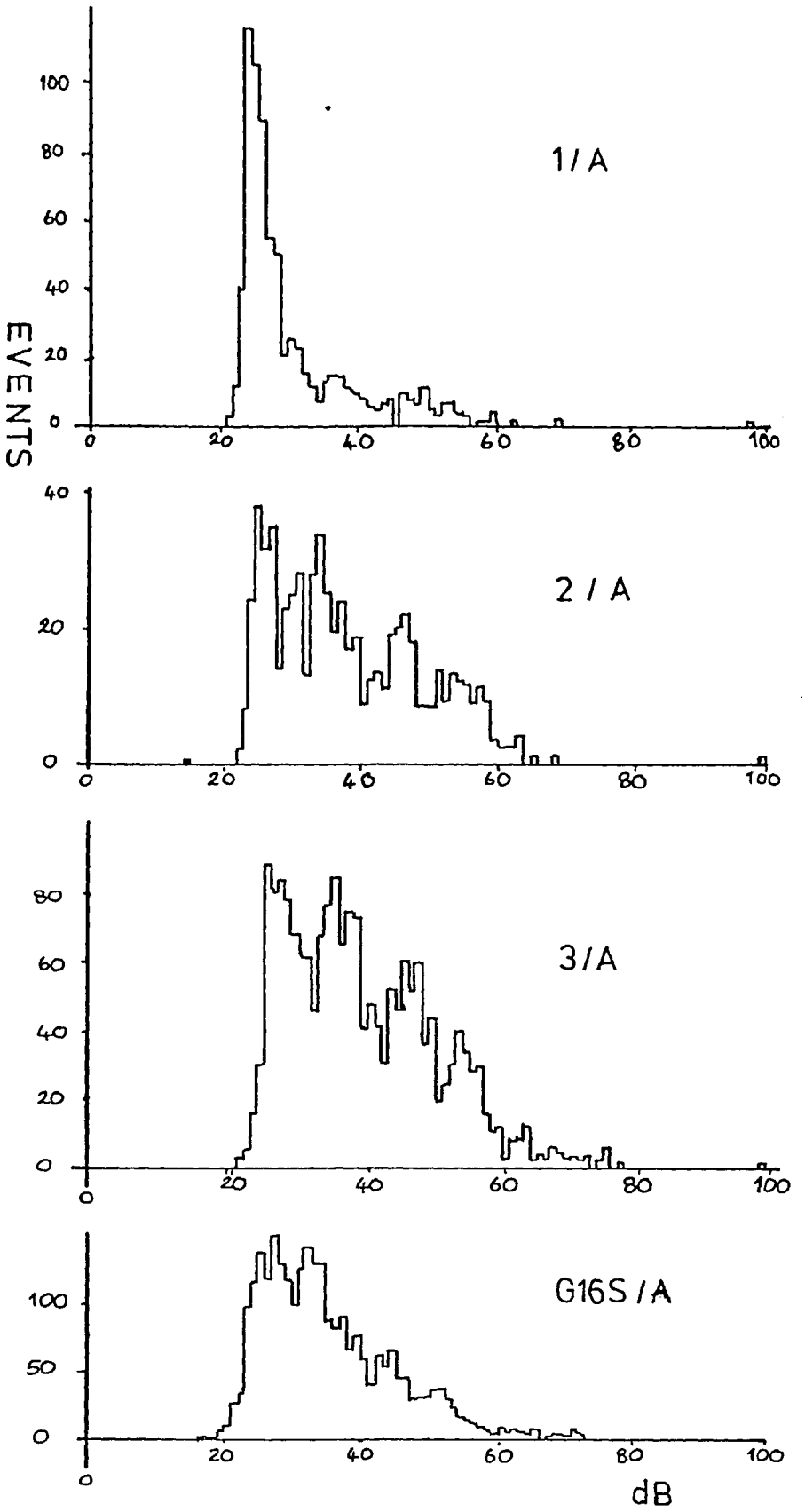

FIGURE 5·7 H

Typical amplitude distributions from systems with anodic coat on various phosphates.

FIGURE 5.71

The amplitude distributions for the various phosphates with a cathodic 2 electrocoat.

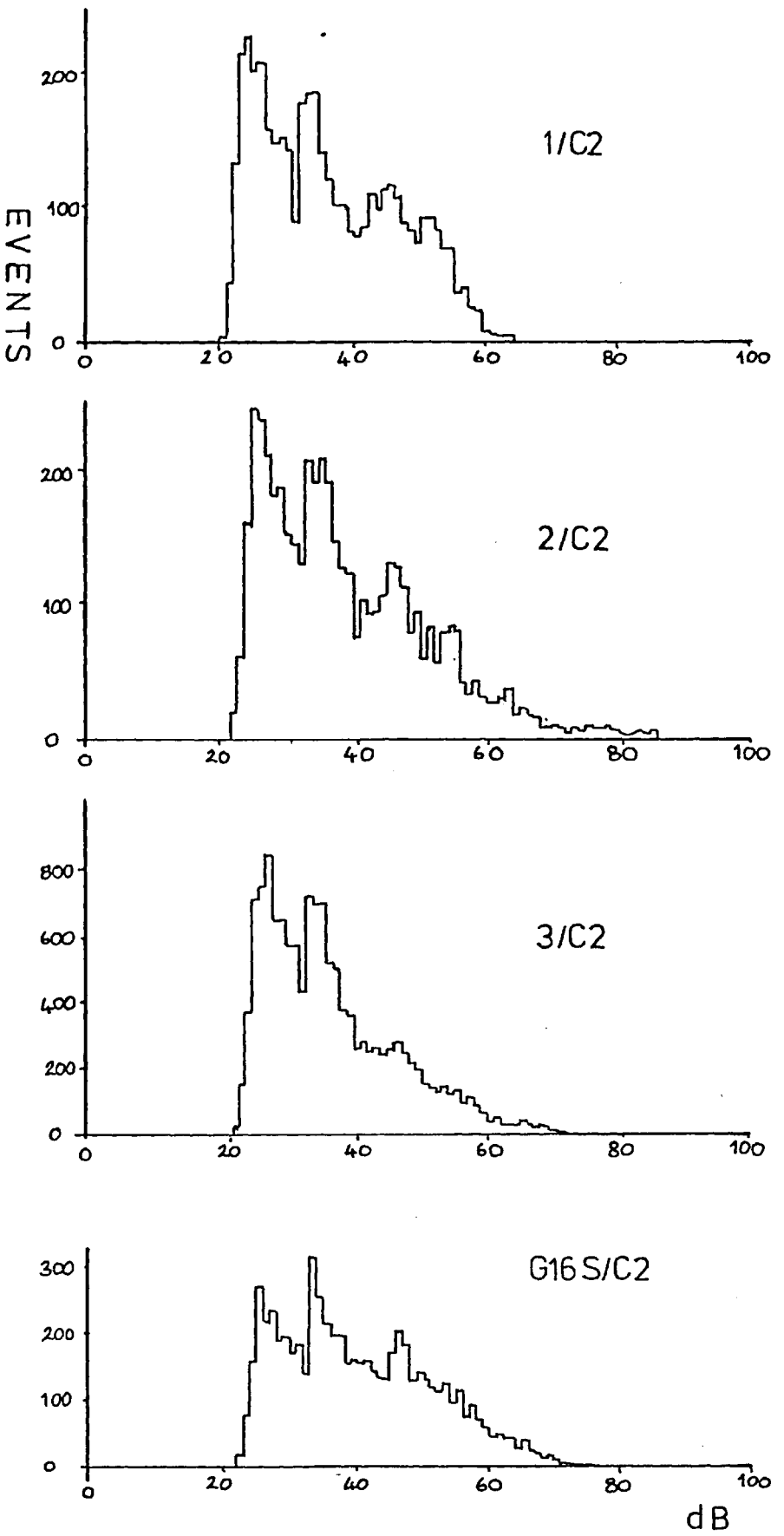
EVENTS
1/C2
2/C2
3/C2
G16 S/C2
dB
0
20
40
60
80
100
200
400
600
800
300

FIGURE 5.7J

Histogram showing the differences in the total events and ringdown counts to failure between the various phosphates and as anodic and cathodic 2 coats are added to the various phosphates.

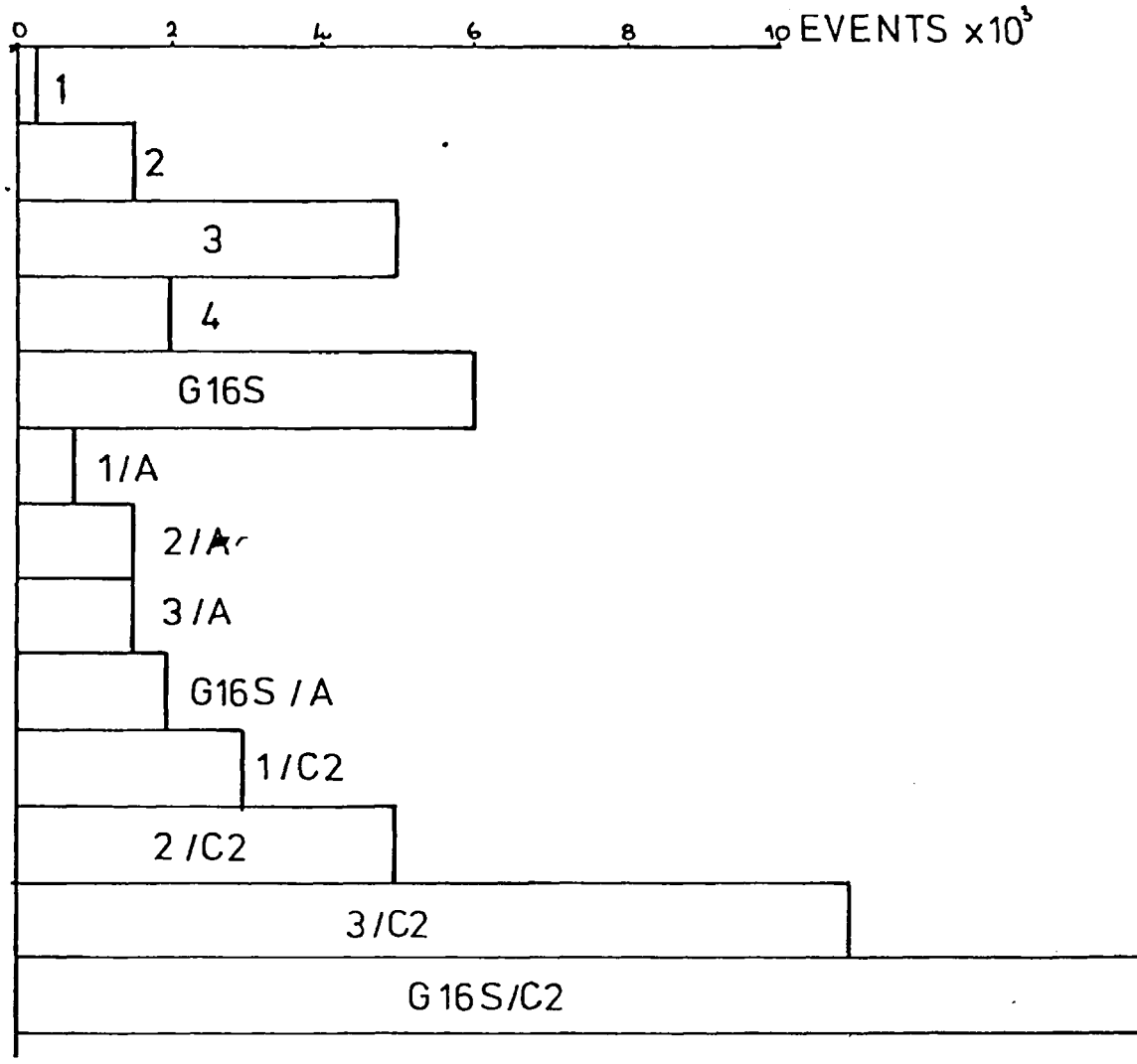
0
2
4
6
8
10
EVENTS x10³
1
2
3
4
G16S
1/A
2/A
3/A
G16S/A
1/C2
2/C2
3/C2
G16S/C2

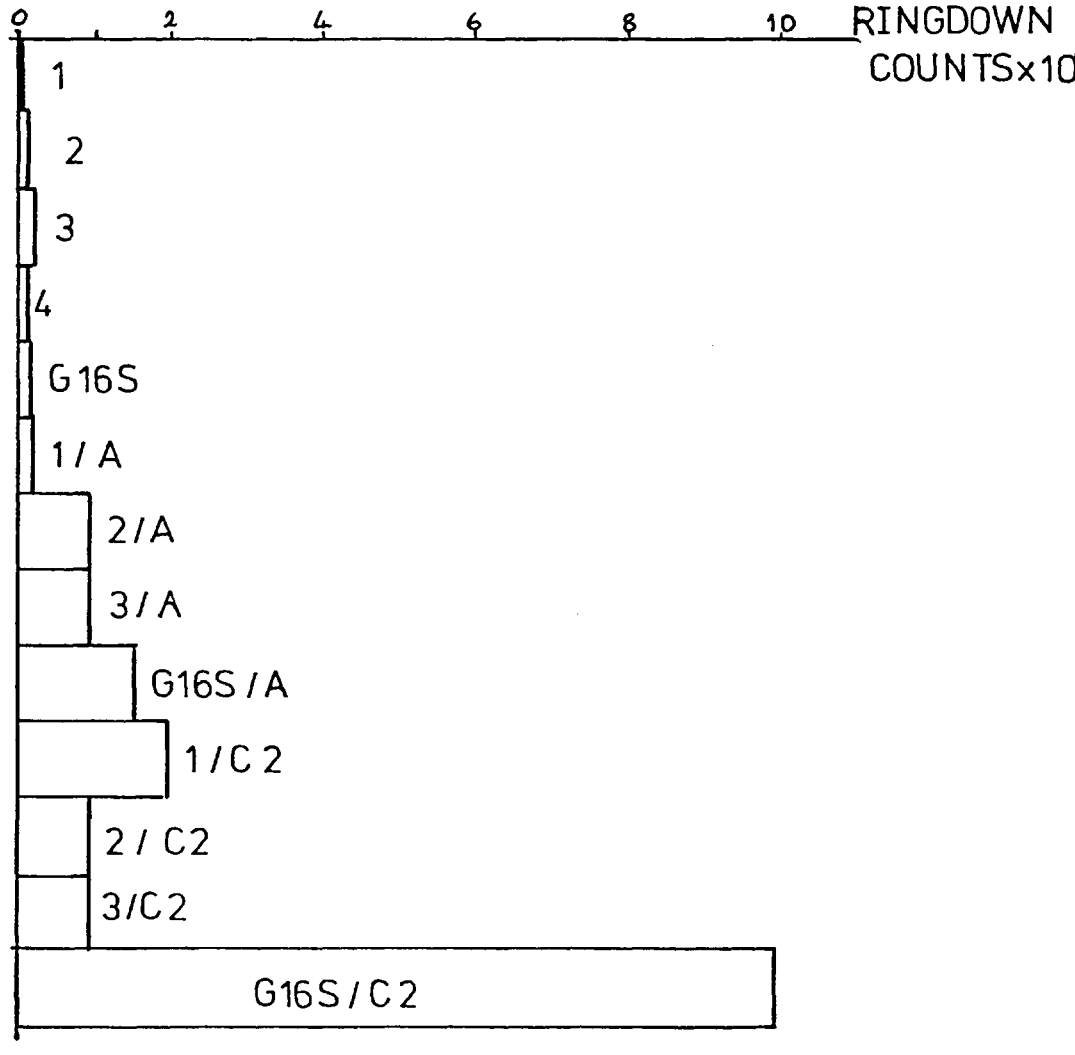
0
2
4
6
8
10
RINGDOWN COUNTS x10⁶
1
2
3
4
G16S
1/A
2/A
3/A
G16S/A
1/C2
2/C2
3/C2
G16S/C2

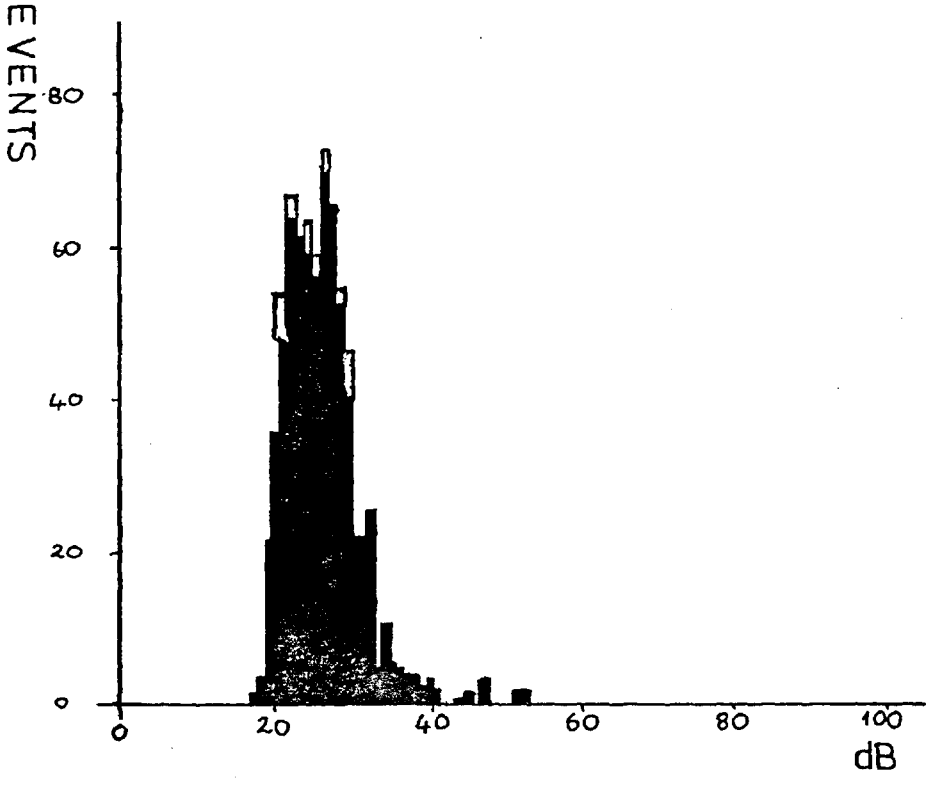

FIGURE 5.8 A

The amplitude distribution for S/P. With the distribution at 15% strain shaded.

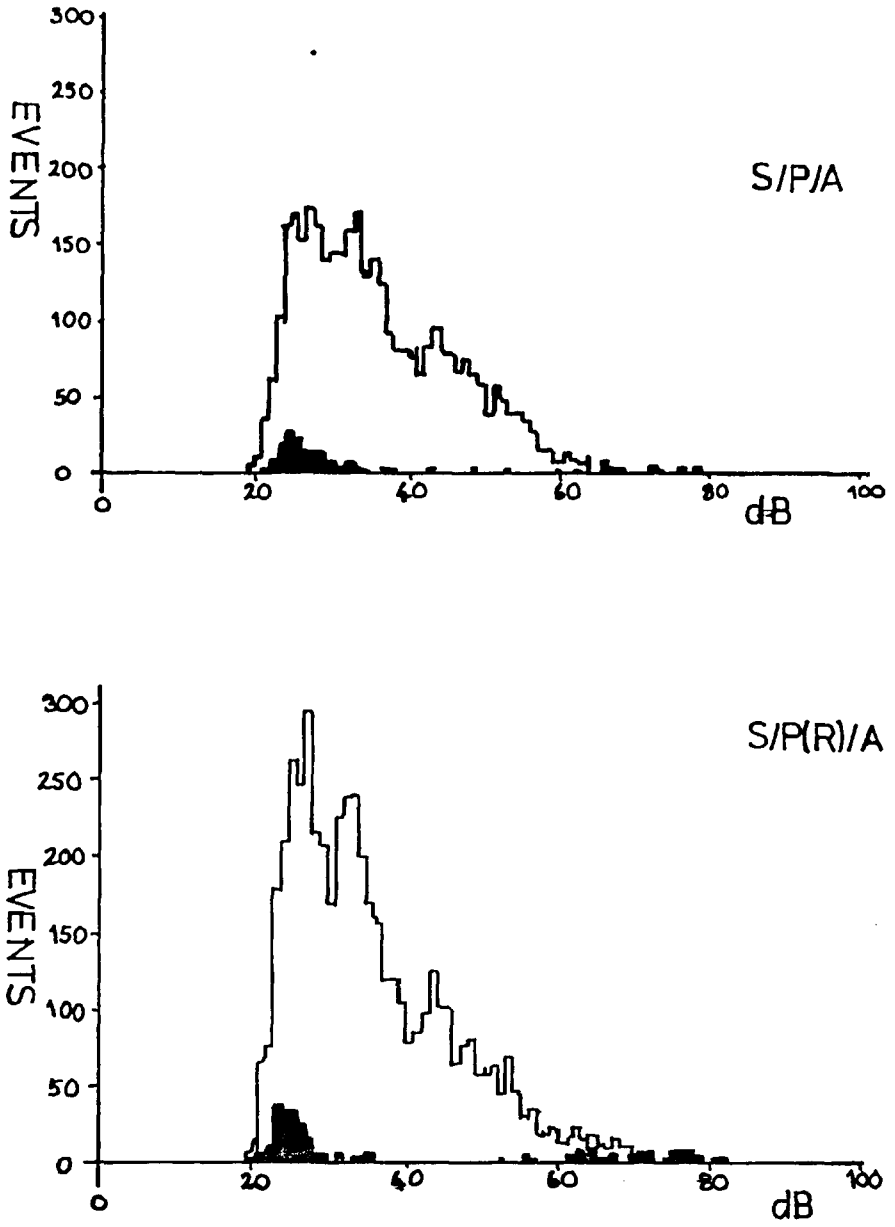

FIGURE 5·8 B

Amplitude distributions for the anodic coats with distributions at 8% strain shaded.

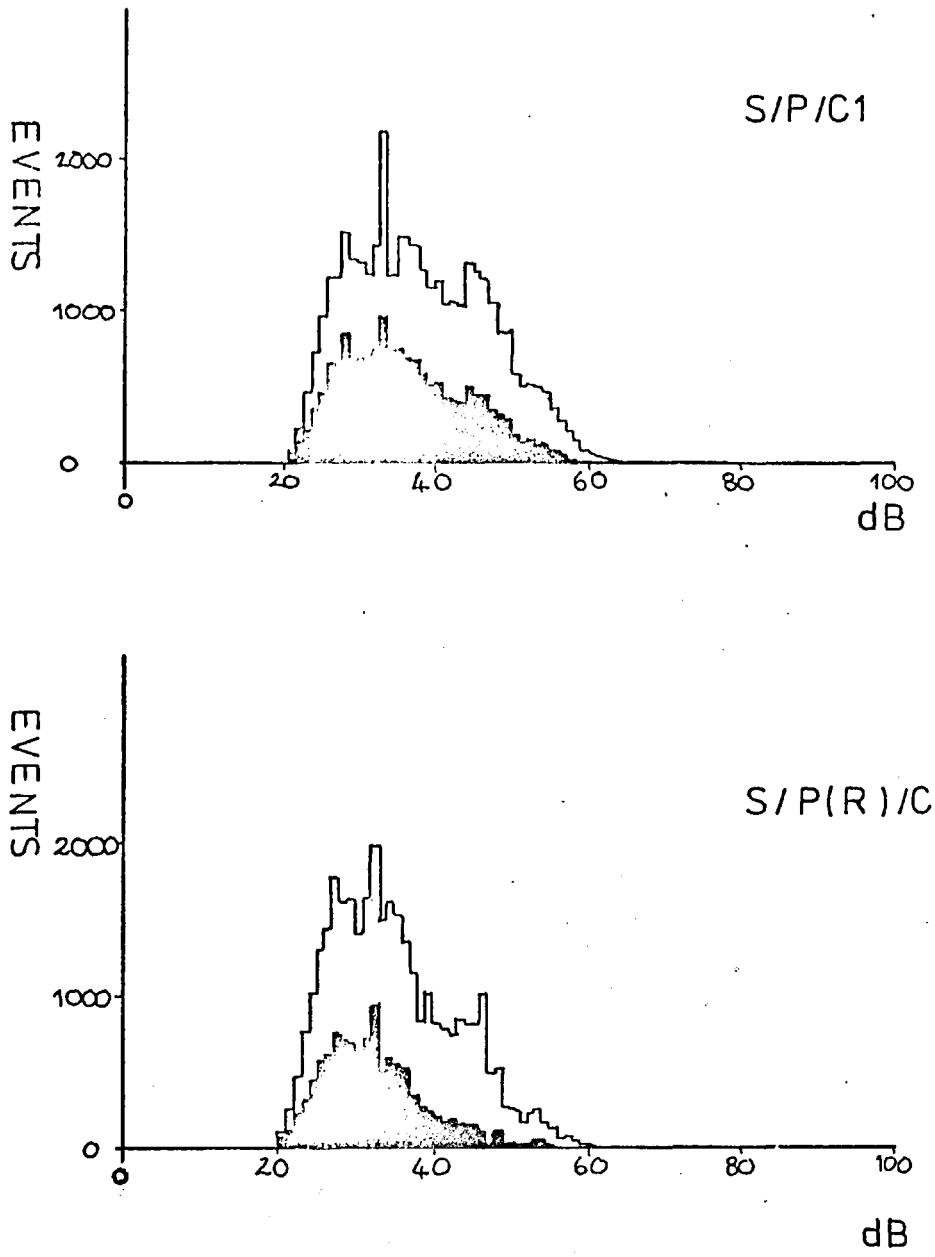

FIGURE 5·8C

Amplitude distributions for S/P/C1 and S/P(R)/C1 with the distributions at 10 and 5% strains shaded respectively.

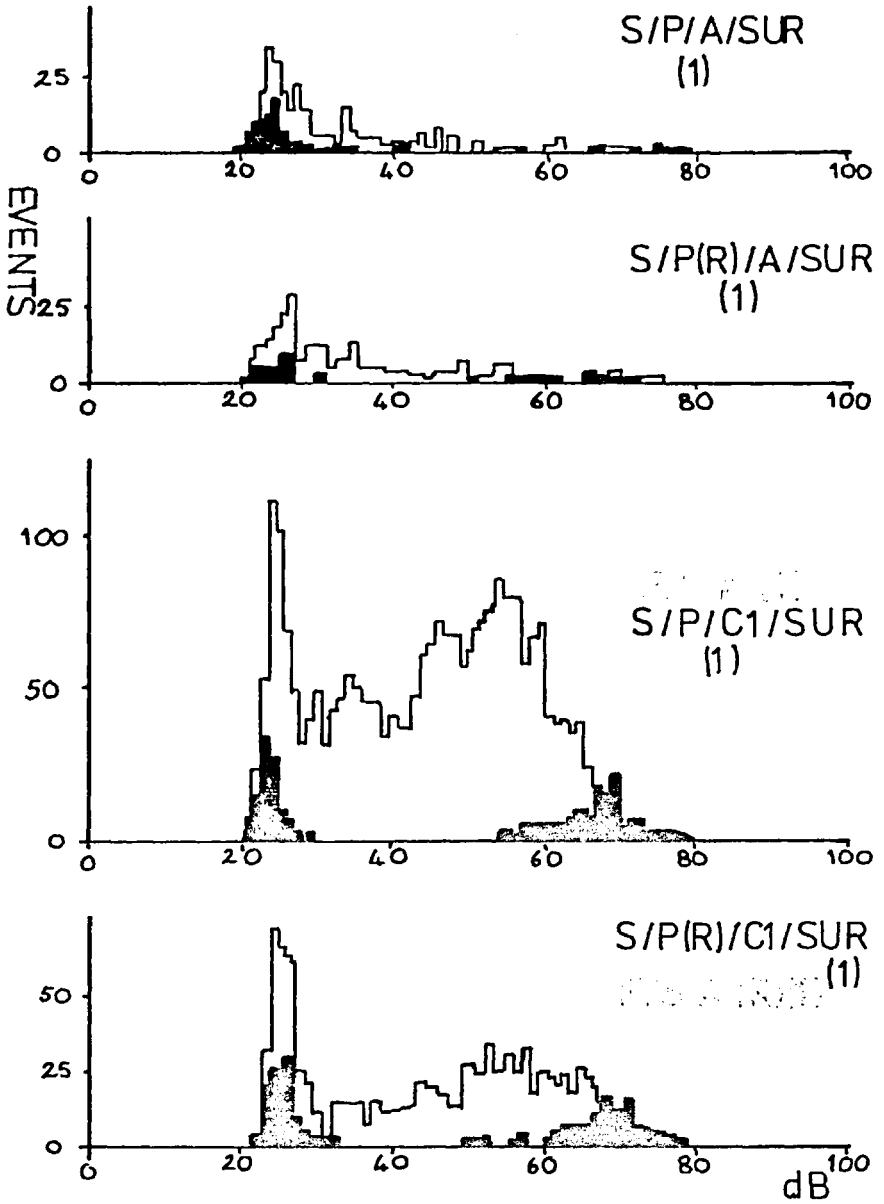

FIGURE 5·8 D

Typical amplitude distributions for systems with a surfacer coat with the distributions at 10% strain shaded.

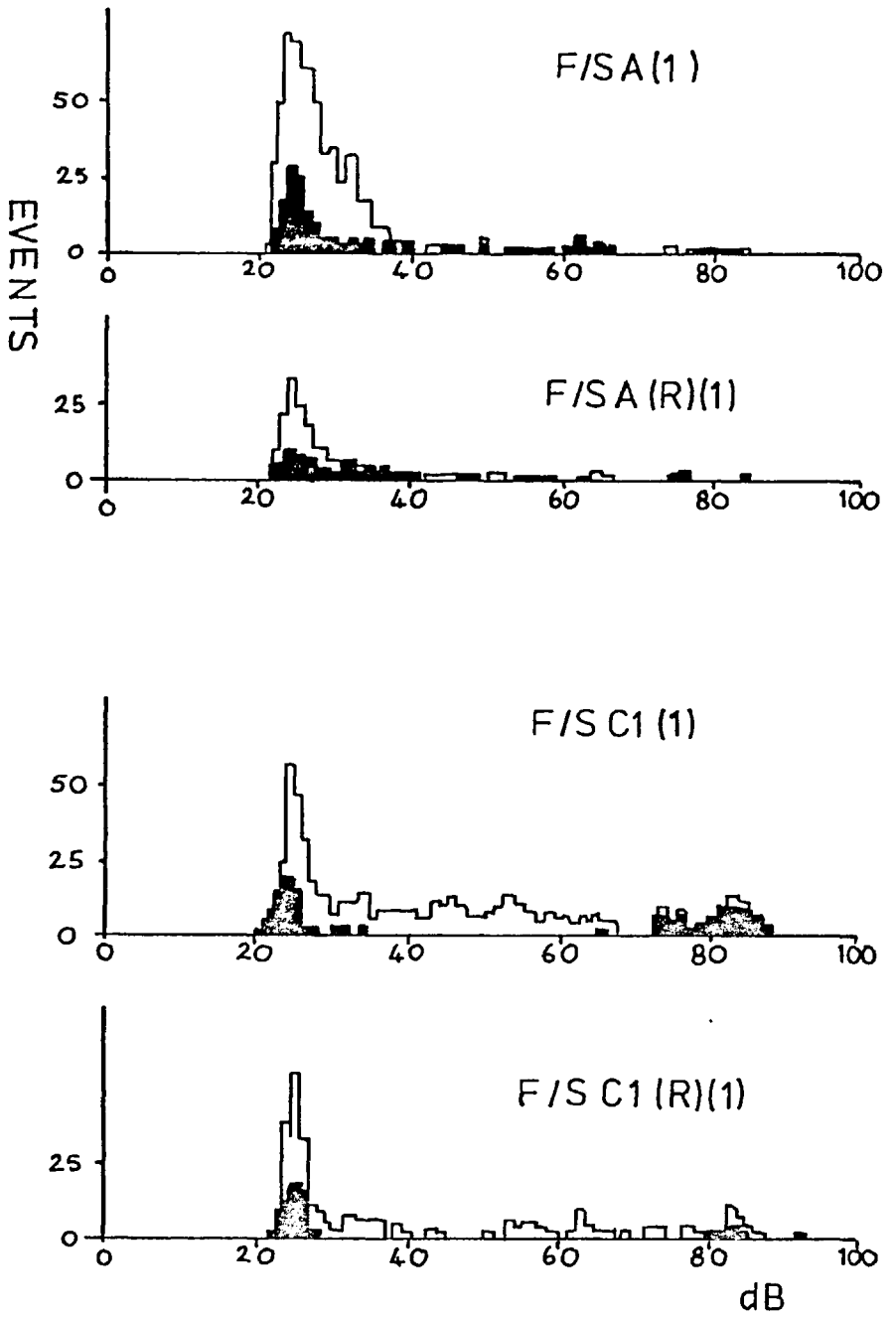

FIGURE 5·8E

Amplitude distributions for the full systems with the distributions at 10% strain shaded (15% for F/S A (1)).

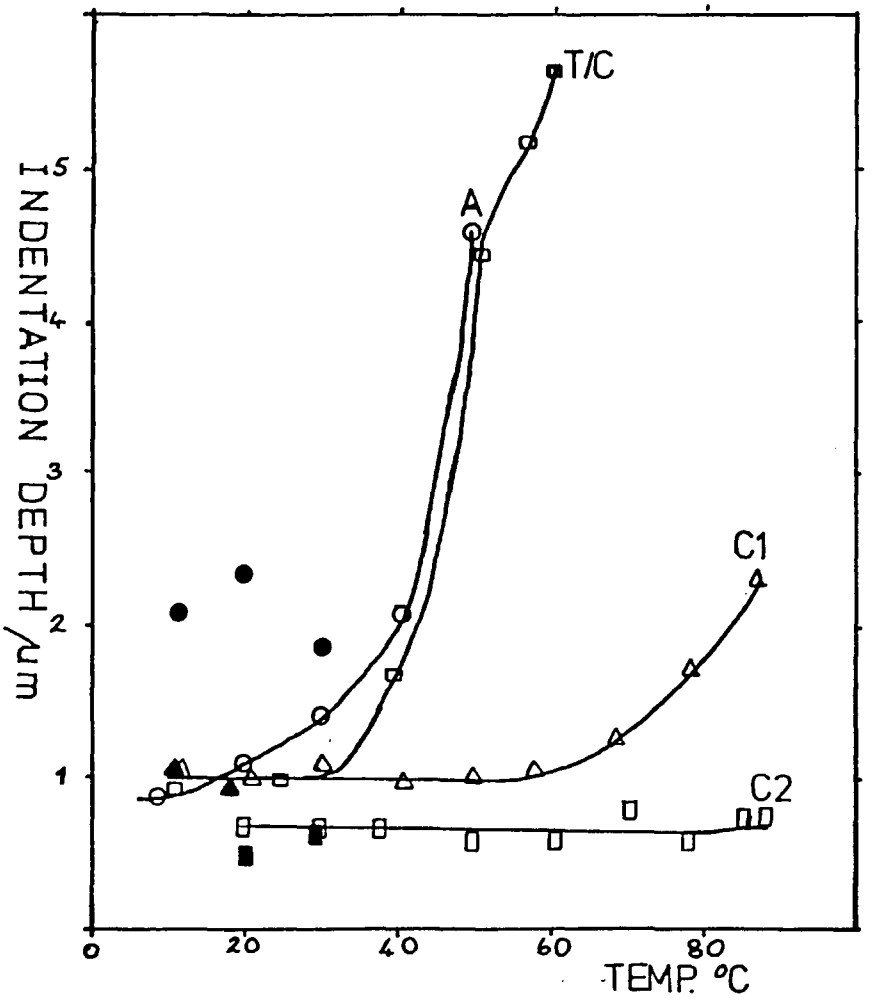

FIGURE 5·10A.

Curves to determine the glass transition temperatures for the coatings.

○ A

△ C1

□ C2

▫ T/C

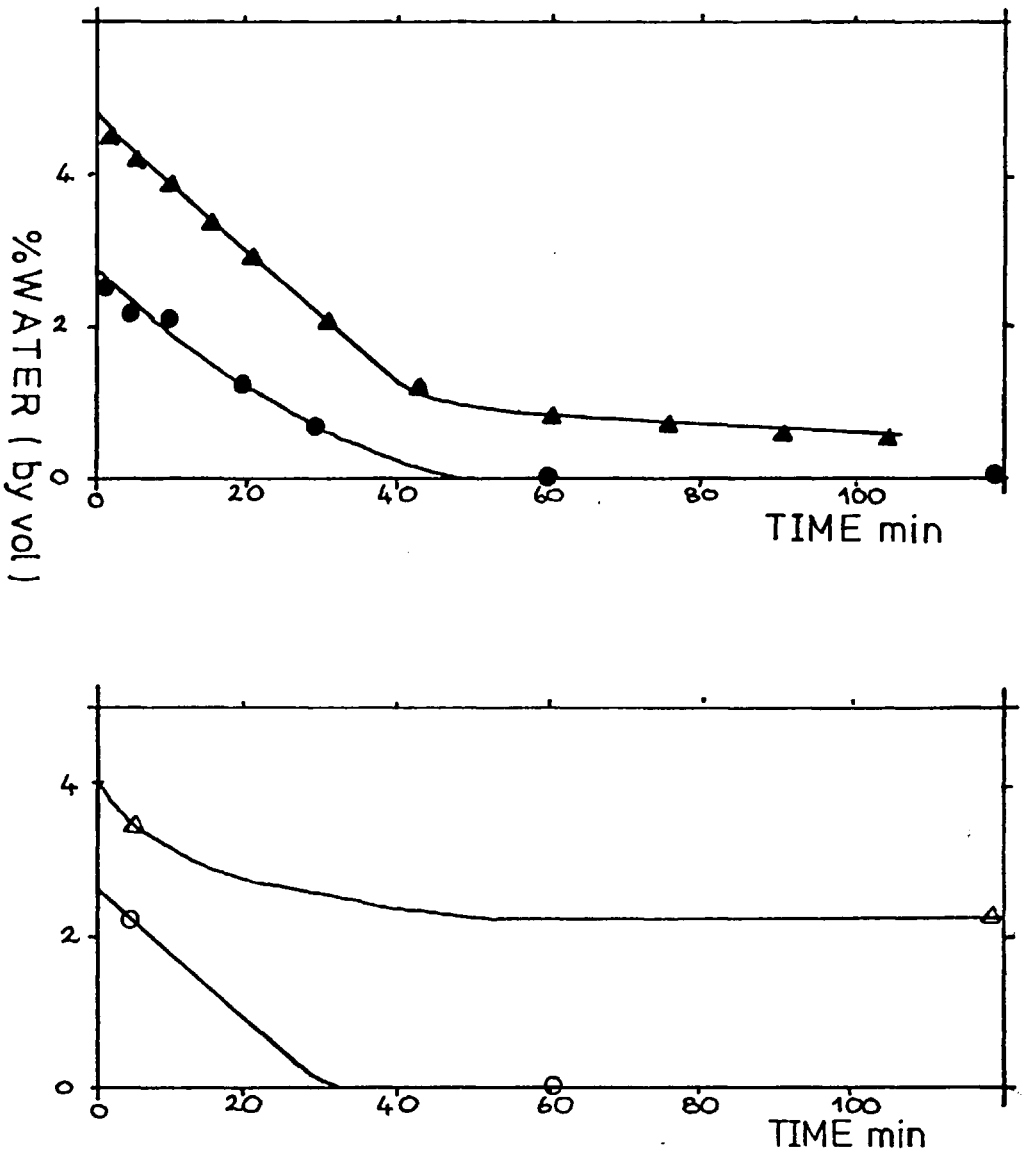

FIGURE 5·11A

Curves to determine the drying times of the coatings.

○ A

● F/S A

△ C1

▲ F / SC1

FIGURE 5.12A

Typical results from cross-hatch tests for several specimens. Note that the tests are of the finishes at several strains.

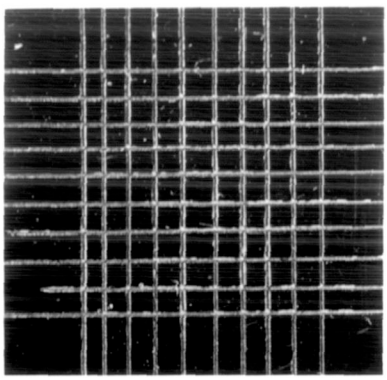

S/P/C1 0% 4mm

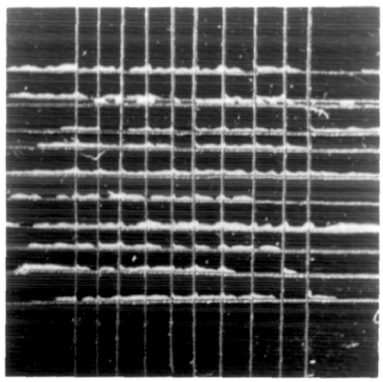

S/P/A 8% 4mm

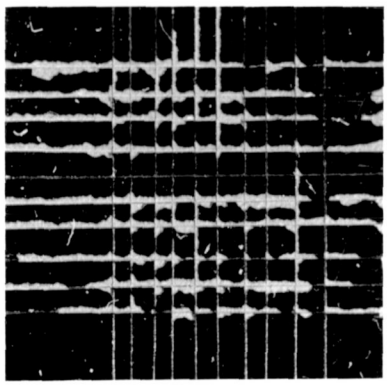

S/P/C2 5% 4mm

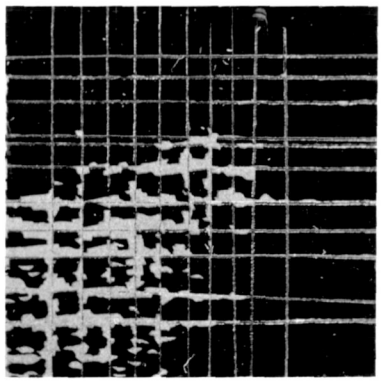

S/P/C1 5% 4mm

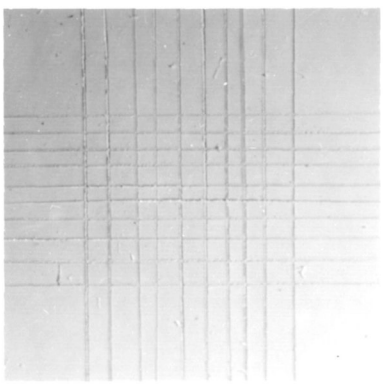

F/S C1 10% 4mm

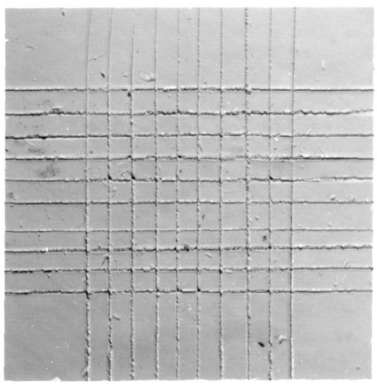

F/S A 10% 4mm

Figure 5.12A Cross hatch tests on various specimens

FIGURES 5.13A and B

Typical stress and acoustic emission vs. strain curves for S/P/A and S/P/Cl respectively. Superimposed are typical photographs showing the gross deformation of the paint films with strain.

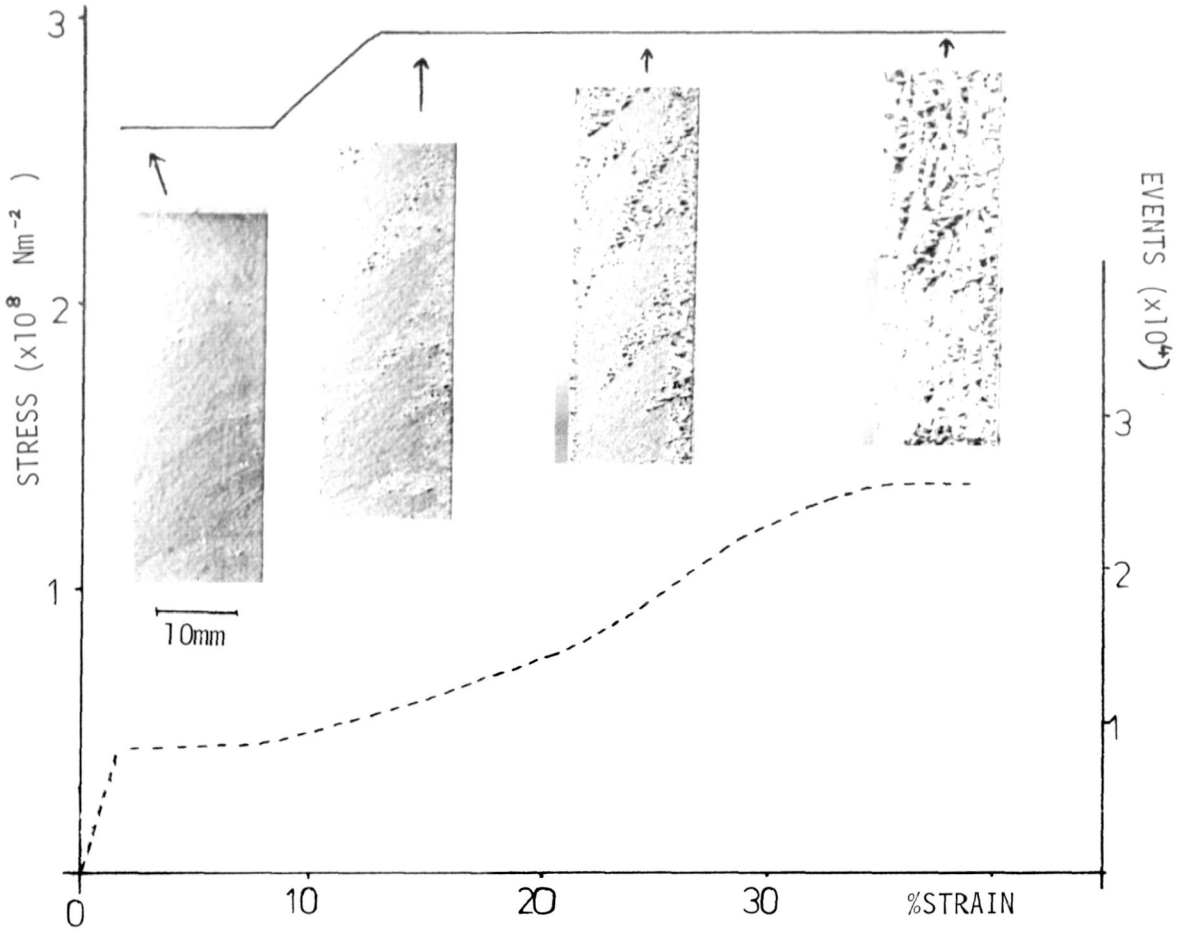

Figure 5.13A S/P/C1

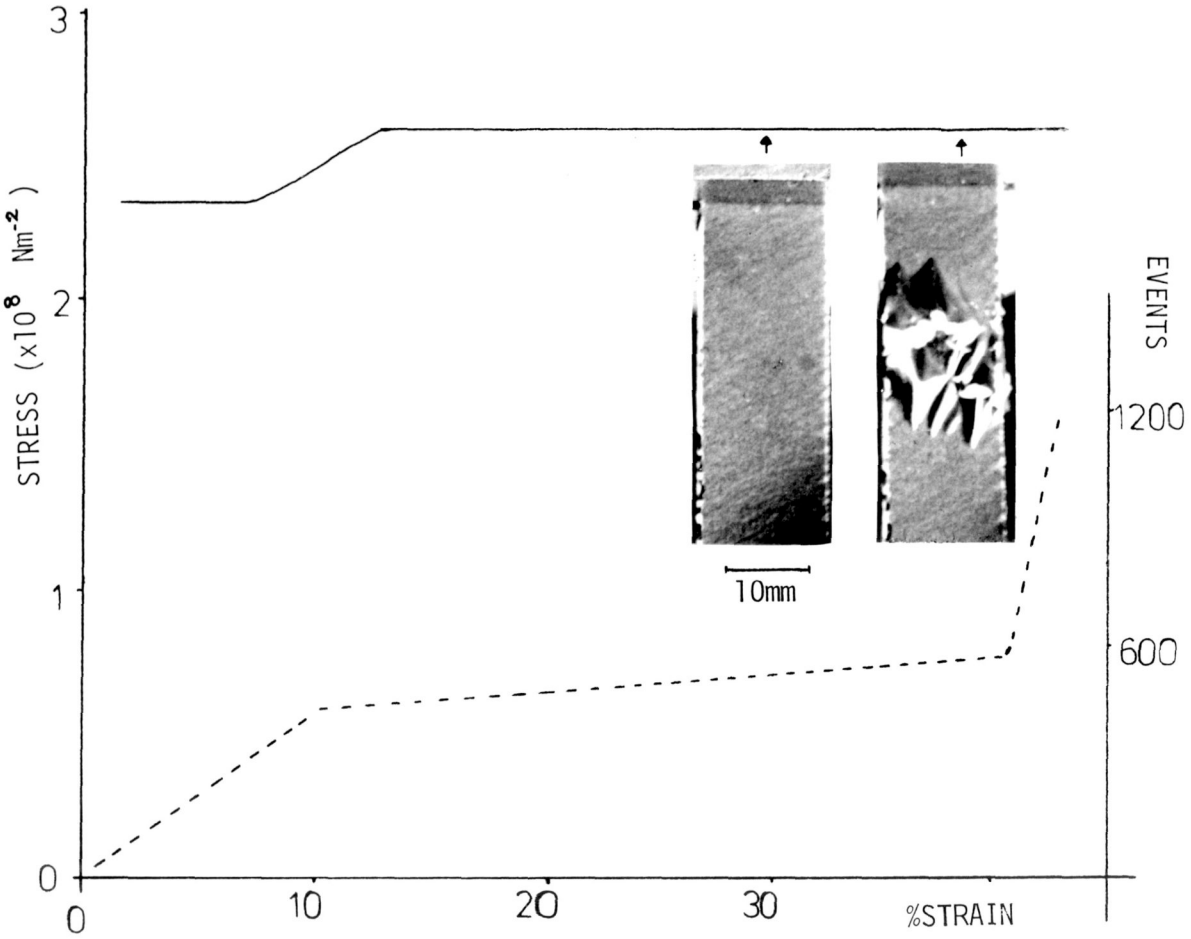

Figure 5.13B S/P/A

FIGURE 5.14A

Scanning electron micrographs showing the surface of the G16S phosphate prior to testing at two magnifications.

FIGURE 5.14B

Scanning electron micrographs of the G16S phosphate after testing to failure. The diagram indicates the inhomogenity along the specimen.

Figure 5.14A S/P

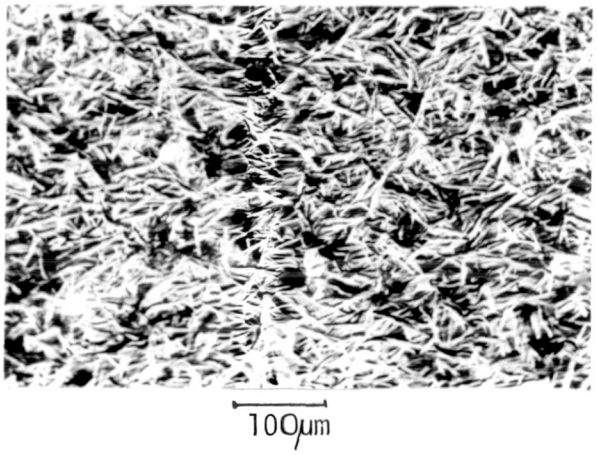

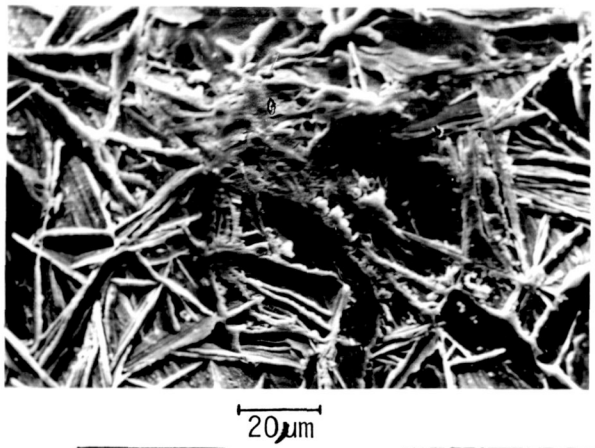

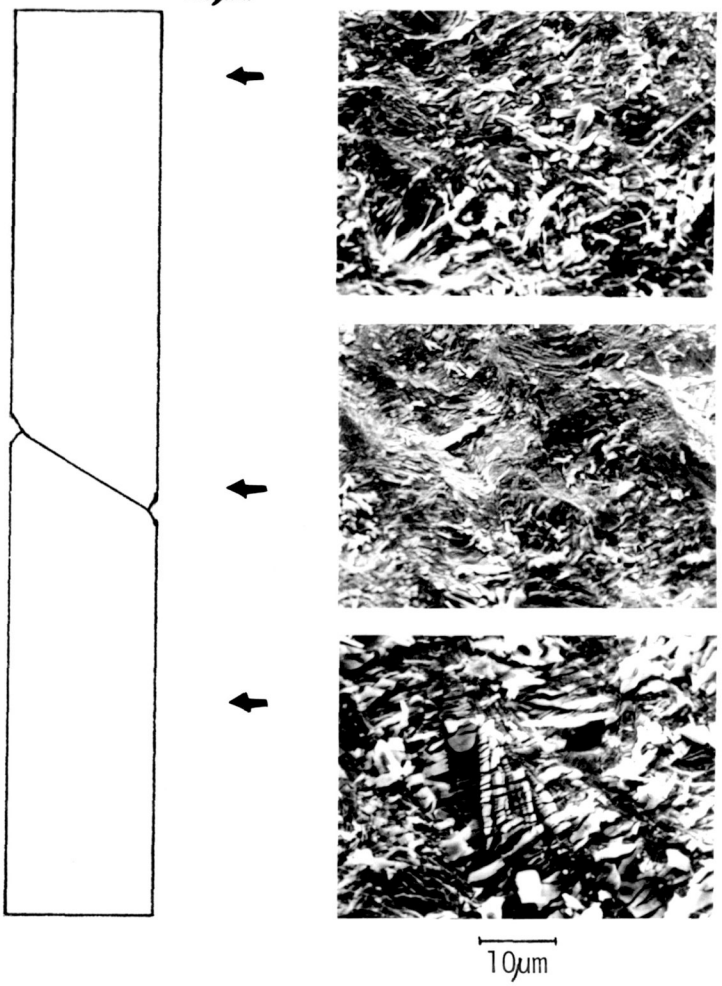

Figure 5.14B S/P

FIGURE 5.14C

Scanning electron micrographs showing the differences in the surface topography between the various phosphates.

Phosphate 1 20μm

Phosphate 2 20μm

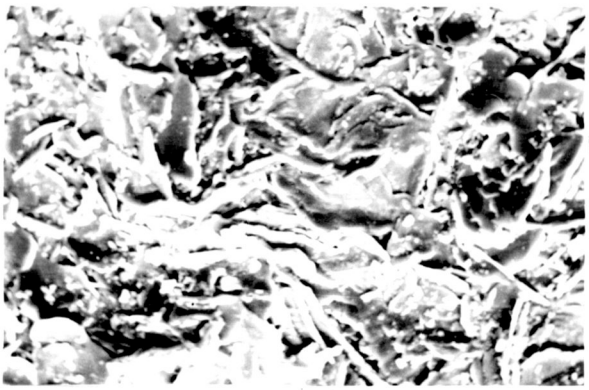

Phosphate 3 20μm

Phosphate 4 20μm

Figure 5.14C Various phosphates

FIGURE 5.14D

Scanning electron micrographs showing the full systems in cross section before testing at two magnifications.

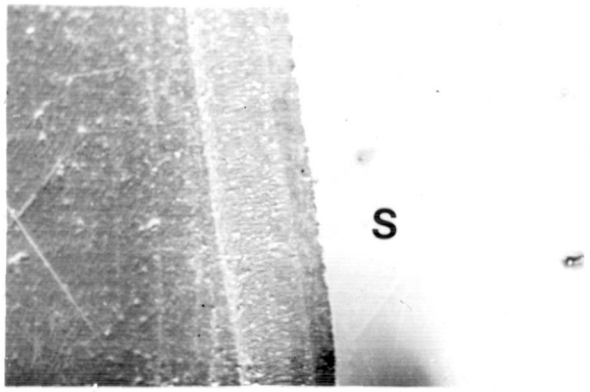

F/S C1 100μm

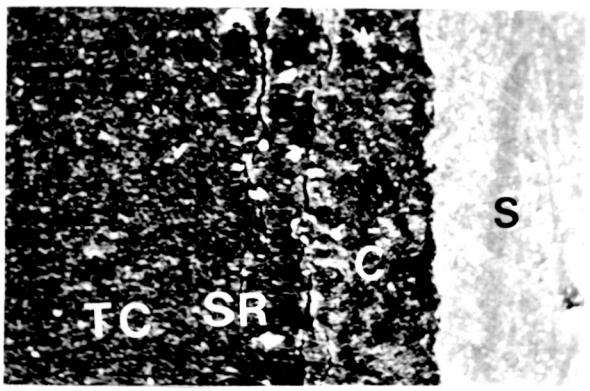

F/S C1 20μm

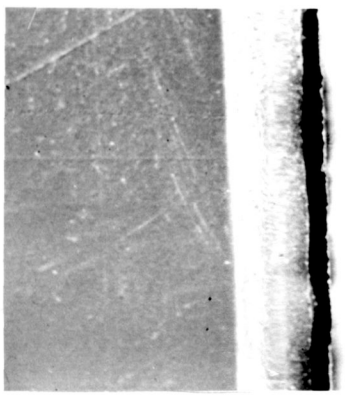

F/S A 100μm

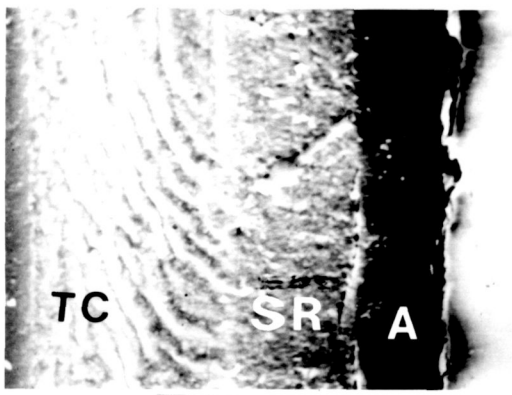

F/S A 20μm

Figure 5.14D

FIGURE 5.14E

Scanning electron micrographs showing the anodic and cathodic 1 electrocoats in cross section at two magnifications, prior to testing.

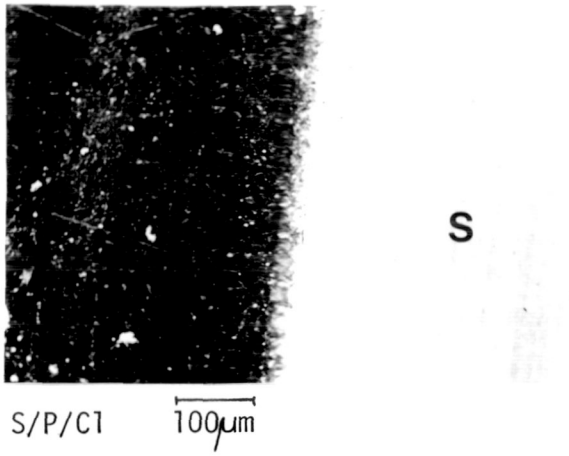

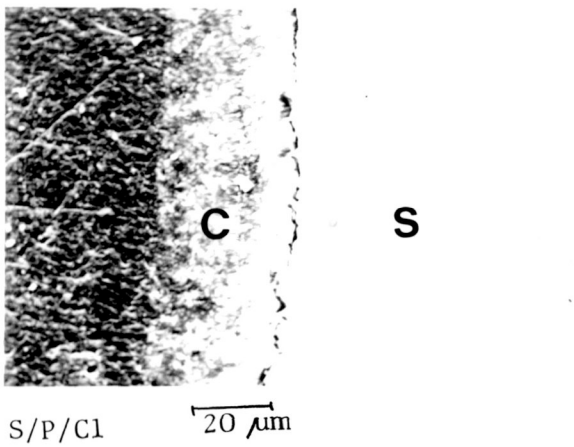

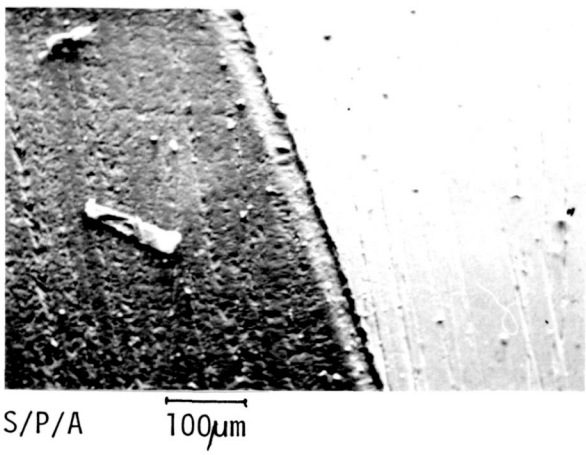

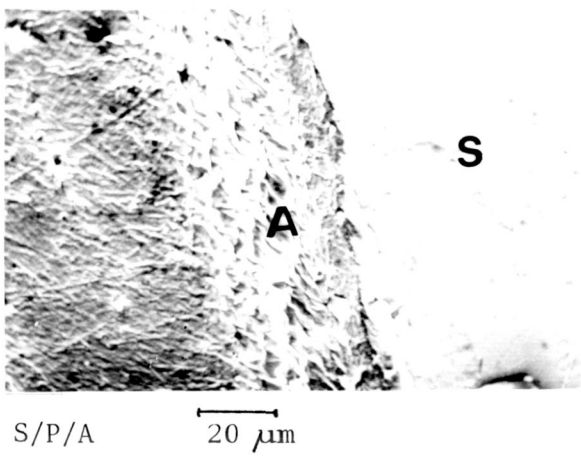

Figure 5.14E

FIGURE 5.14F

Microprobe pictures and zinc traces for S/P, S/P/A and S/P/Cl showing that there is little dissolution of the zinc phosphate by either electrocoat.

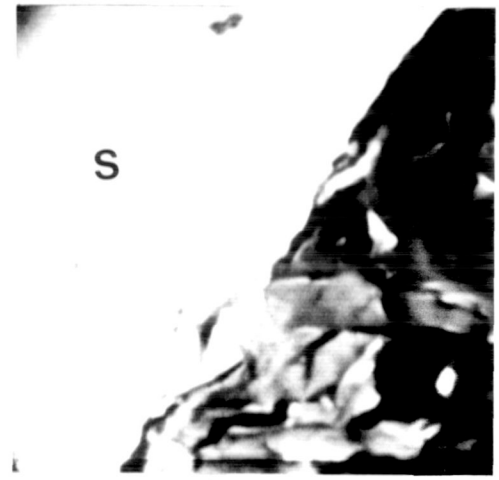

S/P 20μm

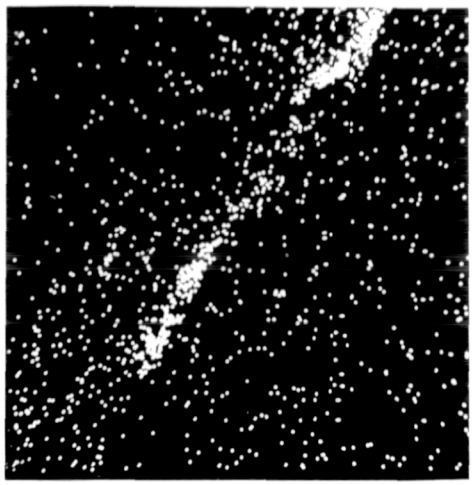

S/P 20μm
Zinc trace

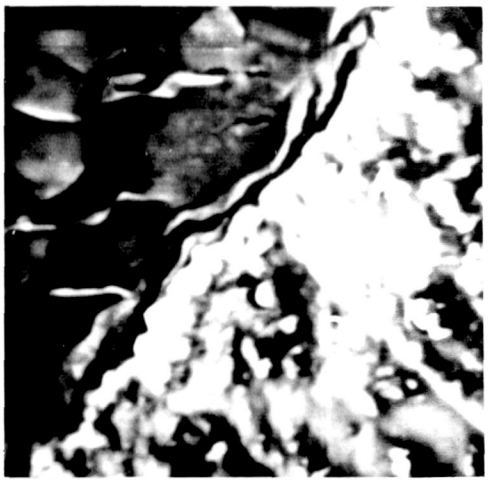

S/P/Cl 20μm

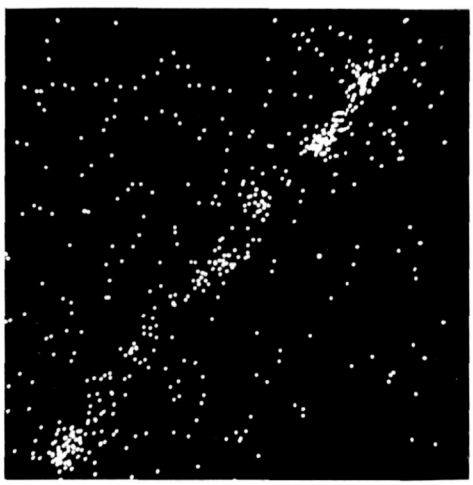

S/P/Cl 20μm
Zinc trace

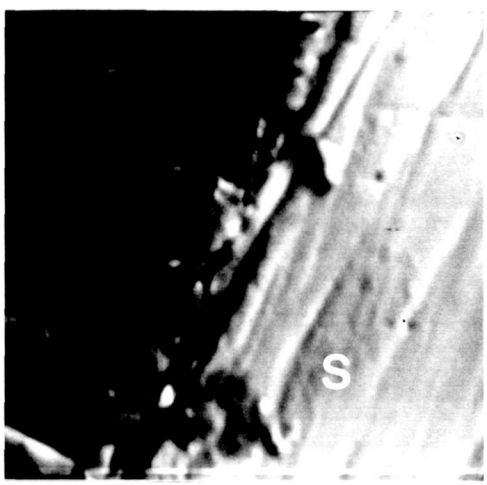

S/P/A 20μm

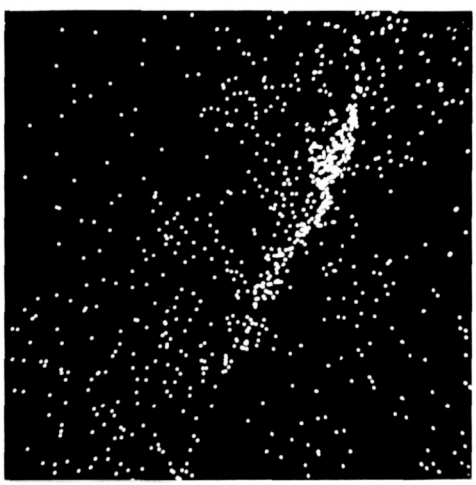

S/P/A 20μm
Zinc trace

Figure 5.14F

FIGURE 5.14G

Scanning electron micrographs showing the anodic and cathodic 1 elctrocoats in cross section at 3% and 8% strain.

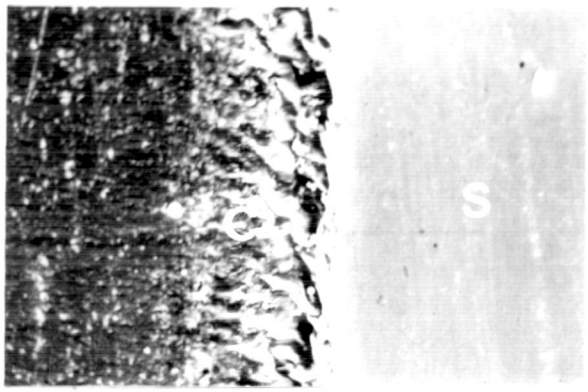

S/P/C1 20μm
(3% strain)

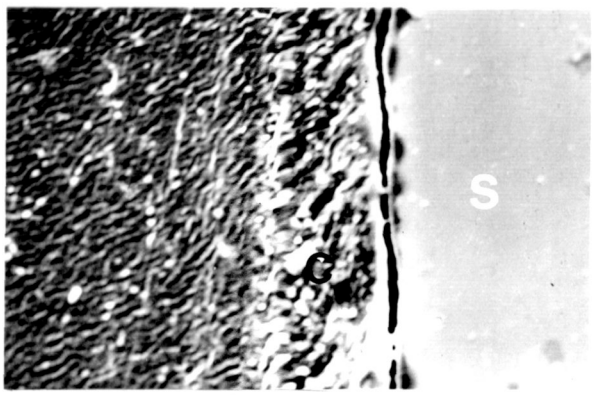

S/P/C1 20μm
(10% strain)

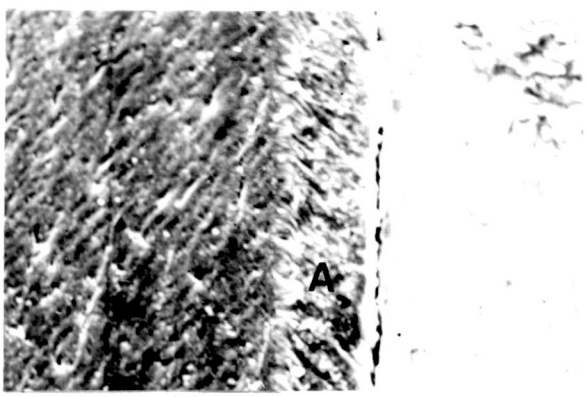

S/P/A 20μm
(3% strain)

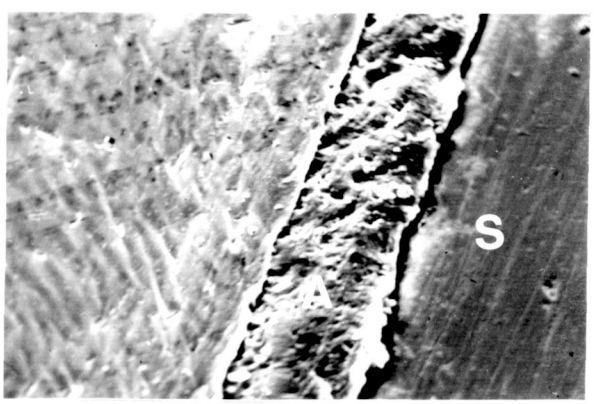

S/P/A 20μm
(10% strain)

Figure 5.14G

FIGURE 5.14H

Scanning electron micrograph showing the electrocoat coming away from the substrate.

FIGURE 5.14I

Scanning electron micrograph showing an interesting shape of crack in the topcoat in cross section.

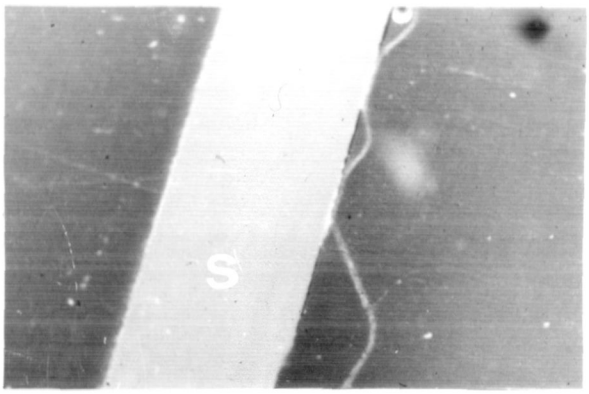

Figure 5.14H S/P/Cl 400μm

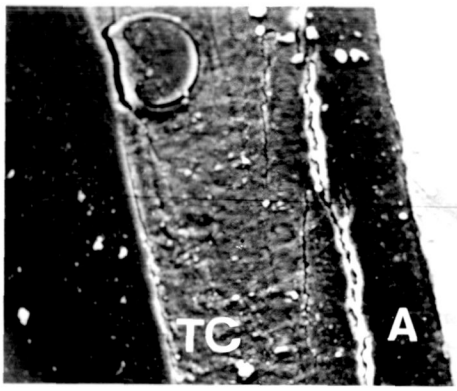

Figure 5.14I F/S A 40μm

Chapter 6. Discussion.

6.1 Luders band formation.

The results of section 5.1 show that, on deformation, uncoated steel gave no Luders region. However, once a coating had been applied to the steel, there were distinct Luders bands on deformation. This was the case for most of the systems tested, with the exception of S/A, S/C2 and the various phosphates, which were coated onto a different batch of steel, of nominally the same composition as that used on the other tests.

To show that this was not a surface effect caused by the coating the coating was ground away, after which the steel continued to show distinct bands when tested. Luders bands arise due to inhomogeneous strain within the specimen, which can be caused by interstitial atoms (such as carbon or nitrogen) pinning dislocations. The strength of the pinning depends on the heat treatment history of the steel, so it is possible that the Luders bands may form, on deformation, due to heat treatment associated with the coating processes. Uncoated steel was annealed at the coating temperatures, but gave no Luders bands on subsequent testing. One possibility is that the hydrogen ions present during the phosphating reaction may diffuse into the steel, giving rise to dislocation pinning during tensile testing. This view is supported by the fact that both the S/A and S/C2 specimens, which were not phosphated, did not show Luders bands. The reason for

the lack of Luders bands in the steels coated with various phosphates other than G16S is not clear, although this may be associated with differences in the phosphating reaction.

6.2 Reproducibility of the acoustic emission.

As noted in section 5.2, the acoustic emission during the tensile testing of paint films exhibited some scatter, but the reproducibility was sufficient to monitor the significant changes between specimens after different coating treatments. To a certain extent the scatter may be attributed to the acoustic emission technique, since it was not possible to control the exact location of the cracking with respect to the transducer. So, although the specimen geometry was kept constant, the reflections and interference of the stress waves in the material, will cause differences in the detected signal, as discussed in section 3.1. Scatter of this order is not unusual in acoustic emission, as bourne out by the work of Tatro (1972) and Curtis (1975). They were able, however,as in the present work, to identify definite trends in the results.

The acoustic emission from paint films may be affected in other ways. The temperature and the humidity would affect the properties of the paint, as would the detailed stress-strain behaviour of the system as a whole, for instance the number of Luders bands initiated in the Luders region. The condition of the steel surface before coating is also important. In several cases the coating seems to have been applied onto a very uneven surface, such as that shown in figure 5.14E. Indeed in some cases

the surface roughness varied along the length of the specimen, and this may affect the adhesion of the paint. Any variation in the deformation behaviour of the paint is likely to affect the acoustic emission from the system. In order to determine whether any of these variables was dominant in causing the scatter, it was attempted to find trends in the amount of acoustic emission for a given system with temperature, humidity, U.T.S., yield stress, %elongation to failure and the distance of final fracture from the transducer. There were no consistent trends in any instance, suggesting that the scatter is due to all or several of these variables, in varying degrees. Fortunately, the differences in the acoustic emission between the systems tested here were so great that , even allowing for the scatter, it was possible to draw several conclusions.

6.3 Acoustic emission during tensile testing of untreated and phosphated steel.

The steel specimens gave very little acoustic emission in comparison with most of the other systems studied. The emissions occurred mainly before ~ 5% strain. It is often found that steels give most emission round yield, particuarly if Luders bands are present (eg. Fisher and Lally (1967), Webborn (1979), Dunegan and Green (1972)). The acoustic emission from metals is generally attributed to dislocation movement, the most likely method of generation being as dislocations break away from pinning points, such as grain boundaries and inclusions. James and Carpenter (1972) suggest that the pulse rate is proportional to the rate of

change of mobile dislocation density.

The differences between the phosphate systems will be discussed in more detail in section 6.9, and the following refers only to the G16S phosphate, which was used for the bulk of the experimental work. This gave considerably more acoustic emission than the untreated steel, as may be expected since there are more possible failure mechanisms, which are themselves likely to be noisier. The main damage sustained by the phosphate is the cracking of the hopeite needles and their loss of adhesion (see figure 5.14B). The adhesion loss seemed to occur between the hopeite and the phosphophyllite, since the microprobe work showed that zinc remained on the substrate, which indicated that some phosphate remained adhered to the steel, and microscopy showed that there were no needles present.

Most of the acoustic emission occurred within the first 10% of strain (figure 5.3A) and, although the situation was complicated by the non-uniform failure of the coating, the microscopy indicated that the majority of the needle cracking and adhesion loss did, indeed, occur below these strains.

6.4 Paint coats.

When a paint system was tested there were almost always two distinct regions of high acoustic emission, although the strains at which they occurred and their magnitude and extent differred between the various systems. This is consistent with Mosle's work (1978), who also observed two distinct peaks during tensile testing of phosphated steels with an electrocoat.

6.4.1 Low strain failure.

The main failure mechanisms at low strains are loss of adhesion and microcracking. Scanning electron microscopy indicated the presence of microcracking by ~ 3% strain in all the systems studied and in all the coats in the full systems. The cracking appears to be worst in the surfacer coat. In the topcoat unusual cracks, as shown in figure 5.14I have been seen. These circular cracks always occur near the outer edge of the paint and the reason for their shape is not understood at present.

In no case have cracks been seen which extend from the outer surface through to the steel. Thus, even though it is likely that microcracking contributes to the acoustic emission it will probably not be a significant failure mechanism in practice. It was attempted to quantify the extent of the microcracking by measuring the crack length as a proportion of the coating area. This was done for various specimens at several pre-failure strains. The results for the anodic and cathodic 1 electrocoats are shown in figure 6.4A, with each point representing a measurement taken from a transverse section through the specimen. It can be seen that there is considerable variation in the amount of microcracking through a given specimen. The scatter is not altogether surprising; at strains in the Luders region the plastic strain through the steel substrate will not be homogeneous due to multiple Luders band nucleation. Indeed, once the damage was visible to the naked eye it was not homogeneously distributed either, consistent with the assumption that

microcracking occurred in localised areas.

The second low strain failure mechanism, that of adhesion loss, was indicated by cross hatch tests (figure 5.12A). In most specimens this low strain adhesion loss occurred considerably before any gross damage was visible on the surface of the specimen, which suggests that it was some minor loss of adhesion, insufficient to cause rucks to form on the surface. (gross adhesion loss will be discussed further in section 6.4.2). It seems likely that Luders bands and dislocation slip steps, which form on the surface of the steel as it deforms, could cause some adhesion loss. The adhesion between a paint and a substrate is often considered to take place along a boundary layer in which the polymer molecules are affected by the proximity of the substrate (Myers and Long,1969). This layer is estimated to be between 1 and 40nm thick. A step caused by Luders bands or slip can be ~ 1μm . at least 25 times the thickness of the adhering layer and would therefore be expected to cause at least some localised adhesion loss. The situation is shown in figure 6.4B. The cross hatch tests showed that the cathodic 1 electrocoat suffered considerably greater loss of adhesion than the anodic coat during the first 10% of strain, it also gave very much more low strain acoustic emission (figure 5.3B). The cathodic 2 electrocoat showed adhesion loss intermediate between the other two coats and also intermediate acoustic emission. This suggests that a weaker adhesive bond gives more acoustic emission. Such a description is reasonable if it is assumed that the Luders step causes a greater area of damage along the remaining interface for the weaker bond. Curtis (1975), working on adhesives, also found

that the failure of weaker bonds gave more acoustic emission.

6.4.2 High strain failure.

The strain at which the onset of higher strain failure occurs depends on the specimen and takes the form of damage visible on the specimen surface. The damage is shown in figures 5.13A and B, and can be described as the peeling of diamond-shaped localised regions, which grew and eventually cracked across. The cracking is perpendicular to the tensile axis, as would be expected, since this is the direction of maximum tensile stress. When sufficient of these diamond-shaped areas were present the paint cracked across the specimen and gross peeling took place. The adhesion loss seems to have occurred mainly within the phosphate layer, since microprobe work indicated the presence of zinc on both the electrocoat back and on the substrate surface after testing, and needles were seen in the electrocoat back in the scanning electron microscope. It is unlikely that the fracture occurred within the phosphophyllite, since, were that the case, the presence of different electrocoats would be unlikely to alter the adhesion. The fracture, then, probably occurred between the hopeite needles and the phosphophyllite.

Although diamond-shaped areas were seen for all the specimens tested here, the more usual shape of damage (Schuh and Theurer,1937) is that of narrow rucks running parallel to the tensile axis. The formation of rucks can be explained by considering the paint to be in tension on the substrate (this is

reasonable since paint often shrinks during cross-linking and solvent evaporation as it dries). The situation is shown in figure 6.4C. While the paint remains adhered it must conform to the deformation of the substrate, although its deformation properties will differ considerably. The deformation will cause the paint to be in compression in the transverse direction, while in the longitudinal direction it will remain in tension. Once adhesion is lost the compression in the transverse direction will cause a ruck to form in the paint film, parallel to the tensile axis; in the longitudinal direction the paint will remain in tension so no ruck will form.

The formation of diamond-shaped areas can be explained by assuming that the coat is initially in compression on the substrate. This is known to be the case for some thermosetting resins, which swell on setting (Myers and Long,1969). Again the paint is forced to conform to the deformation of the substrate by the adhesive forces. This will cause the coating to go into greater compression in the transverse direction, and in the longitudinal direction it will be in tension so reducing the compressive stresses, which will eventually become tensile. This is shown schematically in figure 6.4D. The stresses can eventually become so great as to overcome the bonding forces. If the paint is in compression the loss of adhesion will cause a ruck to form, perpendicular to the compressive stress (similarly to the transverse case in figure 6.4C). If the bonding fails in both the longitudinal and transverse directions it is likely to occur at the same point, hence if the paint is in compression in both the longitudinal and transverse directions, two normal,

intersecting rucks will form and for the paint film to remain in tact this will appear as a diamond shape.

It appeared that the high strain acoustic emission peak began at the same strain that damage was noticed on the specimen surface. It seemed reasonable that the acoustic emission would correlate with the damage on the surface, and, in order to ascertain that this was the case, photographs were taken at regular intervals through a number of tests. The interval was ~ every 2% of strain. The damaged area visible, that is the diamond-shaped areas, and the areas where gross peeling had taken place, were measured using a grid of 1mm squares. This proved remarkably repeatable, to within ∓ 7%. Damage which occurred along the guillotined edge was also included in this analysis, though it was very localised and generally insignificant when compared with the total damaged areas. The results for S/P/A, S/P/Cl, F/S A and F/S Cl are shown in figures 6.4E and F, and are typical of the results obtained from a large number of such analyses, performed for many of the systems tested. It can be seen that the correlation between the acoustic emission in the form of cumulative ringdown counts, and the damaged area visible is extremely good. The second peak , in the acoustic emission often slightly preceded the damaged area visible, as may be expected, since the damaged area may have been too small to be visible when it first formed. These curves are strong evidence for the fact that acoustic emission activity at high strains is largely related to the gross damage in the specimen.

It has thus been established that the low strain acoustic emission is associated with minor adhesion failure and

sub-surface microcracking and that the high strain acoustic emission is associated with the gross failure of the paint film (which can, in turn, be associated with the inability of the coating to conform to the deformation of the substrate). The following sections will explain in detail the differences in behaviour of the various systems studied in the light of the above observations.

6.5 Comparison of systems coated on one side with those coated on both sides.

In most cases the specimens with one or two sides coated showed similar trends between systems in their acoustic emission vs. strain response (see figures 5.3A,B,D and E cf. figures 5.4A,B,C and D). One notable exception was the system with a cathodic 1 electrocoat (S/P/C1(1) on figure 5.4B and S/P(R)/C1(1) on figure 5.4D cf. S/P/C1 and S/P(R)/C1 on figures 5.3B and E respectively). The behaviour of the cathodic 1 electrocoat when coated on one side appears to have been similar to that when tested after immersion (see figures 5.6A and B). Capacitance measurements on the wet films (figure 5.11A) showed that the loss of water from the cathodic 1 electrocoat is slow, and it seems likely that the preparation technique, where the extra coat was ground away on water lubricated SiC papers, caused water to be introduced into the paint film of these specimens. Fortunately this does not seem to have happened for the other systems tested.

The system with one side coated is likely to suffer, in total, only half the damage of a system with both sides coated,

since there will be only half the area of the paint coat, therefore about half the acoustic emission would be expected. Figure 6.5A shows the events vs. strain curves for S/P/A and S/P(R)/A, and S/P/Cl and S/P(R)/Cl respectively. Twice the curves for the same systems coated on one side only are shown for comparison. It can be seen that the systems with the same coatings give approximately the same acoustic emission, with the systems coated on only one side being slightly quieter. This is reasonable since twice the events for the systems with one side coated will also include twice the events from the steel, and it is also possible that the coat had not been ground away completely. The acoustic matching between the paint and the steel is not likely to be perfect, which would also lead to twice the eventsof the system with one side coated being more than the events from the system with one side coated, providing that the transducer is always on the coating.

The similarity between half the acoustic emission from systems with one side coated and that from the same system with both sides coated indicates that the paint is quite well acoustically matched to the steel. This can also be demonstrated by placing the transducer on the uncoated side of a specimen coated on one side only, during testing. Several such tests have been performed and similar acoustic emission is monitored to when the transducer is on the coating.

This good matching between the paint and its substrate suggests that it may be possible to monitor paint failure on large structures, taking advantage of the low attenuation of the stress waves in steel (Webborn,1979).

6.6 Differences between electrocoats.

The results discussed in this section are mainly those from sections 5.3 and 5.4. For all paint systems the rinsing of the phosphate coat seemed to have little effect on the behaviour or the acoustic emission of the dry system. The rinse is introduced mainly in order to improve corrosion resistance (section 2.2.1) so the similarity in mechanical properties is not surprising, indicating only that little corrosion has taken place even when the system is left unrinsed, when it is stored and tested in dry conditions.

In section 6.4 it was pointed out that the acoustic emission occurred in two peaks. In this section again, the low strain peak will be discussed first and then the high strain one.

6.6.1 Low strain failure.

At low strains the anodic electrocoat remained more strongly adhered than the cathodic electrocoats, as shown by the cross-hatch tests at low strains (figure 5.12A). It is reasonable that the anodic electrocoat should adhere more strongly than the cathodic, as can be seen by a consideration of the phosphating and electrocoating equations (given in sections 2.2.1 and 2.2.2). These indicate that the equilibrium of equation 3 in section 2.2.1, where the phosphate is deposited may be reversed by the presence of H^+, which is present during anodic electrocoating (equation 1, section 2.2.2). Thus some of the phosphate is likely

to dissolve in the anodic electrocoat. There is no similar reason for expecting disolution during cathodic electrocoating. Several workers (eg. Cheever and Wojtkowiak, 1970) have detected considerable dissolved phosphate in anodic electrocoats. In this work, however, results from the microprobe (figure 5.14F) suggest that the phosphate layer is similar under both the anodic and cathodic 1 electrocoats. Furthermore, several specimens had the electrocoat removed and the steel and phosphate substrate examined in the scanning electron microscope. Though there was some variation between samples, the microscopy showed that there were some hopeite needles remaining under both the anodic and cathodic 1 coats. This suggests that only a small amount of phosphate is dissolved by this type of anodic coating.

The acoustic emission, however, suggests that there is some dissolution in the anodic electrocoating process which improves the adhesion to some extent, since the anodic coat has more emission in its low strain peak when coated onto unphosphated steel, than when a phosphate layer is present (see figure 5.3C). As any microcracking in the electrocoat would be likely to occur on either substrate the difference in acoustic emission can be attributed to stronger adhesion to the phosphate than to the steel. Another indication that the phosphate layer has a beneficial effect on the adhesion of the anodic coat is that the low strain emission was similar for both the anodic and the cathodic 2 electrocoat on unphosphated steel.

For all the electrocoats the adhesion loss seemed to occur between the hopeite needles and the phosphophyllite, as mentioned in section 6.4, which suggests that mechanical keying is unlikely

to have much effect on the adhesion. For this reason the similar adhesion of the cathodic 2 electrocoat to both phosphated and unphosphated steel, as indicated by the acoustic emission and by the cross-hatch tests is not unreasonable.

The cathodic 1 electrocoat suffered considerably greater adhesion loss at low strains than the other electrocoats, as indicated by both the cross-hatch tests and the acoustic emission. It seems likely that this is largely due to the early onset of the gross deformation in the cathodic 1 coat, as shown by the acoustic emission (figure 5.3E)and by direct observation (figure 6.4E); as will be further discussed later in this section.

This indicates that the differences between electrocoats in their low strain adhesion are less dramatic than was first thought, which is confirmed by a consideration of the acoustic emission at low strains for the full systems (figures 5.4A and B). It is unlikely that the further coats effect the adhesion of the electrocoat (as distinct layers are seen in the scanning electron microscope, eg. figure 5.14C , it is assumed that the interpenetration of the coats is small) yet the low strain acoustic emission of the full system containing an anodic electrocoat was only slightly below that of the full system with a cathodic 1 coat, suggesting that the anodic coat has only slightly better adhesion. The cross-hatch tests on the full systems (figure 5.12A), though inconclusive, also indicated no dramatic differences in the adhesion between those with anodic and cathodic 1 electrocoats.

The second low strain failure mechanism, that of

microcracking, does not entirely account for the differences in the low strain acoustic emission between the full systems. This can be shown by considering the amplitude distributions at low strains (figures 5.8D and E). The full systems show a peak at 26dB and several events at higher amplitudes. It seems reasonable then, to attribute the 26dB peak to adhesion loss, since it occurred in all the systems studied (as will be further discussed in section 6.7) thus the high amplitude events arose due to microcracking. The full system containing a cathodic 1 electrocoat gave more high amplitude events than that with an anodic electrocoat, but insufficient to account for the difference in acoustic emission at low strains. This confirms that there is indeed some difference in the adhesion between the anodic and the cathodic 1 electrocoats.

The formation of microcracks can also be used to account for differences in the low strain acoustic emission as additional coats were added to the electrocoats. The dramatic reduction in the low strain emission once the surfacer coat was added to the cathodic 1 electrocoat (figure 5.4B) is probably due to the gross damage occurring at higher strains (to be discussed further, later in this section). However the smaller reduction in the low strain emission when the surfacer coat was added to the anodic electrocoat is probably due to the reduction of microcracking in the anodic coat and any microcracking that occurred in the surfacer coat being slightly quieter. The further addition of a topcoat increased the low strain emission during tensile testing of the anodic system, and for the cathodic 1 system increased the ringdown counts but reduced the events. A possible explanation of

this difference is that the surfacer coat cracks more on the cathodic 1 than on the anodic electrocoat. The addition of the topcoat reduces the surfacer cracking, but cracks itself, with higher amplitude events. That the microcracking in the sub-surface layers was only reduced, rather than stopped, was indicated by scanning electron microscopy, which shows cracking in all the coats. This description is confirmed by a study of the low strain amplitude distributions (figures 5.8E and F). As suggested previously, the 26dB peak is assumed to arise through adhesion loss and the higher amplitude events from microcracking. In the system with a cathodic 1 electrocoat and a surfacer there were considerably more high amplitude events than in the system with an anodic coat and a surfacer. This indicates that the surfacer coat indeed gave more microcracking on the cathodic 1 than on the anodic electrocoat, as suggested in the previous paragraph. The low strain amplitude distribution of the cathodic 1 full system shows that the topcoat cracking gave higher amplitude events than the surfacer cracking.

The anodic and cathodic 2 electrocoats gave fewer events but more ringdown counts than phosphated steel at low strains (figures 5.3A,B,C,D and E). (The situation in the cathodic 1 electrocoat is complicated by the early onset of the gross damage).This suggests that failure processes within the electrocoats gave fewer but higher amplitude events than those in the phosphate. This is confirmed by the amplitude distributions (figure 5.3 G). The addition of an electrocoat reduces the cracking of the hopeite needles (no cracked needles have been seen on either the substrate or the electrocoat back in the

scanning electron microscope, after testing). This suggests that the microcracking in the electrocoat gave higher amplitude events than the hopeite needles cracking, since the adhesion loss is likely to be of similar amplitudes.

6.6.2 High strain failure.

In section 6.4 it was shown that the acoustic emission at high strains could be attributed to gross damage, visible on the surface of the specimen.

As mentioned in the previous section the gross damage occurred at low strains for the cathodic 1 electrocoat. This was seen directly during testing (figure 6.4E) and the acoustic emission showed considerable overlap between the high and low strain peaks (figure 5.3E). Gross damage would also affect the cross-hatch tests. Differences in the low strain amplitude distributions of the anodic and cathodic 1 electrocoats (figure 5.8B and C) are consistent with there being one dominant failure mechanism in the anodic case, since there is only one peak (that at 26dB) whereas several failure modes are indicated for the cathodic 1 coat, since there are a number of peaks. This is discused in more detail in the next section. The earlier onset of high strain damage for the cathodic electrocoats (and in particular the cathodic 1 electrocoat) compared to the anodic coat can be explained by considering the model proposed in section 6.4. The difference could be due either to the coatings having different mechanical properties or to their being in different degrees of initial compression on the substrate, a

combination of the two seems the most likely. These effects would alter the ability of the coating to conform to the deformation of the steel and hence alter the strain at which the stresses within the coat are sufficient to overcome the bonding forces.

It can be seen that (figures 5.4A and B) the presence of additional coats also affects the onset of the gross damage. As stated previously additional coats are unlikely to alter the adhesion of the electrocoat, but the additional baking and solvent effects may alter the stress situation within the electrocoat, as will the removal of the electrocoat's surface in contact with the air. The stresses within the electrocoat would affect the strains at which the gross damage takes place, the greater the compression on the substrate the earlier the onset of damage (section 6.4). For both the anodic and the cathodic 1 systems the high strain peak in the acoustic emission begins at higher strains when a surfacer is present than when the electrocoat is tested alone. On the further addition of a topcoat the strain at which the acoustic emission increases is reduced. This indicates that the application of the surfacer coat improves the compatibility of the paint system to the steel and the further addition of the topcoat reduced it.

There is a good deal of similarity in the acoustic emission from the full systems containing either electrocoat. The greatest similarity would be expected in this case since the paint is intended to act as a full system so it is its behaviour as such which influences the choice of the paint coats.

The results discussed in this section point the way in which acoustic emission can be used as a useful tool by the paint

scientist. Although it is difficult to compare the adhesion of two electrocoats on the same substrate (because of variations in microcracking) the adhesion of a given electrocoat to various substrates can be easily compared, thus giving an indication of the compatability between the paint system and the substrate. Furthermore a study of the acoustic emission as various coats are added to a system may serve to demonstrate the weak points in that system.

6.7 Amplitude distributions.

As indicated in the preceding sections the amplitude distributions observed in most of the tests appear to consist of a series of component peaks. The power law description (section 3.3.4) commonly used to characterise amplitude distributions, where the distribution is assumed to be

$$n(V) = (V/V_t)^{-b}$$

does not give a good fit to the type of distribution obtained here. A typical cumulative-log plot obtained here is shown in figure 6.7A, and it can be seen that this is not well fitted by a series of straight lines. Holt (1976) points out that a peak could occur in a distribution fitting the power law if several acoustic emission bursts arrive within the deadtime of the apparatus. Only the amplitude of the highest burst would be recorded which could lead to the formation of a peak.

For a series of peaks this would require that only events of similar amplitudes fall within the same deadtime, a situation which seems unlikely here, where many failure processes occur

together, otherwise a peak would only be formed near the threshold. Another error that could be introduced by the dead time is that of an event lasting longer than the dead time. In that case supurious low amplitude events would be recorded. Pulse width measurements (section 5.9) indicate that this did not happen here since all the pulse widths measured were well within the dead time. It appears then, that the series of peaks seen here is a genuine effect.

The amplitude distributions recorded here show a series of peaks centred about several amplitudes, which are similar for all the systems tested. It seems reasonable that each peak could be associated with one failure process in the specimen. This would imply that different failure mechanisms are associated with different energies. Holt (1972) shows that, even with pulses of the same energy, the amplitude will depend in a complex manner on the pulse duration. As the specimens tested here were so small there is likely to be little broadening of the pulse between the source and the transducer, and it is assumed that the pulse duration, in addition to the energy, is a constant for each failure mode.

Holt (1976) has suggested that peaks in the amplitude distributions could be described by log-normal curves. Another description of peak shapes is given by a Lorentzian equation. This is commonly used in Mossbauer spectroscopy, and a computer programme (Appendix 1) is available that distinguishes and quantifies a series of overlapping Lorentzian peaks. The programme uses an iterative technique based on a series of estimates from the operator, to find the best fit to the results.

It is assumed that the total curve is made up of the sum of several Lorentzian equations (depending on the number of peaks). The x-axis is divided into a series of channels and the fitted function at channel i is

$$F_i = B + \Sigma I_l / 1 + (X_i - P_l / W_l)^2$$

where B is the background level

I_l is the intensity of the lth peak

P_l is the position of the lth peak

W_l is the half width of the lth peak

and X_i is the channel number.

This programme was used to verify the existence of the peaks in the amplitude distributions recorded here, and to find their position and intensity. It was possible to constrain the background level to be zero, but the Lorentzian equation is unlikely to give an exact fit to the peak shape as it takes no account of the logarithmic compression of the x-axis, introduced by using decibels.

As the power law often gives a reasonable approximation to the amplitude distribution (Pollock,1973) it was established that the sum of Lorentzian peaks could fit a power law distribution. An idealised bimodal distribution (such as that described in section 3.3.4) with b-values of 1 and 2 was fitted and the result is shown in figure 6.7B, with the triangles representing the original data and the circles the fit. When the fit is exact only the triangles are shown. As can be seen the correspondence is impressive, the only deviations being close to the highest points on the peaks.

It was then attempted to use the programme to fit the data

obtained during the tensile testing of the various finishes. Typical examples of the fitting are shown in figure 6.7C. The results from all the fits are given in table 6.7A, with certain simplifications for clarity. The intensity of each peak has been numbered 1 to 4 for each system, where 1 is the peak of greatest intensity. If two peaks had similar intensities they were assigned the same number. If there were events above 60dB, though insufficient for the programme to fit peaks, as often occurred in the full systems, a tick was placed in the >60dB coloumn in the table. Typical results are shown, and generally the agreement between specimens was good, where the numbering of the peaks disagrees between samples of the same system a black spot was put in the first coloumn of the table, and the data given is that most frequently occurring in the samples tested. The untreated steel has not been included since it gave too few events for a satisfactory analysis.

As can be seen from table 6.7A, there was a lot of disagreement between results for the full systems. This can be attributed to the few events and large scatter at high amplitudes in these cases.

The results indicated that an acceptable approximation to this table could be given by eye, using the peak positions and heights, and this was used to extend the analysis to include systems that were immersed before testing, the various phosphates and the pre-failure distributions (shown in table 6.7B).

The analysis indicates that failure modes in the paint systems occur with amplitudes of 26, 35, 46 and 54dB, with scattered data above 60dB.

TABLE 6.7A

Data fitted by computer, showing the order of the peak intensities in the amplitude distributions.

	Peak centres ±1dB						
SYSTEM	22	26	35	46	49	54	>60
S/P	2	1					
S/P(R)	2	1					
S/P/A(1)		1	2	3			✓
S/P(R)/A(1)		1	2	3			✓
S/P/C1(1)		2	1	3		4	
S/P(R)/C1(1)		2	1	3		4	
S/P(R)/C2		1	2	3		4	
S/P/A/SUR(1)		1	2				✓
S/P(1)/A/SUR(1)		1	2		3		✓
S/P/C1/SUR(1)		1	2	3		4	5
S/P(R)/C1/SUR(1)		1	2	3		2	✓
F/S A(1)		1	2	3			✓
F/S A(R)(1)		1	2				✓
F/S C1(1)		1	4	3		2	
S/A		1	2	3			
S/C2		1	2	3			

TABLE 6.7B

Data fitted by eye showing the order of peak heights in the amplitude distributions.

Systems tested after immersion

SYSTEM	22	26	35	46	54	>60
S/P/A		1	2	3		✓
S/P(R)/A		1	2	3		✓
S/P/C1		2	1	1	2	
S/P(R)/C1		2	1	1	2	
F/S A		1	1	2		✓
F/S A(R)		1	1	2		✓
F/S C1		1	2	3	3	✓
F/S C1(R)		1	2	3	3	✓

Systems containing various phosphates

SYSTEM	22	26	35	46	54	>60
Phosphate 1		1				
Phosphate 2	2	1				
Phosphate 3	2	1	3			
Phosphate 4		1	2			
1/A		1	2			
2/A		1	2	3	4	✓
3/A		1	2	3	4	
1/C2		1	2	3	4	
2/C2		1	2	3	4	
3/C2		1	2	3		✓

TABLE 6.7B continued

Systems at pre-failure strains.

SYSTEM	22	26	35	46	54	>60
S/P 10%	2	1				
S/P/A		1				✓
S/P(R)/A 10%		1				✓
S/P/C1 10%		1	2	3	4	
S/P(R)/C1 5%		1	2	3		
S/P/A/SUR 10%		1				
S/P(R)/A/SUR 10%		1				
S/P/C1/SUR 10%		1				2
S/P(R)/C1/SUR 10%		1				2
F/S A 10%		1				
F/S A(R) 10%		1	2			
F/S C1 10%		1				
F/S C1(R) 10%		1				

The 22dB peak occurs only when the phosphate is the only coating present, and thus must be attributed to the cracking of the hopeite needles. As mentioned in 6.6.1 there is little cracking of the needles when an electrocoat is present.

The 26dB peak occurs for all systems and at low strains, so it seems reasonable to attribute this to adhesion failure in the system.

The high amplitude events, that do not seem to form peaks occur for systems where an anodic, surfacer or topcoat is present, and as in section 6.6.1 are attributed to microcracking. Figures 5.8F and G suggest that microcracking in the topcoat may be of higher amplitude than microcracking in the surfacer coat. No such high amplitude events occur for the cathodic electrocoats, and it can be seen from table 6.7A that the 54dB peak is present only for the cathodic electrocoats. It is thus reasonable to attribute the failure mode producing the 54dB peak to microcracking in the cathodic coats.

This leaves the 35 and 46dB peaks, which must be associated with the gross damage that occurs in all the specimens. As stated in section 5.13, the gross damage involves loss of adhesion on a sufficient scale for the coating to form a ruck, cracking of the film and then peeling. Figures 5.8D,E,F and G show that events of amplitudes around 26dB are present during the gross deformation, and since the 26dB peak has previously been attibuted to adhesion loss it seems reasonable that the loss of adhesion here should also give events of ~ 26dB amplitudes. There is little evidence to assist in the assigning of the other two peaks, though it is assumed that one is associated with the peeling and one with the

cracking.

This can be summarised thus:

22dB cracking of hopeite needles in the phosphate coat.

26dB loss of adhesion.

35dB } gross cracking in the paint film.

46dB } gross peeling of the paint film.

54dB microcracking in the cathodic electrocoat.

>60dB microcracking in the anodic electrocoat, surfacer and topcoat.

A study of the amplitude distributions of the full systems and systems with a surfacer coat (figures 5.4F and H) suggests that there are more peaks than those discussed here, at $\gtrsim$60dB, and that they are associated with the high strain gross damage is indicated by figures 5.8D,E,F and G. Unfortunately there are so few events in each peak they cannot be properly quantified or the associated modes of failure found. There existance is not unexpected since there are a large number of further failure modes possible on the addition of extra coats, eg. surfacer cracking, topcoat cracking and adhesion loss along the electrocoat/surfacer interface.

6.8 The effect of immersion prior to tensile testing.

The results discussed here are given mainly in section 5.6. In this section only, the systems described as full systems are electrocoated on both sides, but the surfacer and topcoat are applied to one side only. Specimens were left in this, as

received state since the immersion period was 96hrs and the extra electrocoat was an efficient way to prevent the steel rusting. As discussed in section 6.5 the side coated with the full system is very much quieter than that with only the cathodic 1 electrocoat, so the acoustic emission will be largely affected by the electrocoat.

A comparison of the wet and dry results (figures 5.6A,B,C and D) reveals a number of striking differences, the most dramatic, perhaps, being in the shape of the ringdown count rate vs. strain curves for the full systems with a cathodic 1 electrocoat. The acoustic emission occurred in only one peak at low strains. The presence of only one peak seems to be due to the extremely early onset of the gross damage in this case. Gross damage was visible on the specimen surface from very low strains. Systems with only the cathodic 1 electrocoat also showed a very much earlier onset of gross damage, though in this case two peaks can be distinguished in the ringdown count rate vs. strain curves.

Though not as dramatic, gross damage also occurred at lower strains when systems with an anodic electrocoat were tested wet than when they were tested dry. This was is seen both directly and by the acoustic emission. The effect is not expected to be so great in the case of the anodic coat as for the cathodic 1 coat, since capacitance measurements (figure 5.11A) indicate that, not only did the anodic coat take up less water during immersion, but also that it would have lost a large amount of the excess water during the course of the test.

A reasonable explanation of the earlier onset of gross

damage after immersion is given by the fact that the paint swells with the water. The film thickness, perpendicular to the tensile axis, of the wet and dry paint films were measured and showed that the paint films did, indeed swell. This swelling forces the paint into greater compression on the substrate which causes the adhesion loss to occur at lower strains.

The low strain acoustic emission appears to be slightly decreased for the cathodic 1 electrocoat. It seems unlikely that the water was acting to prevent microcracking since the 54dB peak remained distinct in the amplitude distribution (figure 5.6F). The height of the 54dB peak seems slightly increased, suggesting that the water promotes microcracking. It does not seem likely that the presence of water improves the adhesion so the reason for the decrease in the low strain acoustic activity is not known at present.

Mosle (1979a) also noticed that the high strain acoustic emission peak occurred sooner during testing after immersion, and he suggested that this was due to water build up along the paint/phosphate interface causing adhesion to be lost along that interface rather than between the hopeite and the phosphophyllite. Examination of the backs of the electrocoats tested here suggests that slightly fewer hopeite needles were present than after the system was tested dry, but the failure still seemed to have occurred mainly along the hopeite/phosphophyllite interface.

The amplitude distributions show a 26dB peak of similar height whether the system is tested wet or dry, which also suggests that the presence of water caused no adhesion loss or

change in the mode of adhesion failure. The other peaks seem to be slightly higher in the case of the wet cathodic 1 coat cf. the dry, suggesting that more cracking and peeling occurred.

Another striking difference between the wet and dry results is that the acoustic emission from the full systems containing a cathodic 1 electrocoat showed a difference between the system with the rinsed phosphate and the one where it was not rinsed. The rinsed system gave considerably less acoustic emission, suggesting improved adhesion. A possible explanation may be that during the immersion some corrosion takes place along the unrinsed phosphate interface, reducing the adhesion. The situation does not occur when an anodic coat is used, probably because the anodic coat presents a more efficient barrier to corrosion. There was little difference in the acoustic emission between rinsed and unrinsed phosphates under the cathodic 1 coat alone, possibly the rusting occurred in both the rinsed and unrinsed case in this instance.

The effect of rinsing the phosphate under a cathodic electrocoat has also been studied by Cooke (1979). He showed that if the cathodic coat was applied by spraying rather than electrocoating the effect still occurred. Thus he attributed the effect to the type of binder used in the coat rather than the coating process. It is possible, though, that neither the cathodically electrocoated nor sprayed coats can prevent the rusting, whereas an anodically applied electrocoat with the same binder would. Unfortunately Cooke did not present the results for an anodic coat applied by spraying. However, the main conclusion of Cooke, that the cathodic electrocoat is

particuarly sensitive to the phosphate is supported by this work.

The acoustic emission during tensile testing of systems containing various types of phosphates will be considered in the next section.

6.9 The effect of various types of phosphates.

Finally the acoustic emission was monitored during tensile testing of several different types of phosphate (as given in table 4.1B) and also of these phosphates coated with anodic or cathodic 2 electrocoats. The results appear mainly in section 5.7.

6.9.1 Phosphated steel.

The G16S phosphate (discussed previously) gave little emission after ~ 10% strain; considerable damage in the form of cracked needles and adhesion loss was found (by scanning electron microscopy)to have occurred during this region. Damage occurring only at low strains has also been seen in the case of oxide layers on steel (Palmer,1973) where similar behaviour would be expected, since both oxides and phosphates are brittle conversion coatings. Palmer also reported that many of the events from the oxides were of high amplitudes, whereas for all the phosphates considered here the amplitude distributions (figure 5.7E) indicated very few events at high amplitudes. This suggests that oxide cracking is a higher energy process than phosphate cracking.

The G16S phosphate has been studied both when rinsed and when left unrinsed, these gave similar acoustic emission (figure 5.3A) as would be expected, since they are stored in dry conditions. The rinsed G16S, however, showed rather less scatter, probably because the unrinsed specimens were beginning to rust, which would cause further variability between the specimens. That rusting does take place is shown in figure 5.14C, where the globular, rather than needle-like growths are commonly attributed to rust (Cooke,1979).

Phosphate number 4 is also a G16 phosphate, but with a lower coating weight. It can be seen from table 5.14 A, that the surfaces of the two appear similar, suggesting that the loss in weight occurs mainly in the bulk of the phosphate. The scanning electron microscopy indicated that, during tensile testing the hopeite needles cracked, but that they largely remained attached to the surface. The final amplitude distibutions are similar for phosphate 4 and G16S, (table 6.7A) both having a 22 and a 26dB peak but events at few other amplitudes. These would be expected to give similar acoustic emission as similar failure mechanisms operate. The phosphate 4, though, gave less emission in total, and also gave some emission at high strains. It is possible that the needle cracking continues to occur at strains of <10%, but that the lower coating weight leads to improved adhesion, with adhesion loss occurring at considerably higher strains. Mosle (1979) found that a thicker phosphate coating led to an earlier onset of more acoustic emission, which he attributes to the fracture of more and coarser crystals, suggesting that the phosphate coatings he studied are different to those investigated

here.

Phosphate 3 gives acoustic emission similar to that of G16S, ie. mainly occurring within the first 10% of strain and gave a similar amplitude distribution. The scanning electron microscope indicates that the emission was due to the cracking of the platelets and their loss of adhesion, and the similarity of the acoustic emission suggests that these processes are similar to the needles cracking and losing adhesion in the G16S.

Phosphate 2 gave a similar amplitude distribution and the microscopy indicated that the emission is due to the cracking of needles and their loss of adhesion. The decreased acoustic emission and the presence of a high (~ 20%) strain region for the ringdown counts suggests that, similarly to phosphate 4, the lower coating weight improves the adhesion.

Phosphate 1 is considerably quieter than the other phosphates, with the emission occurring mainly at higher strains. The amplitude distribution shows events of higher amplitudes and no 22dB peak. The loss of the 22dB peak corresponds with the microscopical observation that the few needles present do not crack. The high strain emission is probably due to loss of adhesion, which since it has a low coating weight, would be expected to occur at high strains.

As described, there are large differences in the behaviour of and the emission from the various phosphates. It is confirmed that needles cracking cause events with ~ 22dB amplitudes and the adhesion loss seems to occur at strains dependant on the coating weight. Cooke (1979) also found that heavier coatings are mechanically fragile.

6.9.2 The effect of electrocoating.

As stated previously, the anodic electrocoat is less sensitive to the phosphate layer than is the cathodic 2 coat. This is also shown by the acoustic emission. The trends in the curves (figures 5.7B,C,E and F) are very similar for all the phosphates when an anodic electrocoat is present, whereas the phosphates with the cathodic coat show the onset of high strain damage at different strains depending on the phosphate. It is assumed that the acoustic emission arises in the same way as described in section 6.4.

The amplitude distributions are similar for all the systems with a cathodic coat (figure 5.7G), however the anodic coat gives a significantly different distribution when applied onto phosphate 1 than when on the others. This distribution (figure 5.7E) shows few events other than a peak at ~ 26dB, which suggests that little failure occurred other than adhesion loss.

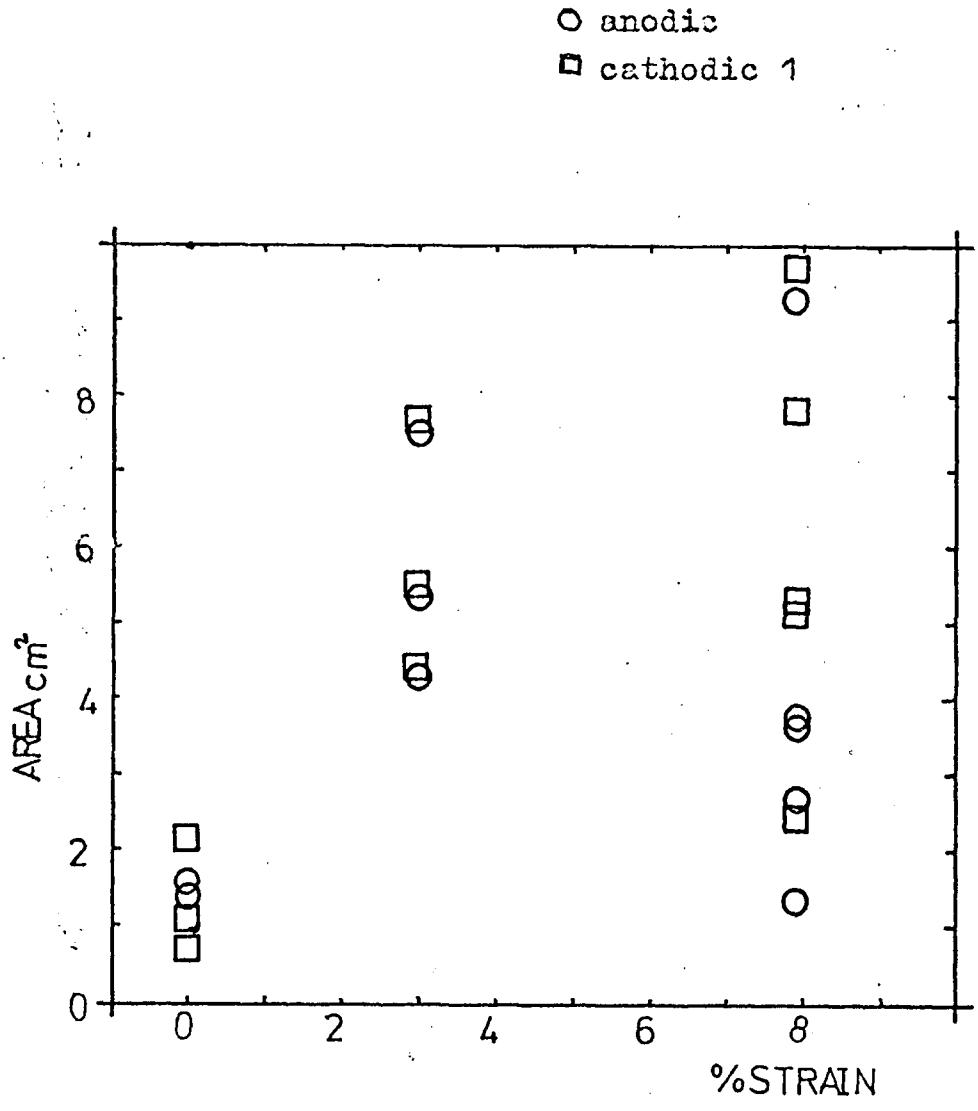

Figure 6.4A.
The area of microcracking as a function of strain for the anodic and cathodic 1 electrocoats.

FIGURE 6·4 B

Schematic representation of a Luders band reaching the surface.

BEFORE

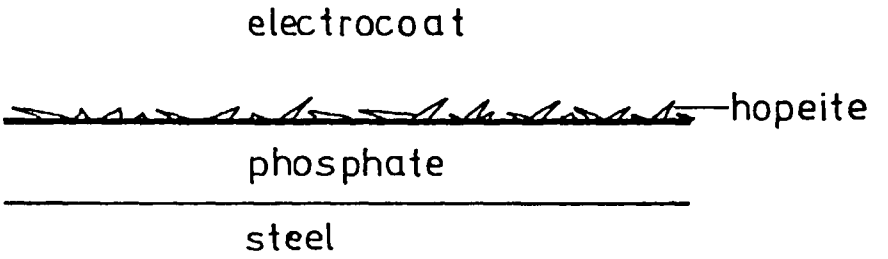

AFTER

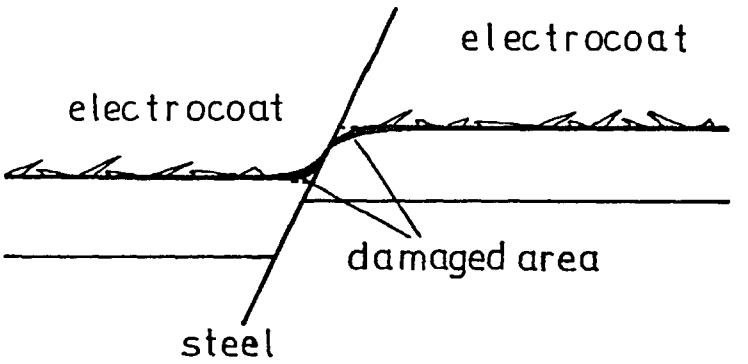

FIGURE 6·4C

Schematic representation of a paint, originally in tension on the substrate, debonding.

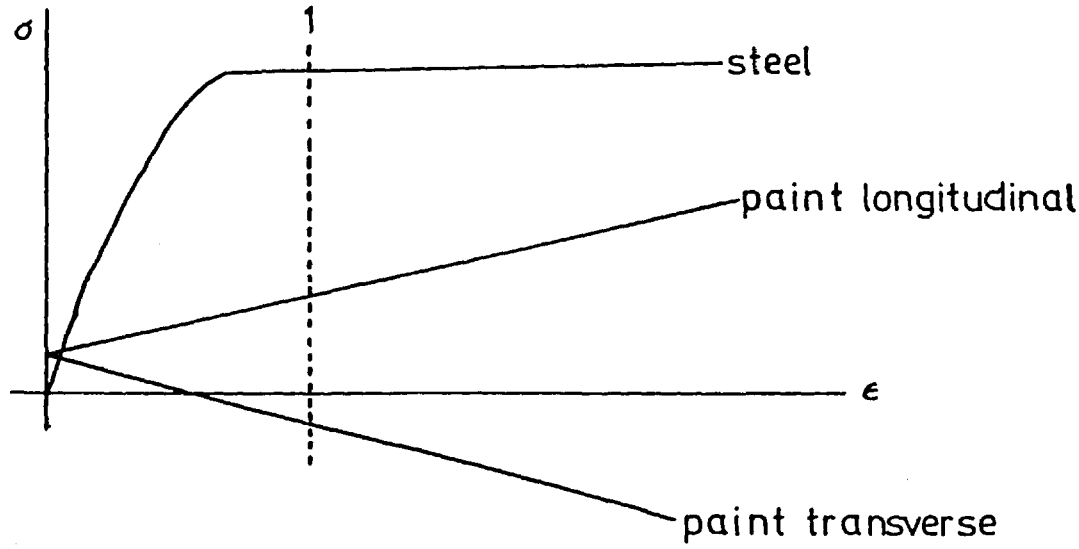

1) Paint debonds in transverse direction. As it was in compression it will form a ruck.

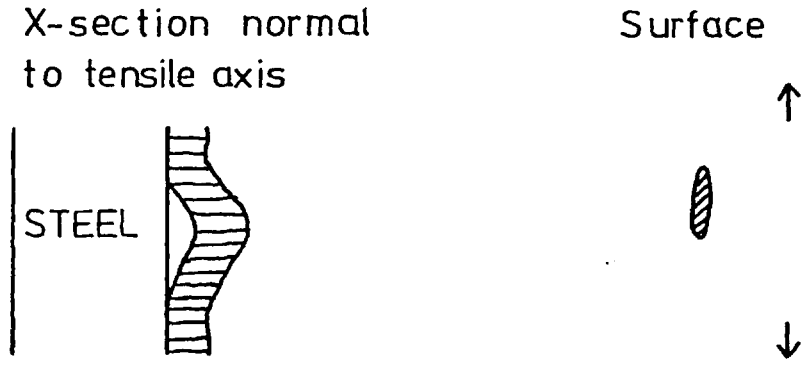

Paint debonds in longitudinal direction. It was in tension so will not form a ruck.

FIGURE 6·4D

Schematic diagram of a paint, originally in compression on the substrate, debonding.

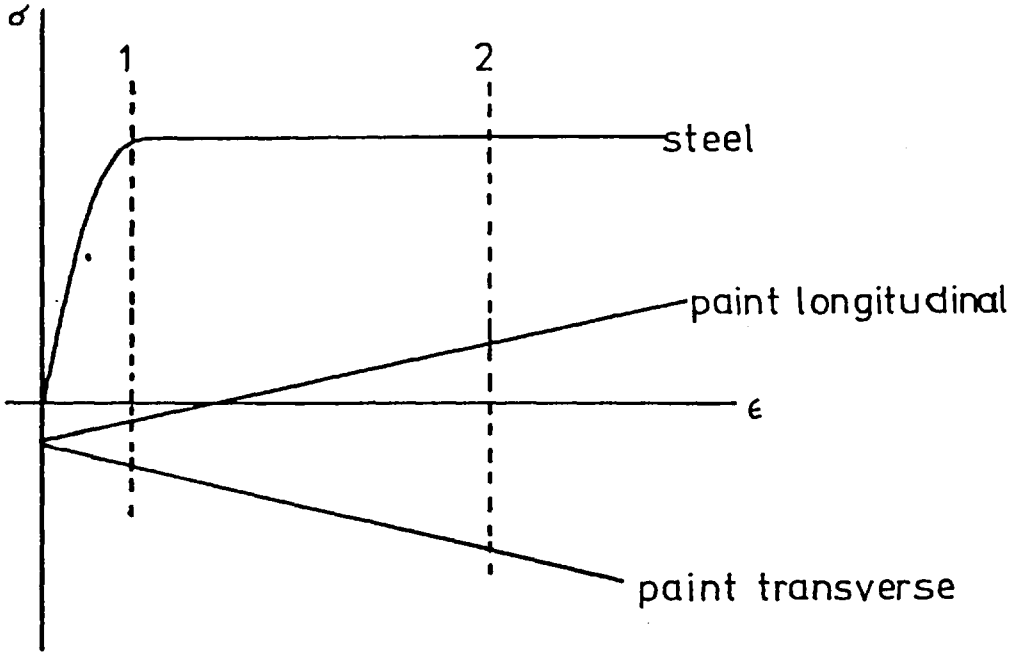

1) Paint debonds in transverse direction.
As it was in compression a ruck forms.

X-section normal to tensile axis.

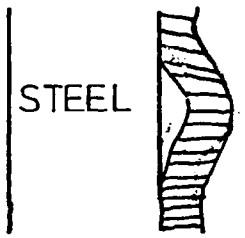

Surface

Paint debonds in longitudinal direction.
It was also in compression so also forms a ruck.

X-section parallel to tensile axis.

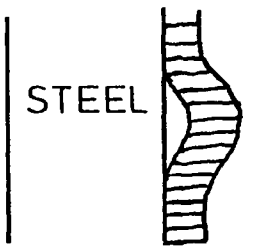

Surface

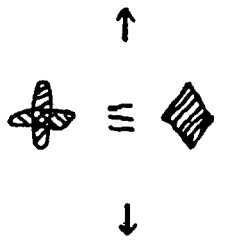

2) Paint cracks across.

X-section parallel to tensile axis.

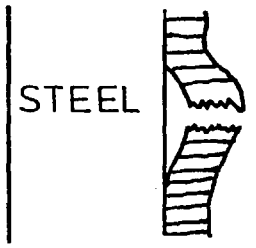

Surface

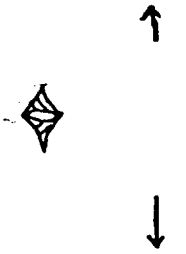

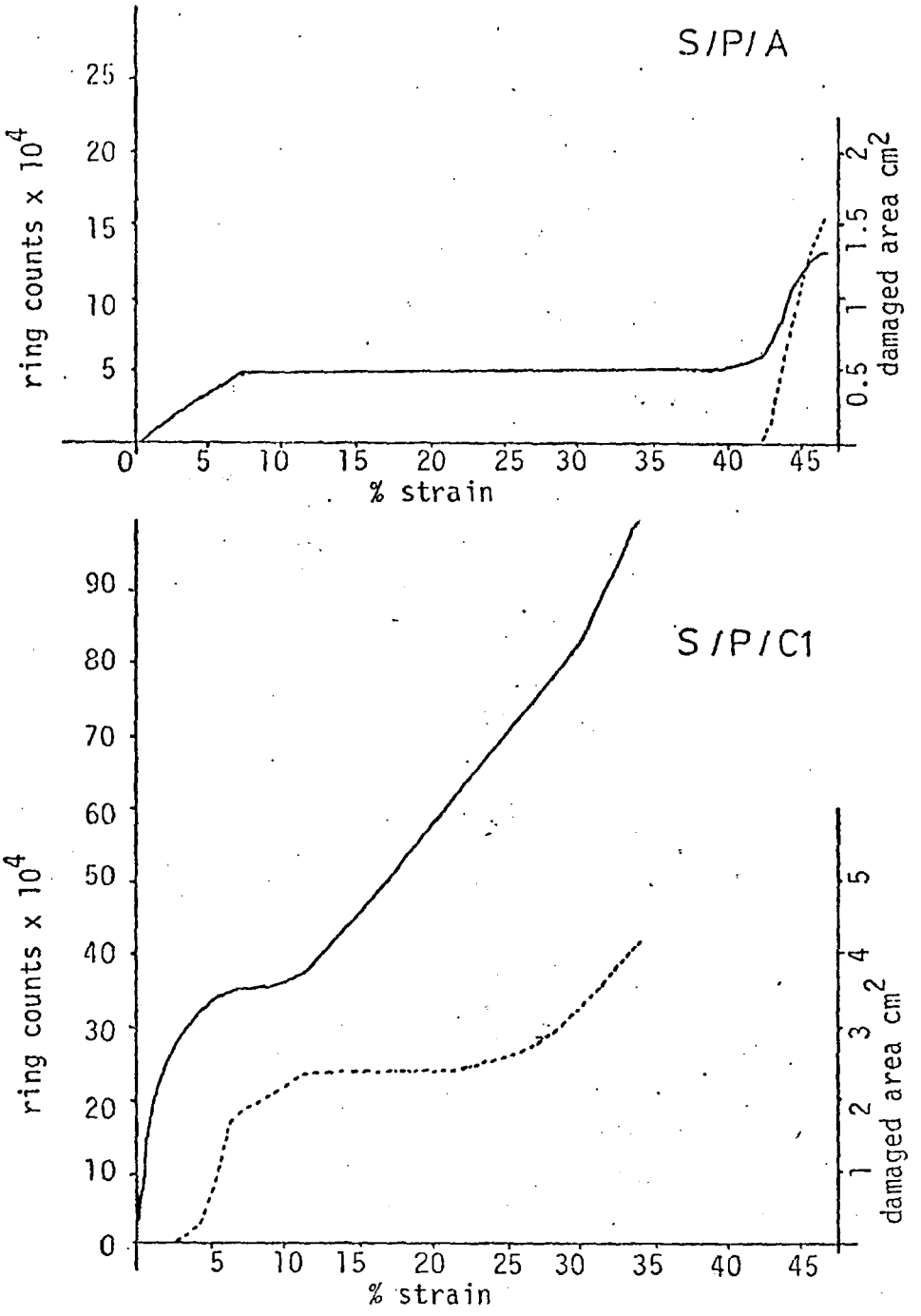

FIGURE 6.4E

Typical ringdown count vs. strain cf. gross damage vs. strain curves.

——— ringdown counts

---------- damaged area

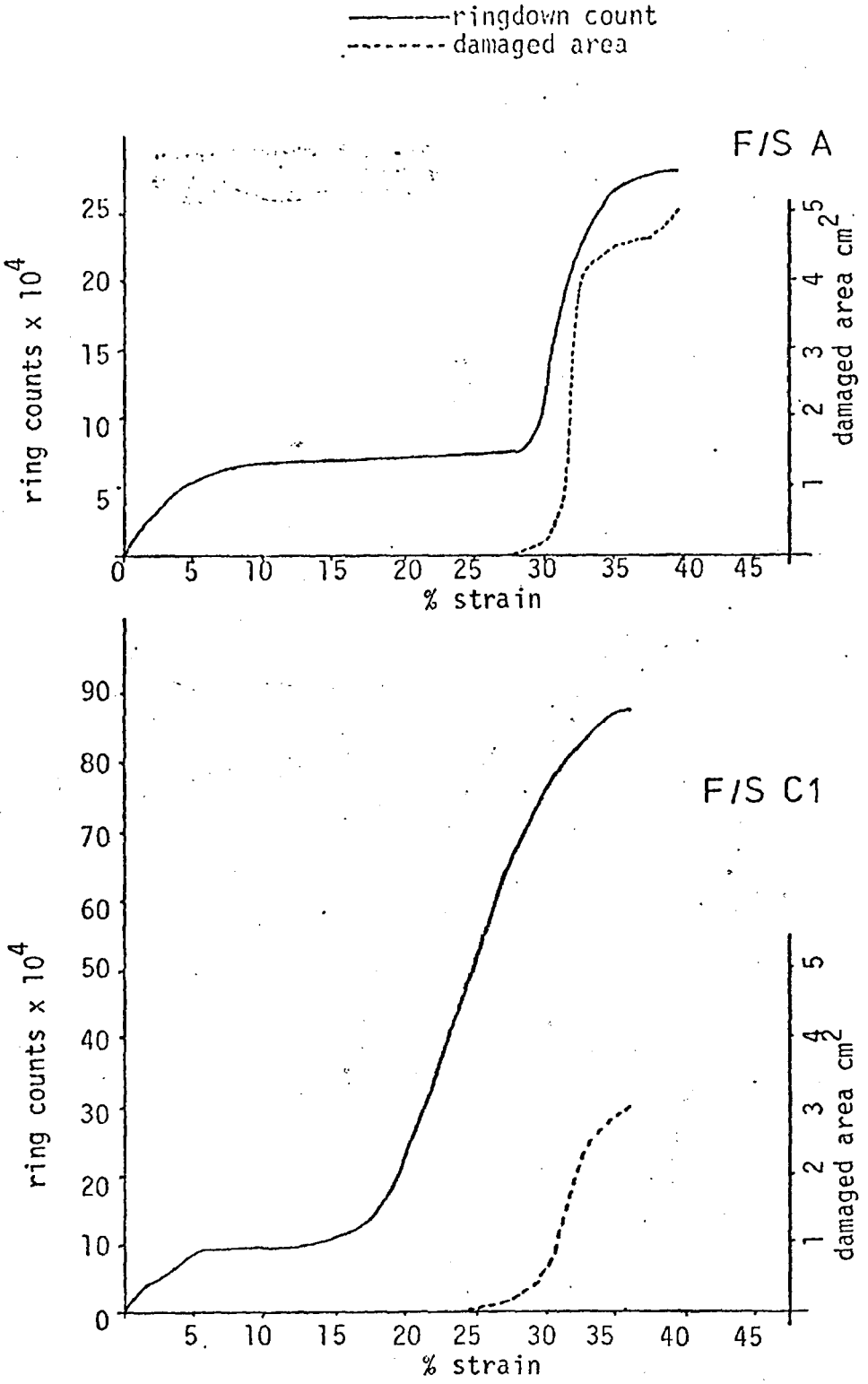

FIGURE 6·4F

Typical damaged area and ringdown count vs. strain curves.

FIGURE 6.5A

The events vs. strain curves for S/P/A and S/P/Cl and twice the events vs. strain curves for S/P/A(1) and S/P/Cl(1), showing that the systems coated on both sides give about twice as many events as the same systems coated on one side only.

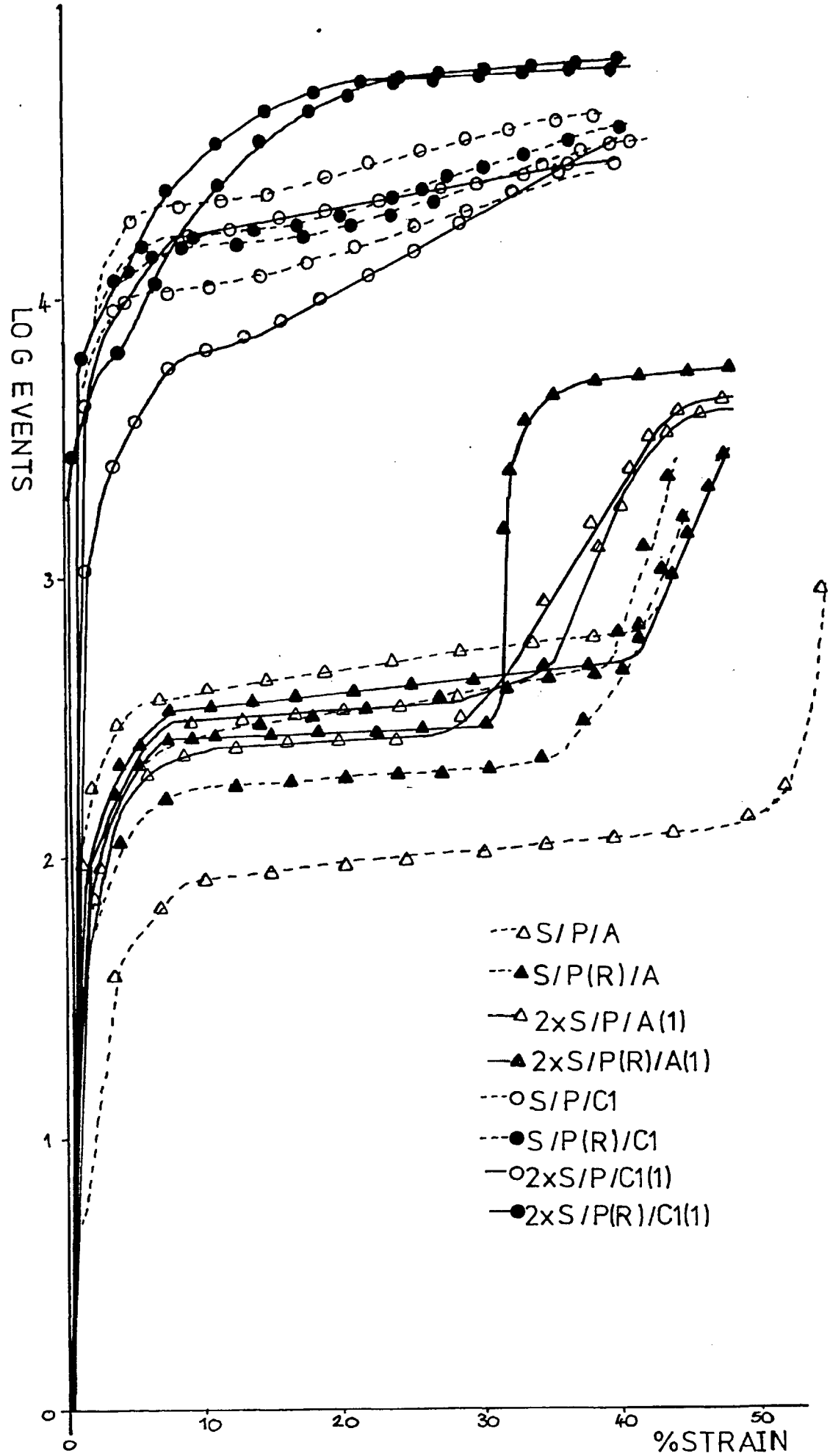
LOG EVENTS
0
1
2
3
4
0
10
20
30
40
50
%STRAIN
S/P/A
S/P(R)/A
2xS/P/A(1)
2xS/P(R)/A(1)
S/P/C1
S/P(R)/C1
2xS/P/C1(1)
2xS/P(R)/C1(1)

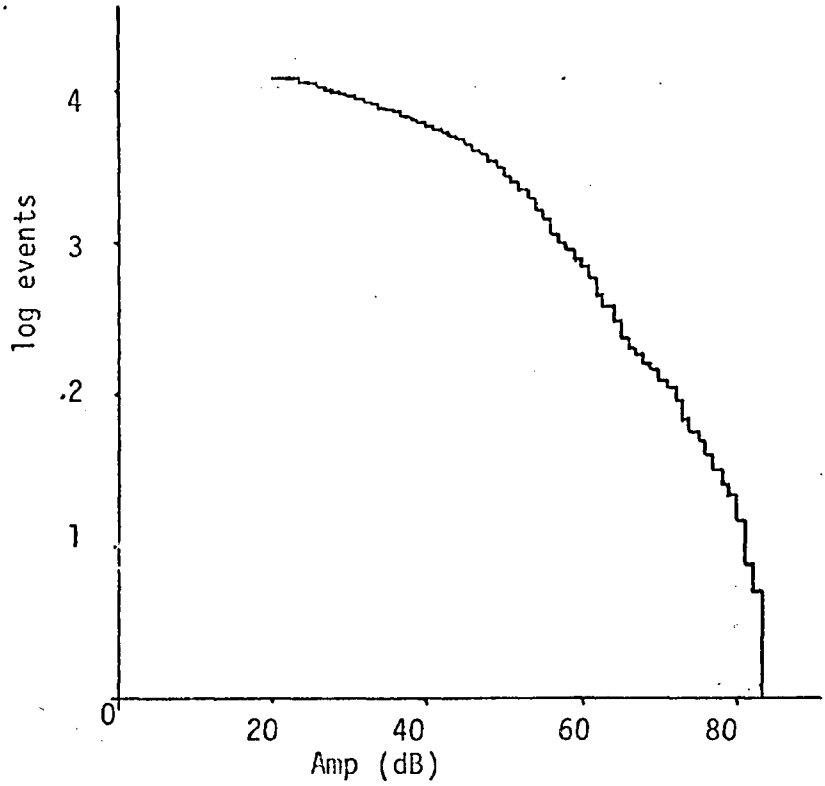

FIGURE 6 7A

A cumulative log plot typical of those obtained here. It does not give a good fit to a straight line.

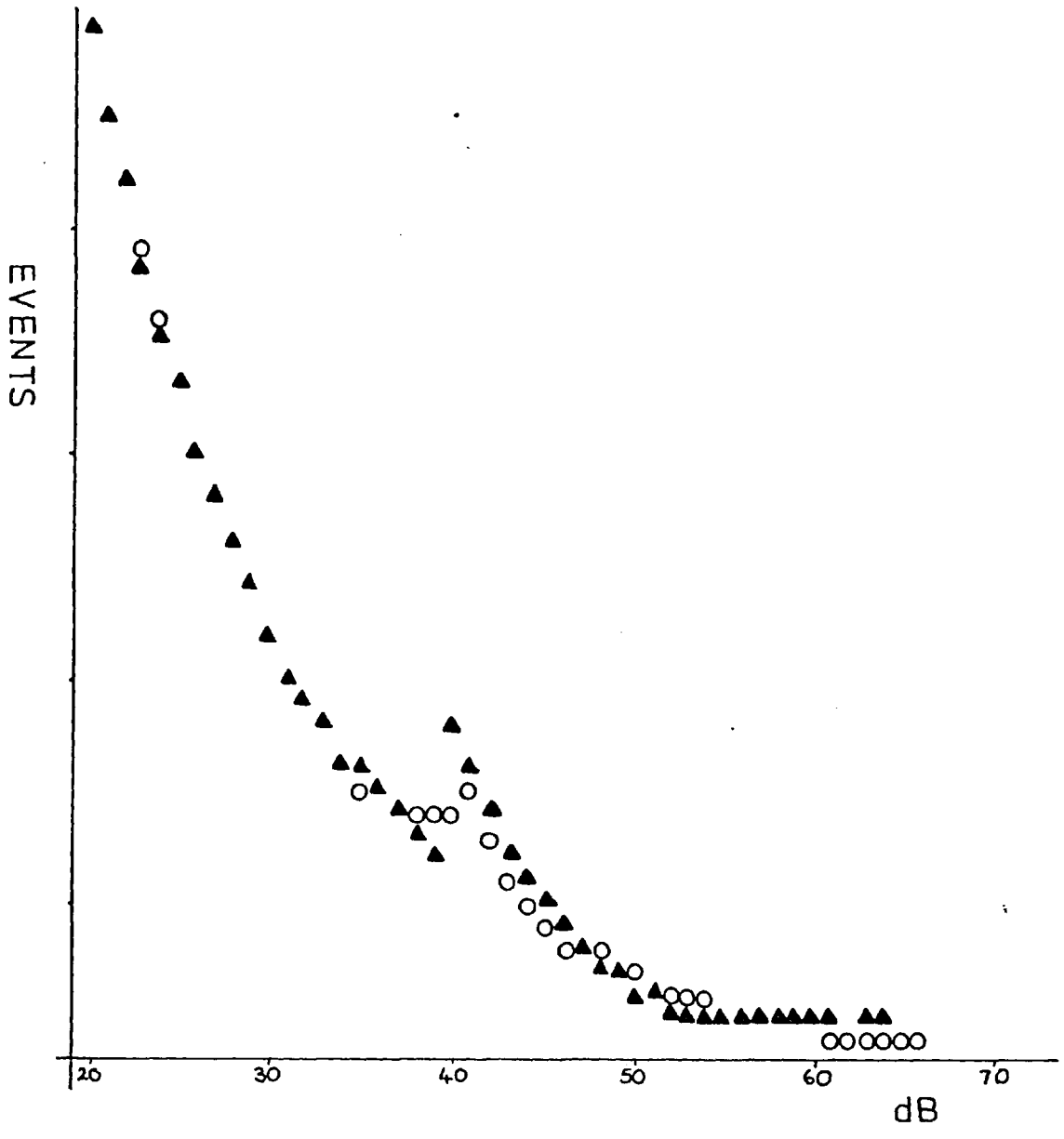

FIGURE 6·7B

A computer fit to a distribution obtained from an idealised cumulative-log plot.

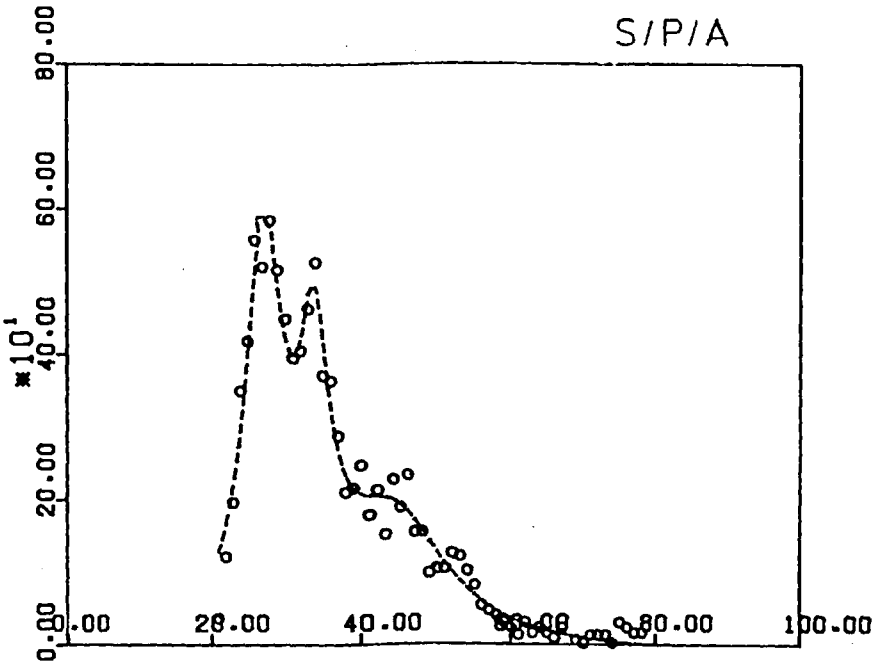

FIGURE 6·7 C

The broken line represents the computer fit to the data represented by circles. Two typical fits are shown.

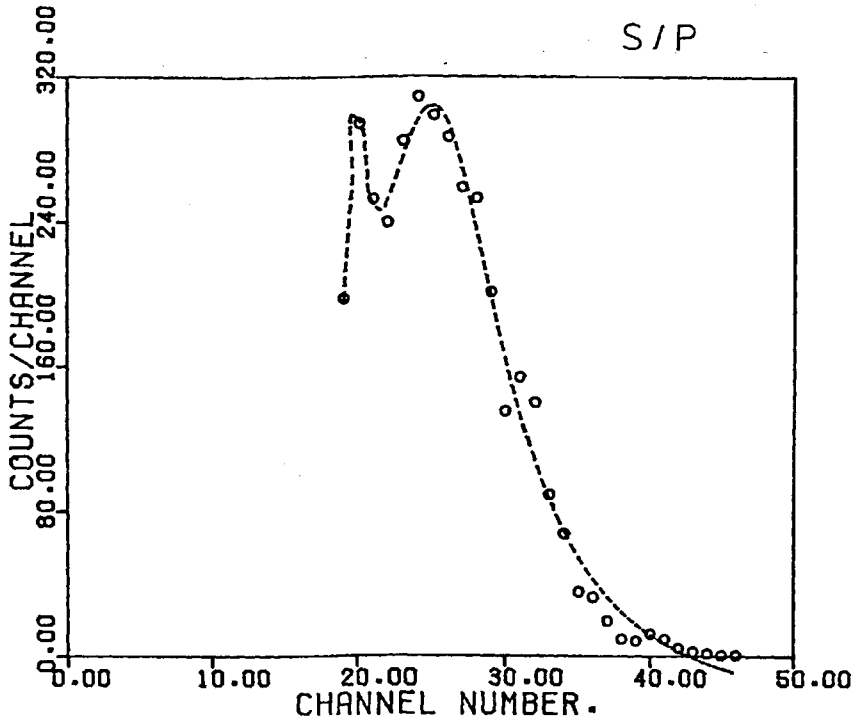

Chapter 7 Conclusions.

The preceding results and discussion allow several general conclusions to be drawn regarding the applicability of acoustic emission to paint testing.

1) Acoustic emission can be used to monitor deformation of automobile finishes with paint coats during tensile testing and gives results which are sufficiently reproducible for differences to be seen between various systems. The results are consistent with the results obtained by longer and more tedious conventional tests.

2) The acoustic emission during tensile testing of automobile finishes occurs in two regions of high activity, centred about strains which are dependant on the system studied. The low strain failure mechanisms of the finishes tested here are microcracking and minor adhesion loss. It has been established that the higher strain region of acoustic activity is associated with damage visible on the surface of the specimen.

3) Differences in the deformation behaviour of the finish which arise due to immersion can be detected by acoustic emission.

4) It is possible to assign peaks in the amplitude distributions of the acoustic emission monitored during tensile testing of automobile finishes to the failure modes that occur within the specimen.

For the particular systems studied here it has also been

established that

5) The steel substrate makes a negligible contribution to the acoustic emission of the finishes.

6) The cathodic electrocoats have poorer adhesion and are more sensitive to the condition of the phosphate than is the anodic coat.

7) The addition of a surfacer coat to the system improves the mechanical behaviour of the finish, whereas the further addition of a topcoat reduces it.

8) The G902 phosphate shows better mechanical performance than the G16, G16S, G2000 or G2500 phosphates.

Chapter 8 Suggestions for further work.

Several areas where further work would be useful arise from Chapter 6.

1) Scanning electron microscopy showed the presence of microcracking in the coatings at low strains. It would be useful to quantify the extent of this cracking for a large number of specimens, in order to compare it with the acoustic emission at low strains more accurately.

Further and more quantitative tests of the adhesion, particuarly of the full systems, should be attempted. Several other tests exist to measure the adhesion than have been utilised here (Schurr,1972).

3) It would be interesting to monitor several other types of electrocoat, in particular another type of anodic coat, for comparison with the results obtained here.

4) The properties of an anodic coat applied by spraying rather than electrocoating should be determined, to establish whether the anodic electrocoating onto phosphate gives particularly good corrosion resistance, as suggested in section 6.8.

In general this technique of monitoring paint films has enormous scope and several areas of further work suggest themselves.

5) Monitoring the acoustic emission during bending tests. In many cases the flexibility of a paint film is determined by bending tests and it would be particularly interesting to monitor

the amplitude distributions in order to determine whether similar failure mechanisms operate.

6) The testing of paint films after immersion yields useful information and this could be extended to testing films after ageing and to testing films in conditions of high humidity.

7) Many other types of paint films could be monitored. It would be interesting to see if the characteristics found in the tests performed here are general to all types of thermosetting resins. It may also be enlightening to study the effects on the acoustic emission of various paint parameters, such as the pigment volume concentration and the types of extenders used.

8) A common way of evaluating a paint's resistance to corrosion is to determine the corrosion about a line scribed through the paint film. Acoustic emission may be a useful addition to such tests, providing information about any underfilm corrosion that may take place.

Appendix 1

Mossbauer programme used for assessing the peaks in the amplitude distributions.

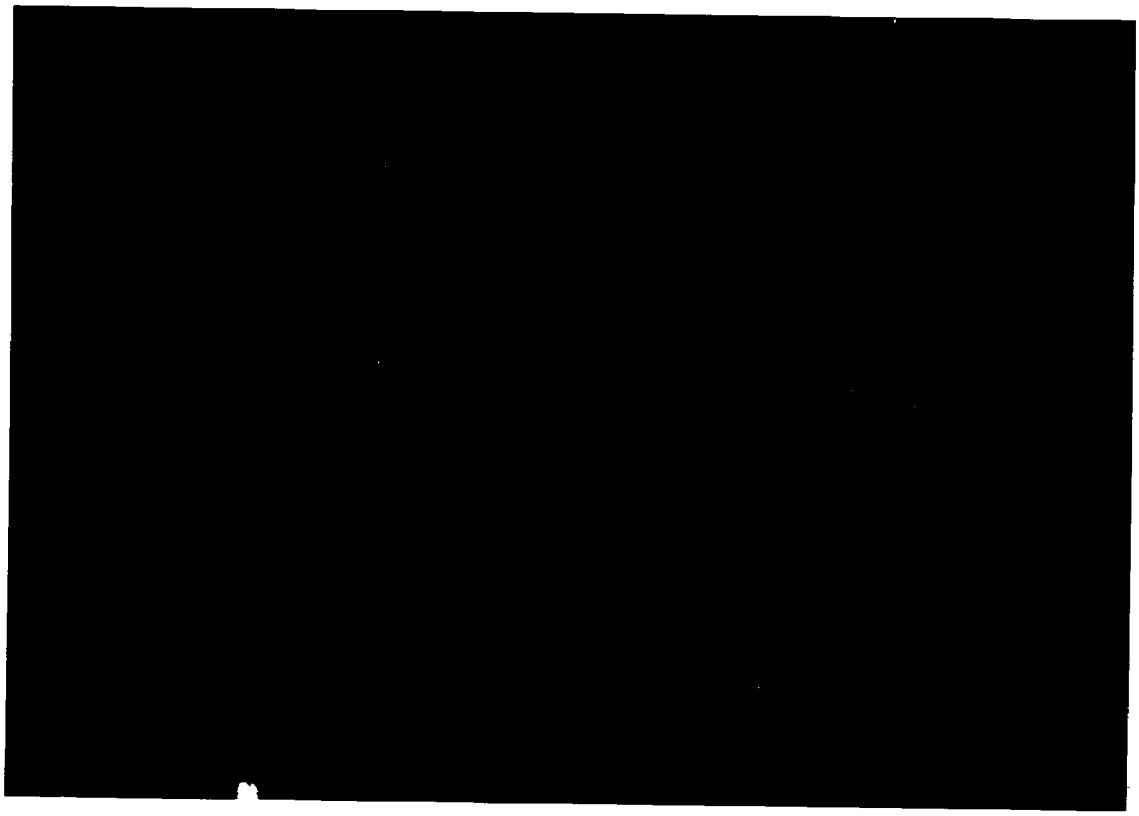

ACKNOWLEDGEMENTS.

I would like to thank Dr. R. D. Rawlings for being an excellent supervisor, his help, encouragement and boundless enthusiasm have been invaluable.

I would also like to thank Ian Morrison for the use of and help with his computer programme, and Paul Grant for allowing me to use the Geology electron microscope.

I am grateful to the Science Research Council for financing this work, and to the members of Imperial Chemical Industries for providing the materials, and the facilities for the conventional tests performed. In particular I would like to thank Dr. M. Coclough and Dr. B. Cooke.

Thanks are also due to the members of my group, to Dr. C. Webborn for his instruction in the use of the acoustic emission equipment, and to A. Halstead and others for adding greatly to my enjoyment of the past three years.

I would like to thank Prof. Pashley and the Metallurgy Department of Imperial College for providing the facilities to carry out this work, and also many of the members of staff for their assistance, in particular F. Huggins, H. Haddow and Dr. Crane.

Finally I would like to thank W. J. Clegg for reading through the thesis and his many helpful suggestions and G. Edwards for her assistance with the typing.

REFERENCES.

Anderson D. et al, J.Coatings Tech. 50(11) 39 1978.

Bacon R. et al, Ind. Eng. Chem. 40(1) 161 1948.

Becht J. et al, Composites 8 245 1976.

Bell S. J.O.C.C.A. 43 466 1960.

Brindley B. and Harrison R. C.E.G.B. report. RD/L/N137/72 1972.

Cheever G. and Wojtkowiak J. J. Paint Tech. 42 409 1970.

Clark J. C.E.G.B. report. R/M/N1024 1978.

Cooke B. Private communication. 1978.

Cooke B. 1st Asian-Pacific Corrosion Control Conf. Singapore, July 1979.

Curtis G. Non-destructive testing 8 249 1975.

Dunegan H. et al. UCID-4868. Lawerence Radiation lab. California. 1964.

Dunegan H. and Green A. A.S.T.M. S.T.P.505. Acoustic Emission. p.100 1972.

Elm A. Off. Dig. 25 750 1953.

Filatov V. et al. Ind. Lab. 39(10) 1638 1973.

Fisher R. and Lally J. Can. J. Phys. 45 1147 1967.

Fitch C. BNWL-1008. Signal analyisis in flat plates. Battelle Northwest, Richland, Washington. 1969.

Gentles J. J.O.C.C.A. 46 850 1963.

Guild F. et al. Composites 7(3) 173 1975.

Hamel F. et al. Ultrasonics 17 125 1979.

Hamstad A. and Mukherjee H. Exp. Mech. 14(1) 33 1974.

Hardy H. A.S.T.M. S.T.P.505 Acoustic emission

p.41 1972.

Harris D. and Dunegan H. Exp. Mech. 14 71 1974.

Holt J. C.E.G.B. report. RD/L/N106/72. 1972.

Holt J. and Evans A. C.E.G.B. report. RD/L/N40/76. 1976.

Jacobsen A. Ind. Eng. Chem. 30(6) 660 1938.

James D. and Carpenter S. J. Appl. Phys. 42(12) 4685 1971.

Kaiser J. PhD.thesis. Technische Hochschule, . Munich. 1950.

Mason W. et al. Phys. Rev. 73(10) 1213 1948.

Mason W. et al. Physical Acoustics and the Properties of Solids. pub. Van Nostrand Co. Inc. New Jersey 1958.

Mayne J. British Corr. J 5 106 1970

Monk C. and Wright T. J.O.C.C.A. 48 520 1965.

Mosle H. et al. Z. Werkstofftechnik 9(8) 265 1978.

Mosle H. et al. Conf. on Surface Protection by Organic Coatings. Budapest. May 1979a.

Mosle H. et al. Symp. on Acoustic Emission. Bad Nauheim. Apr. 1979.

Myers R. and Long J. Treatise on Coatings. Vol. 2. pt. 1. pub. Marcel Dekker. New York. 1969.

Nylen S. and Sunderland P. Modern Surface Coatings. pub. Wiley and sons. 1965.

Ono K. and Usick L. Mat. Eval. 34 32 1976.

Palmer I. Mat. Sci. Eng. 11 227 1973.

Peters C. and Larson C. Non-destructive testing 9 197 1976.

Pollard H. Sound waves in Solids. pub. Pion Ltd. London. 1977.

Pollock A. Non-destructive testing 6 264 1973.

Redwood M. Ultrasonics 2 174 1964.

Schlotz C. Bull. Seism. Soc. Am. 38 399 1968.

Schuh A. and Theuerer H. Ind. Eng. Chem. 9(1) 9 1937.

Schurr G. A.S.T.M. S.T.P.500. Paint testing Manual p.333 1972.

Scruby C. and Wadley H. J. Phys. D: Appl. Phys. 11 1487 1978.

S.M.M.T. Standard no. 57. Water Immersion Test. 1956.

Strivens T. Private communication. 1979.

Swindlehurst W. Non-destructive testing 6 152 1973.

Swindlehurst W. and Wilshaw T. J. Mat. Sci. 11 1653 1976.

Tatro C. A.S.T.M. S.T.P.505. Acoustic Emission. p.84 1972.

Walker P. Off. Dig. 37 1561 1965.

Webborn C. PhD. Thesis. Imperial College. 1979.

Williams J. C.E.G.B. report. RD/L/N37/73. 1973.

Williams J. and Lee S. Non-destructive testing 12 5 1979.

Wojtkowiak J. and Bender H. J. Coat. Tech. 50(642) 86 1978.

TABLE 4.1A.

SYMBOL	SPECIMEN
S	Steel
S/P(R)	Steel with a phosphate coat (rinsed)
S/P	Steel with a phosphate coat (unrinsed)
S/P(R)/A	Steel with a rinsed phosphate & anodic electrocoat
S/P/A	Steel with an unrinsed phosphate & anodic electrocoat
S/P(R)/C1	Steel with a rinsed phosphate & cathodic 1 "
S/P/C1	Steel with an unrinsed phosphate & cathodic 1 "
S/P(R)/C2	Steel with a rinsed phosphate & cathodic 2 "
S/P/C2	Steel with an unrinsed phosphate & cathodic 2 "
S/A	Steel with anodic electrocoat applied directly
S/C2	Steel with cathodic 2 electrocoat applied directly
F/S A(R)	Steel with a rinsed phosphate & anodic electrocoat, with surfacer and topcoat on one side
F/S A	Steel with an unrinsed phosphate & anodic electrocoat with surfacer and topcoat on one side
F/S C1(R)	Steel with a rinsed phosphate & cathodic 1 coat with surfacer and topcoat on one side
F/S C1	Steel with an unrinsed phosphate & cathodic 1 coat with surfacer and topcoat on one side

Systems with the coating only on one side.

S/P(R)/A(1)	Steel with a rinsed phosphate & anodic electrocoat
S/P/A(1)	Steel with an unrinsed phosphate & anodic electrocoat
S/P(R)/C1(1)	Steel with a rinsed phosphate & cathodic 1 "
S/P/C1(1)	Steel with an unrinsed phosphate & cathodic 1 "
S/P(R)/A/SUR(1)	Steel with a rinsed phosphate, anodic electrocoat and surfacer
S/P/A/SUR(1)	Steel with an unrinsed phosphate, anodic electrocoat and surfacer
S/P(R)/C1/SUR(1)	Steel with a rinsed phosphate, cathodic 1 electrocoat and surfacer
S/P/C1/SUR(1)	Steel with an unrinsed phosphate, cathodic 1 electrocoat and surfacer
F/S A(R)(1)	Steel with a rinsed phosphate, anodic electrocoat surfacer and topcoat
F/S A(1)	Steel with an unrinsed phosphate, anodic electrocoat surfacer and topcoat
F/S C1(R)(1)	Steel with a rinsed phosphate, cathodic 1 electrocoat surfacer and topcoat
F/S C1(1)	Steel with an unrinsed phosphate, cathodic 1 electrocoat, surfacer and topcoat

F/S - full system
On photographs the topcoat is designated TC.

TABLE 4.1B

SYMBOL	SPECIMEN
1	Granodine 902
1/A	Granodine 902 with anodic electrocoat
1/C2	Granodine 902 with cathodic 2 electrocoat
2	Granodine 2500
2/A	Granodine 2500 with anodic electrocoat
2/C2	Granodine 2500 with cathodic 2 electrocoat
3	Granodine 2000
3/A	Granodine 2000 with anodic electrocoat
3/C2	Granodine 2000 with cathodic 2 electrocoat
4	Granodine 16